Design, Characterization and Biomedical Applications of Cyclopropanated Lipidic Mesophases

---

Dissertation
zur

Erlangung der naturwissenschaftlichen Doktorwürde

(Dr. sc. nat.)

vorgelegt der

Mathematisch-naturwissenschaftlichen Fakultät

der **Universität Zürich**

von

Livia Salvati Manni
aus Italien

Promotionskomitee

Prof. Dr. Kim K. Baldridge

Prof. Dr. Ehud M. Landau

Prof. Dr. Jay S.Siegel

Prof. Dr. Anthony Linden

Prof. Dr. Raffaele Mezzenga

Zürich, 2017

Abstract

This multidisciplinary project begins with one overarching aim: to elucidate the role of the rigidity of the lipid tail on the phase transitions of lipidic mesophases. Previous studies have demonstrated that the position and the number of *cis* double bonds in monoacylglycerols determine the chain splay of the molecule, establishing how this parameter was essential in influencing the phase behavior. Following on from this, novel lipids which are inspired by naturally occuring cyclopropanated lipids have been synthesized, and their phase behavior elucidated. The chain rigidity has been systematically varied by locking the *cis* configuration of the double bond on the alkyl chain in a confined geometry. To understand the relationship between chain rigidity and phase behavior a library of new lipids has been synthesized replacing the *cis* double bond by a geometrically confined cyclopropyl ring. The replacement of the double bond with a chemically analogous cyclopropyl group was designed in order to maintain a similar chain splay and CPP parameter. The insertion of an additional carbon into the lipidic chain doesn’t significantly change the length or the curvature of the chain but varies substantially the packing frustration and the lateral stress of the lipid.

The phase behavior of these novel lipids with identical head group and different alkyl chains has been investigated with utmost care. Small angle X-ray scattering (SAXS) measurements at different hydration level and at different temperatures have been used to study the thermal behavior of these lipid and the effect of this novel motif on the lipidic packing, with particular attention to low temperature effects.

Since cyclopropanated lipids are present in several dairy products, and since lipidic nanoparticles have been proved to be excellent drug delivery systems, digestion studies of cubosomes and hexosomes formed by the novel synthesized cyclopropanated lipids have been performed. Time resolved synchrotron SAXS has been used to monitor the phase changes during the enzymatic reaction.

In order to test the utility of the cyclopropanated lipidic systems for membrane protein crystallization the novel lipidic cubic phase (LCP) matrices have been employed in crystallization studies with the membrane protein model system bacteriorhodopsin (bR).

Finally, the successful crystallization attempts for membrane protein structural studies of the chloride channels EcClC and Rm1ClC, as well as the lipopolysaccharide transporter LptD-LptE show the broad applicability of the LCP crystallization method and the utility of tuning crystallization conditions, including a screening of different lipids, to optimize crystal growt.

Zusammenfassung

Das übergeordnetes Ziel dieses interdisziplinären Projektes, ist die Rolle der Rigidität der Lipidkette auf die Phasenübergängen der lipidischen Mesophasen zu untersuchen. Frühere Studien haben gezeigt, dass die Position und die Anzahl der *cis*-Doppelbindungen in Monoacylglycerolen deren Spreizung wesentlich beeinflussen und zudem wirken sich diese Parameter auf das Phasenverhalten aus. Ausgehend von diesen Erkenntnissen wurden neue, von den natürlich vorkommenden cyclopropylierten Lipiden inspirierte Moleküle synthetisiert und deren Phasenverhalten untersucht. Die Rigidität der Lipidkette wurde systematisch variiert, indem *cis*-Doppelbindungen in verschiedenen Molekülen durch Cyclopropylgruppen ersetzt wurden und die Position und Anzahl der Cyclopropylringe in der Alkylkette verändert wurde. Diese Substitution wurde gewählt, weil dabei eine ähnliche Geometrie eingenommen und der CPP (Kritischer Packungsparameter) Parameter nicht signifikant verändert wird. Das damit zusätzlich eingefügte Kohlenstoffatom in die Lipidkette verändert die Länge beziehungsweise die Krümmung der Kette in geringem Ausmass, hat jedoch einen Einfluss auf die Packungsfrustration und den lateralen Stress des Lipids.

Das Phasenverhalten dieser neuartigen Lipide mit identischen Kopfgruppen und unterschiedlichen Alkylketten wurde akribisch untersucht. Kleinwinkel-Röntgenstreuungs-Messungen (SAXS) auf verschieden Hydratisierungsstufen und bei verschiedenen Temperaturen wurden verwendet um das thermale Verhalten von diesen Lipiden zu untersuchen. Zudem wurde der Effekt der Cyclopropylgruppe auf die lipidische Packung, mit Berücksichtigung der Tieftemperatureffekten erforscht.

Da cyclopropylierte Lipide in Milchprodukten vorkommen und lipidische Nanopartikel exzellente Drug Delivery Systeme sind, wurde die Enzymkinetik des Abbaus dieser neuen cyclopropylierten Lipide in Cubosomen und Hexosomen untersucht. Mittels zeitaufgelösten Synchrotron SAXS Messungen wurden die Phasenübergänge während der enzymatischen Reaktion über die Zeit verfolgt.

Um die Anwendung der cyclopropylierten Lipidsysteme in der Proteinkristallisation in neuartigen Lipiden zu testen, wurden kubischen Phasen (LCP) in Kristallisationsstudien mit dem Membranprotein-Modellsystem Bakteriorhodopsin (bR) verwendet. Die erfolgreichen Kristallisationen für die Membranprotein-Struktur-Untersuchung der Chloridkanäle EcClC und Rm1ClC, sowie des Lipopolysaccharid Transporters, beweisen die breite Anwendbarkeit dieser LCP-Kristallisationsmethode.

Zudem wurde die Nützlichkeit der möglichen Feinabstimmung der Kristallisationsbedingungen inklusive des Screenings von verschiedenen Lipiden um das Kristallwachstum zu optimieren, gezeigt.

Table of contents

Chapter 4: Digestion of monoacylglycerols and their cyclopropanated derivatives: molecular structure and nanostructure determine rate of digestion……………………………………….59

Chapter 5: Membrane protein crystallization…………………………………………….71

Chapter 1

Introduction

1.1 Lipidic mesophases

Lyotropic liquid crystals are viscous materials that have intermediate characteristics between liquid and solid crystalline materials. They are formed by the spontaneous assembly of amphiphilic molecules in presence of a solvent. In these mesophases, the molecules are 'liquid-like' as they are mobile, but can only diffuse within an ordered geometry characteristic of crystalline solid. The dual molecular nature of amphiphiles, composed of a hydrophobic tail and a hydrophilic head group, governs the assembly process of these molecules in polar solvents such as water, resulting in formation of various materials with several geometries and different physical characteristics. Generally, lipids have the ability to form supramolecular structures in aqueous systems, assembling in different phases according to pressure, temperature, molecular shape and composition. This phenomenon is known as lipid polymorphism (*1*). Typical lipidic liquid crystalline phases are lamellar ($L\alpha$), micellar (L), hexagonal (H) and cubic (Q). The $L\alpha$ phase consists of stacked planar lipidic bilayers separated by water. In micelles, lipid molecules are arranged in a spherical geometry that encompasses water.

Of particular interest to this work are the 3D and 2D mesophases which will be discussed in more detail in section 1.4 and 1.5. Briefly, cubic phases comprise of a single curved lipidic bilayer arranged spacially in an infinite periodic minimal surface that delineates two identical, but not interconnected aqueous channels (*2*). The type of surface symmetry can vary, resulting in the formation of different cubic phases, namely with gyroid (*Ia3d*), double diamond (*Pn3m*), or primitive symmetry (*Im3m*). In the 2D hexagonal phase, the lipidic molecules aggregate in cylinders that are packed in a hexagonal lattice. These curved systems can be divided into two main groups: oil-in-water or normal phases, in which the lipidic tails aggregate due to hydrophobic effect so as to avoid contact with water, while the polar head groups protrude to the external part of the aggregate and are in contact with water (H_I, L_1); and water-in-oil or inverse structures in which the water is confined in pores constituted by the polar head groups, while the lipidic tails point out of the aggregate (H_{II}, L_2) (**Figure 1**).

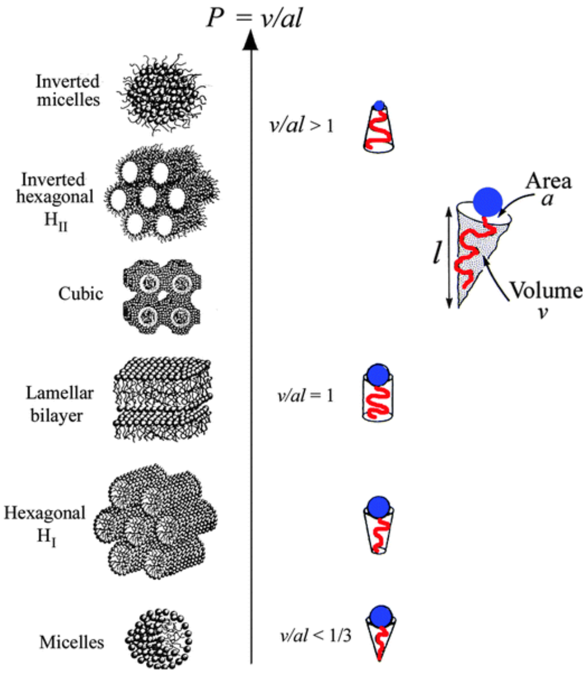

Figure 1. Schematic illustration of lipid polymorphism in water. The phase sequence is expressed in accordance with the critical packing parameter, CPP = *v/al*, where *v* is the volume of the lipidic chain, *a* is the cross-sectional area of the head group, and *l* is the length of the molecule. Reproduced with permission from (*3*)

In this context, *cis*-monoacylglycerols are a class of lipids known for their unique lyotropic liquid crystalline polymorphism, and for their ability to undergo phase transition to non-lamellar phases. They have been intensely studied due to their ability to form lipidic bicontinuous cubic phases (LCPs) in particular (*4*), the latter being used in numerous biomedical applications.

This distinct family of lipids is naturally synthesized by the enzymatic hydrolysis of the more abundant triglycerides, thereby yielding amphiphiles that consist of one molecule of glycerol connected to a *cis* unsaturated fatty acid via an ester bond (**Figure 2**).

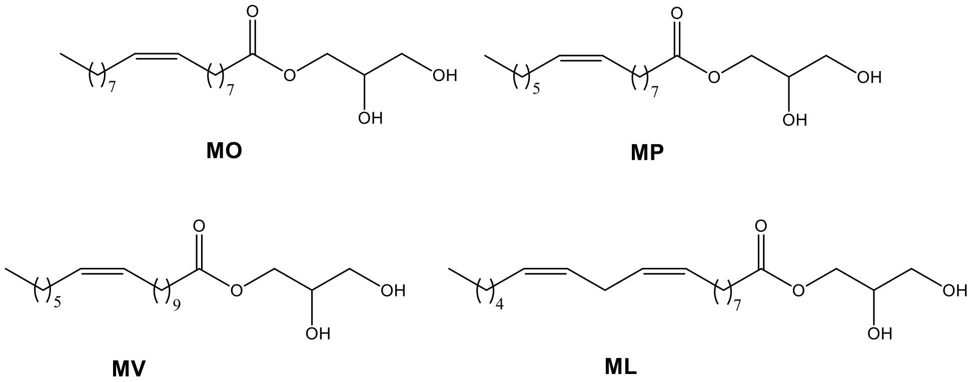

Figure 2. Four *cis*-monoacylglycerols of interest in this study. They exhibit different hydrophobic chain lengths, different number of *cis* double bonds and different position of the unstauration: monoolein (MO), monopalmitolein (MP), monovaccein (MV), and monolinolein (ML).

The physicochemical properties of the hydrophilic and hydrophobic moieties of amphiphiles determine their phase behavior upon hydration. Specifically, the capability of the head group to form H-bonds, the size and hydrophilicity of the lipid, together with the presence of an isoprenoid or unsaturated hydrocarbon chain are considered fundamental factors to allow a diversified polymorphism and for the formation of LCPs. Variation of the head group of these lipids, through the introduction of different moieties such as sugars or pentaerythritol in order to preserve the ability to form strong H-bonds, have been attempted and have led to the synthesis of novel synthetic lipids with alternative chemical properties but similar phase behavior (*5-8*). While the possibility of altering the head group, albeit with certain limitations and problems, has been explored in the past, the presence of a *cis* double bond or an isoprenoid structure in the lipidic chain seems to be a necessity for the formation of the different cubic phases (*9*). The branched chain of the isoprenoid moiety, or the presence of one or more *cis* double bonds, provide in most cases the correct curvature and rotational and translational motions in order to obtain inverse structures in general, and LCPs in particular (*10*).

1.2 Lipid molecular shape and properties of the ensuing mesophase

In order to be able to control and tune the phase behavior in general, and the phase transitions in particular, as well as the fundamental characteristics of each geometrical phase, chemical and physical aspects of the lipidic building blocks have to be taken into consideration.
The driving force for formation of the aggregates is the hydrophobic effect: In order to avoid water-oil interactions, surfactants associate forcing the lipidic chains to aggregate so as to exclude contact with water (*11*). In order to minimize the dissolution energy of the system, the hydrophobic effect avoids decreasing of entropy connected with the solvation of lipidic moieties by water. The bilayer formation and its conformation is the result of the sum of various complex attractive and repulsive interactions. For the inverse curved bilayer, like those found in LCPs, these interactions are even more complicated because the tendency of the surface to attain its curvature is controlled by the repulsive lateral pressure in the chain region, the interfacial pressure and the lateral stress around the head group (H-H bond, steric and hydrational interactions) (*12*).

One of the first parameters developed to explain such lipid behavior is the tendency of a monolayer to bend into a particular curvature as a function of the molecular shape of the lipidic building block. The critical packing parameter (CPP, **Equation 1**) correlates the ratio between the splay of the hydrocarbon chain (volume and length) and the effective head group area, with the capacity of lipids to form inverse structures (**Figure 1**) (*13*).

$$CPP = v/al \qquad (1)$$

Where v is the volume of the incompressible hydrocarbon chain, a is the cross-sectional area of the head group, and l is the maximum length that the chain can assume. This model, which is useful as an indication for amphiphilic self assembly, does not explain the existence of intermediate bicontinuous cubic phases (*9*).

The free energy of the system is an extremely important factor in the formation of inverse phases. It is determined by the competition between the tendency of the membrane to achive a curvature and the packing frustration of the hydrocarbon chains (**Equation 2**) (*14, 15*).

$$g_{tot} = g_c + g_p \qquad (2)$$

In this model, the free energy of the system (g_{tot}) is expressed as the sum of two contributions: g_c = the free energy associated with the curvature of the system, which can be calculated for each lipid in each geometry starting from **Equation 1** and g_p = free energy associated with the packing frustration.

For a curved geometry, the packing frustration is generated by the necessity of the lipidic chains to assume different lengths to fill up the available space. For the molecular shape and the splay of the lipidic chain to force the system to become curved, the free energy of the system would be minimized when the mean curvature of the bilayer is constant and the lipidic length is identical for each molecule. Fulfilling these two requirements is not possible for curved systems, and therefore the free energy of curved phases is always frustrated. As a result, in order to relieve the frustration, a change in global curvature or a phase transition will occur in response to lateral stresses imposed on the surfactant monolayer when environmental parameters (e.g. temperature, pressure, solvation, and additives) change. This balance of forces makes these systems able to switch phases and change curvature under the influences of external parameters.

Despite the availability of these models, due to the complexity and the number of interactions and energies involved in the formation of each packing geometry, rules that can precisely predict *a priori* the phase behavior and transition temperatures and concentrations of various lipids based on their molecular structure alone are not available. For this reason, engineering of novel lipidic molecules that demonstrate lipid polymorphism, thus enabling the possibility of switching phases in a controlled manner is still a formidable challenge. Molecular design of lipidic building blocks that control the phase behavior of the ensuing matrix is a long-term goal that can only be achieved by starting from phase behavior studies on common lipids or on novel lipids with small, systematic mutations.

1.3 Phase behavior of the monoolein-water system

Within the *cis*-monoacylglycerol family, the best characterized and most utilized lipid is monoolein (MO). MO is especially popular for its ability to form stable LCPs at room temperature and in an excess of water. MO was one of the first lipids discovered that form bicontinuous cubic phases upon hydration and is one of the most used lipids in drug delivery and membrane protein crystallization studies.

MO is comprised of a single oleoyl chain linked to a glycerol head group by an ester bond (**Figure 2**). The phase behavior of hydrated MO and the structure and properties of various phases formed have been well established (**Figure 3**) (*16*).

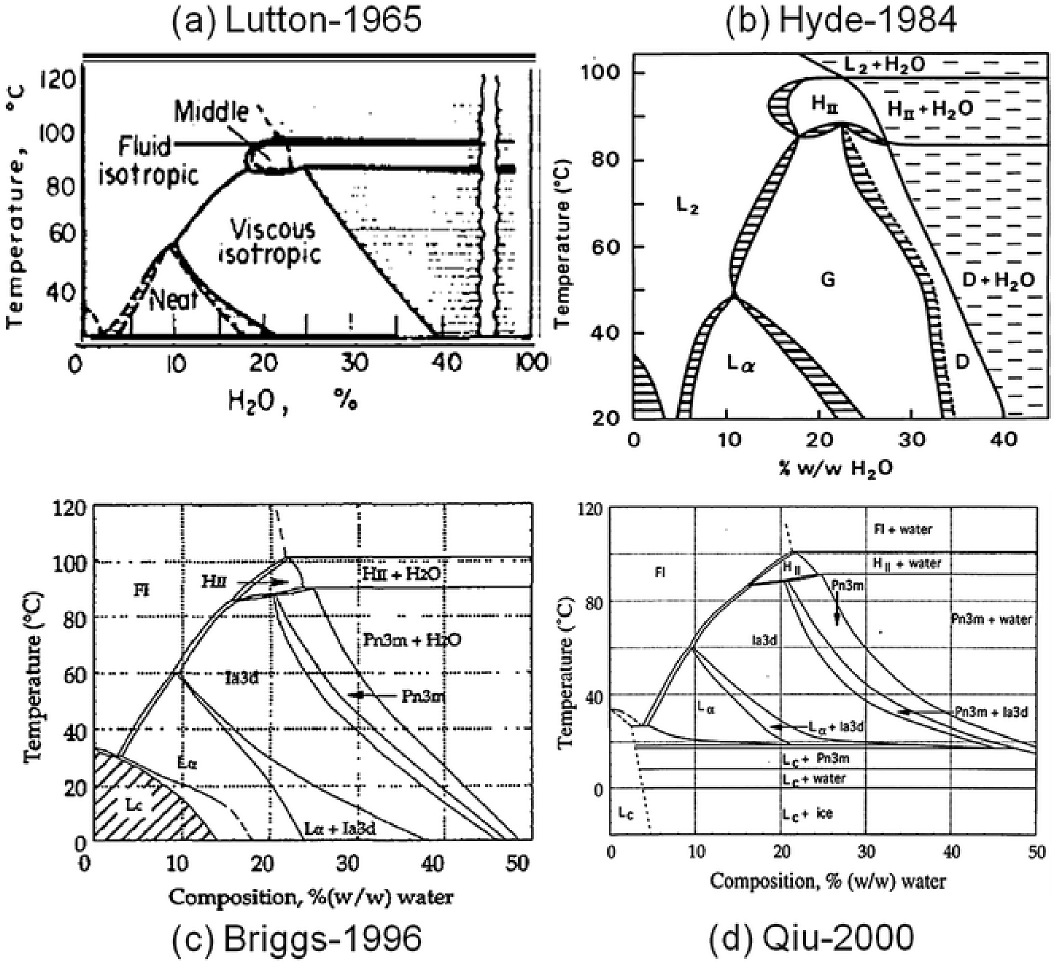

Figure 3. Comparison of monoolein-water phase diagrams studied from 1965 to 2000. a) The viscous isotropic phase described by Lutton in 1965 (*17*) corresponds to the isotropic cubic phase characterized

by Luzzati in 1968 (*4*). b) Hyde determined the geometry of the low hydration cubic phase, reporting in 1984 a transition between a gyroid (*Ia3d*) and diamond (*Pn3m*) cubic phase (*18*). c) Briggs extended the phase studies to low temperature in 1996 (*19*). d) Supercooling effect with a low temperature thermodynamic instability of LCPs was reported by Qui in 2000 (*20*). Reproduced with permission from (*16*).

MO polymorphism has been reported in several phase diagram studies reported in **Figure 3**, in which hydration and temperature were varied in a systematic way and phase transitions were determined by small angle x-ray scattering (SAXS), light microscopy or differential scanning calorimetry (DSC) (*17-20*). Upon hydration at ambient temperatures, MO shows transition from a lamellar crystalline phase (*Lc*), in which lipidic molecules are organized in a solid crystalline bilayer to L_α, a liquid crystalline phase in which the planar bilayer has higher mobility and the molecules can diffuse laterally. By increasing the temperature of the systems at low hydration, the first transition is to the isotropic fluid (*FI*), composed of inverse micelles of surfactant and water (L_2). At higher water contents, the lamellar geometry undergoes a reorganization, forming three dimensional bicontinuous cubic phase initially with *Ia3d,* and subsequently with *Pn3m* geometry, the latter being stable in excess of water. By increasing the temperature of systems with a water content higher than 15% to 85°C, the cubic geometry collapses into a highly curved inverse hexagonal phase. The resulting H_{II} phase is stable in excess of water at temperatures up to 100°C. The ability to switch phases by increasing hydration and, most importantly, temperature, makes these mesophases appealing for several applications in which order-to-order transitions can be induced to change properties of the material (diffusion coefficient, interface availability etc.).

1.4 Lipidic cubic phases

Bicontinuous cubic phases are thermodynamically stable lipidic mesophases that can form in various defined space group geometries: the double gyroid (*Ia3d*) cubic phase with three-fold water channels, the double diamond (*Pn3m*) one with four-fold water channels, and the primitive (*Im3m*) cubic phase with six-fold water channels (*2, 18*). These geometries are depicted **in Figure 4**. These 3D architectures exhibit different symmetries, but they share the following features: they are constituted by a curved lipid bilayer that forms an infinite periodic minimal surface with zero mean curvature, which is surrounded by two identical, but non-intersecting aqueous channels. Moreover, in the fully hydrated systems i.e. *Pn3m* and *Im3m,* lipid and water molecules can diffuse within their respective molecular compartments, and water can diffuse between the channels and an excess reservoir (*21*). A discontinuous cubic structure, which consists of reverse micelles packed in cubic crystalline domains (*Fd3m*) has also been intensely studied (*8*).

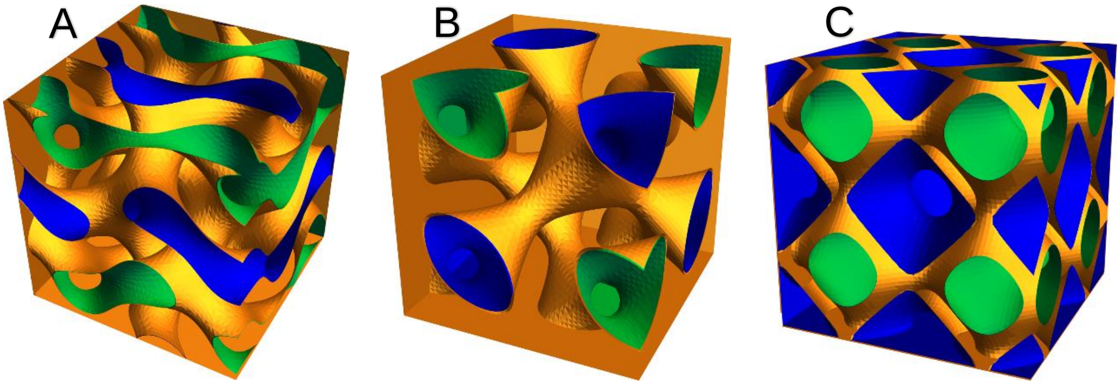

Figure 4. Representation of the topology of the three bicontinuous cubic phases with particular attention to the aqueous channel geometry. The water channels are depicted in blue and green, while the lipidic bilayer is colored in gold-yellow. A) *Ia3d* double gyroid cubic phase, B) *Pn3m* double diamond cubic phase, and C) *Im3m* primitive cubic phase.

Geometrical considerations can be used in order to calculate the aqueous channel radius. For the inverse bicontinuous cubic phases, the water-lipid interface is assumed to be parallel to the underlying minimal surface (TPMS) (*22*). By knowing from SAXS measurements the geometry and the lattice parameter a, and knowing the lipid volume fraction of the sample ϕ, the length of the lipid tail, *l*, can be calculated by solving the following cubic equation (*23*):

$$\Phi = 2A_0\left(\frac{L_{lip}}{a}\right) + \frac{4}{3}\pi\chi\left(\frac{L_{lip}}{a}\right)^3 \qquad (3)$$

where A_0 is the area of the surface in the unit cell in which the lattice parameter is equal to unity, and χ is the Euler-Poincare characteristic. Depending on the specific cubic phase they have the following values: $A_0 = 3.091$ and $\chi = -8$ for *Ia3d;* $A_0 = 1.919$ and $\chi = -2$ for *Pn3m;* and $A_0 = 2.345$ and $\chi = -4$ for *Im3m*. For the radius of the aqueous channels, *r* the following equations are valid for the *Ia3d*, *Pn3m* and *Im3m* phases, respectively (*19*):

$$r = 0.248a - L_{lip} \qquad (4a)$$

$$r = 0.391a - L_{lip} \qquad (4b)$$

$$r = 0.3055a - L_{lip} \qquad (4c)$$

1.5 Hexagonal phase

In the hexagonal symmetry, lipidic monolayers form cylinders that are organized in a hexagonal packing arrangement. Monoacylglycerols usually present an inverse hexagonal phase, with the water confined into cylinders formed by the polar headgroups of lipids, while the hydrophobic tails protrude into the external interface of the aggregates (*24*). For hydrated monoacylglycerols the H_{II} phase appears at high temperatures (70-100 °C), as is the case for MO (*20*). These systems are highly curved and the lipidic chains are densely packed and stressed. To overcome the free energy related to the lipidic chain stress, the curvature required from the lipid molecular shape needs to be optimized. For these systems, the lipidic wedge shape increases at high temperature when H-bonds between the lipid's polar head groups and water molecules are broken. This loss of hydration sphere results in decrease of the head group cross sectional area.

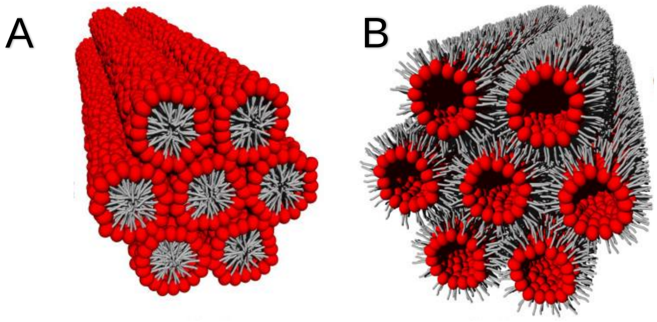

Figure 5. Schematic representation of A) normal, and B) inverse hexagonal phases formed from aggregation of lipid molecules in the presence of water. Polar head groups are shown in red, apolar chains are shown in grey. The highly curved lipidic monolayers constitute cylinders that are organized in a hexagonal packing arrangement. In the normal phase, the water is confined to the external interface of the cylindrical aggregates, while in the inverse phase the cylinders constitute the aqueous channels. Reproduced with permission from (*25*).

Calculation of the aqueous channel radius of the H_{II} phase must take into account both the cylindrical geometry and the packing frustration of the hydrophobic chains in the interstitial spaces. Therefore starting from the lattice parameter a, and the lipid volume fraction ϕ, the radius r, of the H_{II} phase can be calculated using the following equation (*26*):

$$r = a(1-\phi)^{1/2}\left(\frac{\sqrt{3}}{2\pi}\right)^{1/2} \qquad (5)$$

1.6 Properties and applications of lipidic mesophases

The amphiphilic nature of the mesophases renders these materials ideal to encapsulate molecules with different polarities, sizes and chemical characteristics (*27*). In the case of the two phases of interest, *Pn3m* and H_{II}, the characteristic thermodynamic stability in excess of water opens up a plethora of applications, most importantly in the fields of drug delivery and membrane protein crystallization. The presence of aqueous nanopores with a regular structure and repetition enables the possibility to confine water-soluble drugs or small hydrophilic proteins in a controlled manner (*28*, *29*). Most significantly, the high porosity of the system maximizes the interface between water and the lipidic layer, making these materials interesting for interfacial studies (*30*).

1.6.1 Bulk mesophases and lipidic dispersions as drug delivery systems

The amphiphilic properties, biocompatibility and high surface area of these lipidic mesophases render them ideal for application in drug delivery. The release of hydrophilic drugs incorporated into the mesophases has been shown to be a diffusive process regulated by the size of the aqueous channels and the symmetry of the mesophase: in particular, the order for release rate is 3D *LCP* >> 2D *Lα*>> 1D H_{II} (*31, 32*). Additionally, the mesophases and actives can be tailored to suit each other in order to optimize the incorporation and release of selected drugs (*33, 34*). *In vivo* studies, have demonstrated the low toxicity of cubic phases, which maintain their mesophase nanostructure and controlled release characteristics when subcutaneously injected (*35*) or orally dosed (*36*).

A recent development in this field is the design of stimuli responsive drug delivery systems, which takes advantage of the ability to dynamically switch between the different lipidic nanostructures. These smart nanomaterials can be loaded with soluble drugs and an 'on-demand' release can be triggered by light, pH or temperature with the aim to significantly reduce or eliminate side effects (*37-40*).

The ability of LCPs and the H_{II} phase to coexist with an excess of water enables the formation of dispersed nanostructured particles in the presence of a stabilizer - cubosomes and hexosomes - with the same complex internal structures as those of the gel materials (*41*). Thus important properties such as biodegradability, amphiphilicity, geometry and lattice parameters of the bulk lipidic phases are correspondingly preserved in the dispersions (*42*). Additionally, the issues associated with the size and complexity of the system, as well as difficulties in handling the viscous, sticky bulk mesophases can be avoided by using these dispersed nanostructured particles.

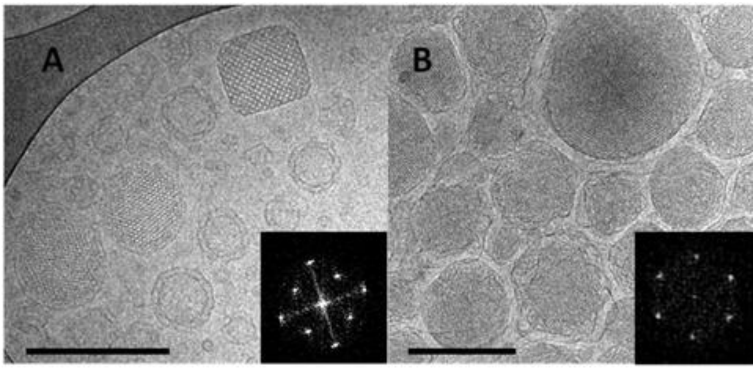

Figure 6. Cryo-TEM images of A) cubosomes and B) hexosomes. The internal structure organization is shown by Fast Fourier Transform (FFT) analysis. Reproduced from (*43*).

Cubosomes have been largely studied as drug delivery systems for small hydrophilic molecules. However, these systems are problematic as they exhibit burst release upon dilution (*44*). In order to overcome this phenomenon, stimuli responsive lipidic particles have been developed (*37, 38*). The ideal system would be a drug delivery dispersed mesophase that can switch from a slow releasing geometry such as liposomes or hexosomes to a fast one like cubosomes, by dynamically changing environmental factors such as the pH (*45*), and through the application of external stimuli such as light activation (*46*), or during enzymatic hydrolysis (*47*). These methods of dynamically altering phase behavior have have been conceived as the optimal trigger mechanism for the dynamic, controlled release of encapsulated drugs (*48*).

1.6.2 Membrane protein crystallization

Membrane proteins play a central role in all physiological processes in cellular systems, regulating vital functions such as transport, signal transduction and energy conversion. Knowledge of the structures of these proteins is an obligatory step towards understanding their function, dynamics and assembly. Moreover, membrane proteins are essential for the correct function of cells, and their malfunction causes several diseases such as Alzheimer's, Parkinson's, diabetes, cancer, heart failures and various other dysfunctions. It is not surprising, therefore, that membrane proteins constitute around 60% of the targets of approved drugs and the elucidation of their three-dimensional structure is fundamental for drug design (*49*). The difficulties in studying membrane proteins are mainly due to their large hydrophobic surfaces, flexibility and lack of stability once they are removed from their native membrane environment (*50*). These problems make it extremely challenging to handle membrane proteins, with difficulties related to their expression, purification, stabilization and crystallization. In particular, structural analysis by X-ray crystallography requires well diffracting crystals that are obtained by a slow and organized nucleation and crystal growth. In order to solubilize membrane proteins and avoid a fast precipitation they are purified in detergent solutions in which micelles act as a "membrane like" hydrophobic environment.

The use of LCPs as an alternative bilayer matrix for membrane protein crystallization was introduced in 1996 (*51*) and since then, bulk LCPs have been shown to be an ideal matrix for the entrapment and crystallization of membrane proteins (*51-53*). The presence of a bilayer (LCP) or a "bilayer-like" (H_{II}) lipidic environment provides matrices which act as excellent mimics of cellular membranes and give the possibility to embed, reconstitute and crystallize membrane proteins, and to incorporate other hydrophobic molecules (*27, 51, 54*). Their capacity to mimic the cell membrane in their characteristic lipophilicity, curvature, thickness and lateral pressure makes these materials the perfect candidate for membrane protein studies.

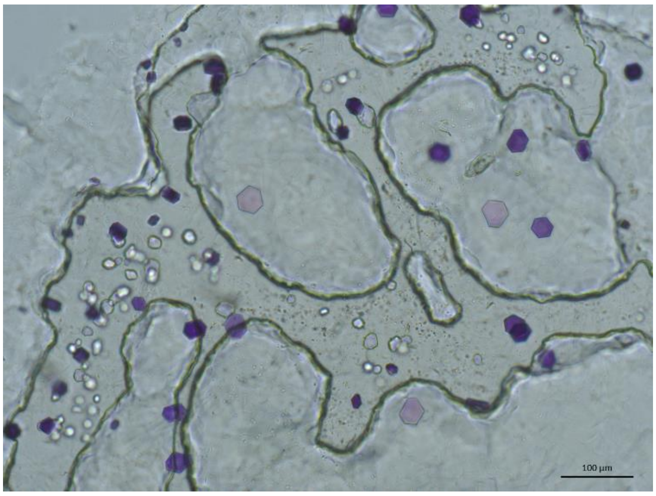

Figure 7. Purple hexagonal bacteriorhodopsin (bR) crystals grown in LCPs.

Thus introduction of LCPs as tools into molecular membrane biology has revolutionized the field, enabling the crystallization of membrane proteins previously unseen (*53*). Over the last two decades, the capacity to produce well diffracting crystals from LCPs has resulted in an exponential increase of unique structures of membrane proteins (*53*). The families of membrane proteins that have been crystalized in this way range from microbial rhodopsins (**Figure 7**) to outer membrane proteins and transporters (*53*). Most importantly, LCP crystallization has led to the elucidation of high-resolution structures of numerous G protein-coupled receptors (GPCRs), (*52*, *55-57*) essential for the understanding of cellular signal transduction pathways. Recent developments of LCP injectors for serial femtosecond crystallography at X-ray free electron lasers (XFELs) has made it possible to determine high resolution membrane protein structures of microcrystals grown in LCPs, overcoming one of the few disadvantages of LCP crystallization: while LCP crystals are usually very well ordered, they are generally smaller than protein crystals obtained using vapor diffusion techniques (*58-60*). Advances in the field have resulted in impressive progress in a very short period of time. The last successful project that would have been the dream of any membrane biologist only two decades ago is the recording of a three-dimensional atomic movie of the light induced structural changes in the proton pump bacteriorhodopsin embedded in LCP using XFEL serial femtosecond crystallography (*61*).

In addition to crystallization, the functional solubilization and reconstitution of membrane proteins has also been achieved, demonstrating the capacity of both cubic and hexagonal matrices to host active membrane proteins (**Figure 8**) (*54, 62-64*).

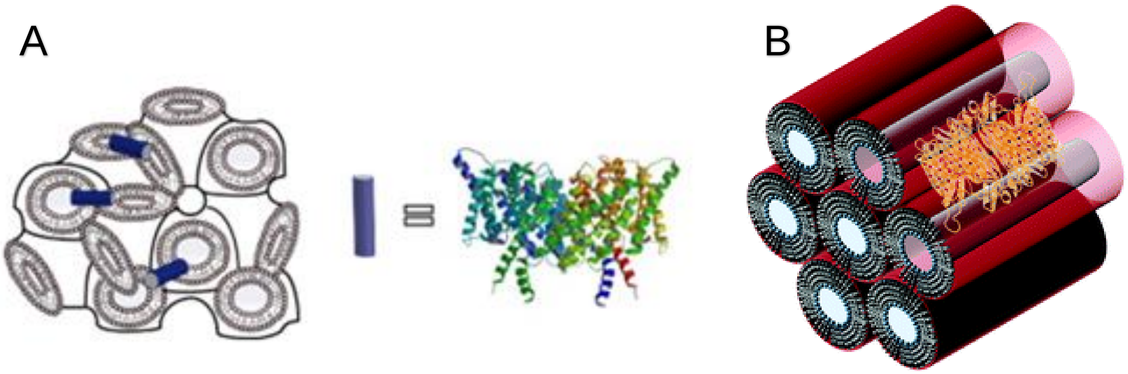

Figure 8. Schematic representation of the functional reconstitution of A) chloride channel ec-1 (EcClC) in *Pn3m* cubic phase; B) outer membrane protein F (ompF) in H_{II} phase. Figures reproduced with permission from (*54, 64*).

As can be seen, these multicompartmentalized nanomaterials can be utilized in important biomedical applications. Understanding the fundamental forces that govern the self-assembly of the lipid molecules into the different geometries is essential to design these systems for their specific applications. In order to achieve this, amphiphiles that can form lipidic mesophases need to be understood on a fundamental level in order to control and manipulate transitions between the different mesophases.

1.7 Aim of the thesis

Development of alternative lipids that can form lipidic mesophases with interesting properties is called for, given the the increasing number and scope of applications of these systems in drug delivery, as bio-compatible sensors and for membrane protein studies. The design of novel molecules that show complex polymorphism is hard to achieve, and thus systematic studies to explore the effect of small structural changes of the lipidic building blocks on the lipidic phase behavior are essential to understand the rules that govern phase formation. Starting from the consideration that replacing *cis* double bonds by cyclopropanated systems retains most of the chemical and geometrical properties, we hypothesized that cyclopropanated lipids will maintain the complex phase behavior of the parent monoacylglycerides, and that the resulting new materials can be usefully utilized for several applications.

Thus the aims of this project are to:

- Design and synthesize novel lipids which are inspired by naturally occuring cyclopropanated lipids;
- Study of the phase behavior of these novel lipids by SAXS measurements at different hydration levels and at different temperatures, with particular attention to low temperature effects;
- Elucidate the role of the lipid tail's rigidity on the phase behavior of lipidic mesophases by comparison of the molecular structure and the phase transition bundaries of the novel lipids with those of commonly used monoacylglycerols;
- Test the utility of the synthesized cyclopropanated lipids as building blocks of drug delivery systems forming lipidic suspensions, and monitor their enzymatic digestion by time resolved synchrotron SAXS.
- Establish the applicability and the advantages of varying lipids for *in cubo* membrane protein crystallization.

References

1. V. Luzzati, A. Tardieu, T. Gulik-Krzywicki, Polymorphism of lipids. *Nature* **217**, 1028-1030 (1968).
2. S. T. Hyde, Bicontinuous structures in lyotropic liquid crystals and crystalline hyperbolic surfaces. *Curr Opin Solid State Mater Sci* **1**, 653-662 (1996).
3. O. G. Mouritsen, Lipidology and lipidomics-quo vadis? A new era for the physical chemistry of lipids. *Physical Chemistry Chemical Physics* **13**, 19195-19205 (2011).
4. V. Luzzati, A. Tardieu, T. Gulik-Krzywicki, E. Rivas, Reisshus.F, Structure of cubic phases of lipid-water systems. *Nature* **220**, 485-488 (1968).
5. M. Hato, J. Yamashita, M. Shiono, Aqueous phase behavior of lipids with isoprenoid type hydrophobic chains. *J Phys Chem B* **113**, 10196-10209 (2009).
6. J. Yamashita, M. Shiono, M. Hato, New lipid family that forms inverted cubic phases in equilibrium with excess water: Molecular structure - aqueous phase structure relationship for lipids with 5,9,13,17-tetramethyloctadecyl and 5,9,13,17-tetramethyloctadecanoyl chains. *J Phys Chem B* **112**, 12286-12296 (2008).
7. V. Vill, R. Hashim, Carbohydrate liquid crystals: Structure-property relationship of thermotropic and lyotropic glycolipids. *Curr Opin Colloid Interface Sci* **7**, 395-409 (2002).
8. J. M. Seddon, N. Zeb, R. H. Templer, R. N. McElhaney, D. A. Mannock, An fd3m lyotropic cubic phase in a binary glycolipid/water system. *Langmuir* **12**, 5250-5253 (1996).
9. C. Fong, T. Le, C. J. Drummond, Lyotropic liquid crystal engineering-ordered nanostructured small molecule amphiphile self-assembly materials by design. *Chem Soc Rev* **41**, 1297-1322 (2012).
10. V. P. Dmitriev, G. R. Ouriques, Cubic phases of amphiphilic molecular aggregates. *Eur Phys J B* **12**, 421-429 (1999).
11. C. Tanford, Hydrophobic effect and organization of living matter. *Science* **200**, 1012-1018 (1978).
12. J. M. Seddon, R. H. Templer, Cubic phases of self-assembled amphiphilic aggregates. *Philos T Roy Soc A* **344**, 377-401 (1993).
13. J. N. Israelachvili, D. J. Mitchell, B. W. Ninham, Theory of self-assembly of hydrocarbon amphiphiles into micelles and bilayers. *J Chem Soc Farad T 2* **72**, 1525-1568 (1976).
14. P. M. Duesing, R. H. Templer, J. M. Seddon, Quantifying packing frustration energy in inverse lyotropic mesophases. *Langmuir* **13**, 351-359 (1997).
15. G. C. Shearman *et al.*, Calculations of and evidence for chain packing stress in inverse lyotropic bicontinuous cubic phases. *Langmuir* **23**, 7276-7285 (2007).
16. C. V. Kulkarni, W. Wachter, G. Iglesias-Salto, S. Engelskirchen, S. Ahualli, Monoolein: A magic lipid? *Physical Chemistry Chemical Physics* **13**, 3004-3021 (2011).
17. E. S. Lutton, Phase behavior of aqueous systems of monoglycerides. *J Am Oil Chem Soc* **42**, 1068-1170 (1965).
18. S. T. Hyde, S. Andersson, B. Ericsson, K. Larsson, A cubic structure consisting of a lipid bilayer forming an infinite periodic minimum surface of the gyroid type in the glycerolmonooleate-water system. *Z. Kristallogr.* **168**, 213-219 (1984).
19. J. Briggs, H. Chung, M. Caffrey, The temperature-composition phase diagram and mesophase structure characterization of the monoolein/water system. *J Phys II* **6**, 723-751 (1996).

20. H. Qiu, M. Caffrey, The phase diagram of the monoolein/water system: Metastability and equilibrium aspects. *Biomaterials* **21**, 223-234 (2000).
21. W. B. Lee, R. Mezzenga, G. H. Fredrickson, Self-consistent field theory for lipid-based liquid crystals: Hydrogen bonding effect. *J Chem Phys* **128**, 074504 (2008).
22. U. S. Schwarz, G. Gompper, Bending frustration of lipid-water mesophases based on cubic minimal surfaces. *Langmuir* **17**, 2084-2096 (2001).
23. D. C. Turner, Z. G. Wang, S. M. Gruner, D. A. Mannock, R. N. Mcelhaney, Structural study of the inverted cubic phases of di-dodecyl alkyl-beta-d- glucopyranosyl-rac-glycerol. *J Phys II* **2**, 2039-2063 (1992).
24. J. M. Seddon, Structure of the inverted hexagonal (hii) phase, and non-lamellar phase-transitions of lipids. *Biochim Biophys Acta* **1031**, 1-69 (1990).
25. G. Tresset, The multiple faces of self-assembled lipidic systems. *PMC Biophys* **2**, 3 (2009).
26. R. Mezzenga *et al.*, Shear rheology of lyotropic liquid crystals: A case study. *Langmuir* **21**, 3322-3333 (2005).
27. M. Komisarski, Y. M. Osornio, J. S. Siegel, E. M. Landau, Tailored host-guest lipidic cubic phases: A protocell model exhibiting nucleic acid recognition. *Chemistry* **19**, 1262-1267 (2013).
28. E. M. Landau, G. Rummel, S. W. CowanJacob, J. P. Rosenbusch, Crystallization of a polar protein and small molecules from the aqueous compartment of lipidic cubic phases. *J Phys Chem B* **101**, 1935-1937 (1997).
29. J. Bender *et al.*, Lipid cubic phases for improved topical drug delivery in photodynamic therapy. *J Control Release* **106**, 350-360 (2005).
30. S. Salentinig, S. Phan, A. Hawley, B. J. Boyd, Self-assembly structure formation during the digestion of human breast milk. *Angew Chem Int Ed* **54**, 1600-1603 (2015).
31. L. M. Antognini, S. Assenza, C. Speziale, R. Mezzenga, Quantifying the transport properties of lipid mesophases by theoretical modelling of diffusion experiments. *J. Chem. Phys.* **145**, 084903 (2016).
32. L. Sagalowicz, R. Mezzenga, M. E. Leser, Investigating reversed liquid crystalline mesophases. *Curr Opin Colloid Interface Sci* **11**, 224-229 (2006).
33. J. Clogston, G. Craciun, D. J. Hart, M. Caffrey, Controlling release from the lipidic cubic phase by selective alkylation. *J Contr Release* **102**, 441-461 (2005).
34. E. Nazaruk *et al.*, Design and assembly of ph-sensitive lipidic cubic phase matrices for drug release. *Langmuir* **30**, 1383-1390 (2014).
35. Y. Sadhale, J. C. Shah, Stabilization of insulin against agitation-induced aggregation by the gmo cubic phase gel. *Int J Pharmaceut* **191**, 51-64 (1999).
36. K. W. Lee, T. H. Nguyen, T. Hanley, B. J. Boyd, Nanostructure of liquid crystalline matrix determines in vitro sustained release and in vivo oral absorption kinetics for hydrophilic model drugs. *Int J Pharm* **365**, 190-199 (2009).
37. N. Rahanyan-Kagi, S. Aleandri, C. Speziale, R. Mezzenga, E. M. Landau, Stimuli-responsive lipidic cubic phase: Triggered release and sequestration of guest molecules. *Chemistry* **21**, 1873-1877 (2015).
38. S. Aleandri, C. Speziale, R. Mezzenga, E. M. Landau, Design of light-triggered lyotropic liquid crystal mesophases and their application as molecular switches in "on demand" release. *Langmuir* **31**, 6981-6987 (2015).
39. R. Negrini, R. Mezzenga, Ph-responsive lyotropic liquid crystals for controlled drug delivery. *Langmuir* **27**, 5296-5303 (2011).
40. W. K. Fong, T. Hanley, B. J. Boyd, Stimuli responsive liquid crystals provide 'on-demand' drug delivery in vitro and in vivo. *J Control Release* **135**, 218-226 (2009).
41. S. Andersson, M. Jacob, S. Lidin, K. Larsson, Structure of the cubosome – a closed lipid bilayer aggregate. *Z Kristallogr - Cryst Mater* **210**, 315 (1995).

42. W. K. Fong, R. Negrini, J. J. Vallooran, R. Mezzenga, B. J. Boyd, Responsive self-assembled nanostructured lipid systems for drug delivery and diagnostics. *J Colloid Interface Sci* **484**, 320-339 (2016).
43. S. Helvig, I. Azmi, S. Moghimi, A. Yaghmur, Recent advances in cryo-tem imaging of soft lipid nanoparticles. *AIMS Biophysics* **2**, 116-130 (2015).
44. B. J. Boyd, Characterisation of drug release from cubosomes using the pressure ultrafiltration method. *Int J Pharmaceut* **260**, 239-247 (2003).
45. S. Salentinig, L. Sagalowicz, O. Glatter, Self-assembled structures and pka value of oleic acid in systems of biological relevance. *Langmuir* **26**, 11670-11679 (2010).
46. J. D. Du *et al.*, Phospholipid-based self-assembled mesophase systems for light-activated drug delivery. *Phys Chem Chem Phys* **17**, 14021-14027 (2015).
47. W. K. Fong *et al.*, Generation of geometrically ordered lipid-based liquid-crystalline nanoparticles using biologically relevant enzymatic processing. *Langmuir* **30**, 5373-5377 (2014).
48. M. Kang, G. Huang, C. Leal, Role of lipid polymorphism in acoustically sensitive liposomes. *Soft Matter* **10**, 8846-8854 (2014).
49. H. Yin, A. D. Flynn, Drugging membrane protein interactions. *Annu Rev Biomed Eng* **18**, 51-76 (2016).
50. C. G. Tate, Practical considerations of membrane protein instability during purification and crystallisation. *Heterologous Expression of Membrane Proteins: Methods and Protocols* **601**, 187-203 (2010).
51. E. M. Landau, J. P. Rosenbusch, Lipidic cubic phases: A novel concept for the crystallization of membrane proteins. *Proc Natl Acad Sci USA* **93**, 14532-14535 (1996).
52. D. M. Rosenbaum *et al.*, Gpcr engineering yields high-resolution structural insights into beta(2)-adrenergic receptor function. *Science* **318**, 1266-1273 (2007).
53. V. Cherezov, Lipidic cubic phase technologies for membrane protein structural studies. *Curr Opin Struct Biol* **21**, 559-566 (2011).
54. C. Speziale, L. Salvati Manni, C. Manatschal, E. M. Landau, R. Mezzenga, A macroscopic h+ and cl- ions pump via reconstitution of ecclc membrane proteins in lipidic cubic mesophases. *Proc Natl Acad Sci USA* **113**, 7491-7496 (2016).
55. V. P. Jaakola *et al.*, The 2.6 angstrom crystal structure of a human a2a adenosine receptor bound to an antagonist. *Science* **322**, 1211-1217 (2008).
56. W. Liu *et al.*, Structural basis for allosteric regulation of gpcrs by sodium ions. *Science* **337**, 232-236 (2012).
57. V. Cherezov *et al.*, High-resolution crystal structure of an engineered human beta2-adrenergic g protein-coupled receptor. *Science* **318**, 1258-1265 (2007).
58. U. Weierstall *et al.*, Lipidic cubic phase injector facilitates membrane protein serial femtosecond crystallography. *Nat Commun* **5**, 3309 (2014).
59. W. Liu *et al.*, Serial femtosecond crystallography of g protein-coupled receptors. *Science* **342**, 1521-1524 (2013).
60. L. C. Johansson *et al.*, Lipidic phase membrane protein serial femtosecond crystallography. *Nature Methods* **9**, 263-265 (2012).
61. E. Nango *et al.*, A three-dimensional movie of structural changes in bacteriorhodopsin. *Science* **354**, 1552-1557 (2016).
62. A. Zabara, R. Negrini, O. Onaca-Fischer, R. Mezzenga, Perforated bicontinuous cubic phases with ph-responsive topological channel interconnectivity. *Small* **9**, 3602-3609 (2013).
63. A. Hochkoeppler *et al.*, Photochemistry of a photosynthetic reaction center immobilized in lipidic cubic phases. *Biotechnol Bioeng* **46**, 93-98 (1995).
64. A. Zabara, R. Negrini, P. Baumann, O. Onaca-Fischer, R. Mezzenga, Reconstitution of ompf membrane protein on bended lipid bilayers: Perforated hexagonal mesophases. *Chem Commun* **50**, 2642-2645 (2014).

Chapter 2

Synthesis of novel lipids for lipidic mesophase studies.

Cyclopropanated lipids

Several lipidic systems show a complex phase behavior, known as lipidic polymorphism in presence of water. By varying the level of hydration, they are able to generate aggregates with different curvatures, geometries and physical proprieties (*1*). Due to the liquid crystalline nature of these phases they are known as mesophases: both water and lipid are free to diffuse maintaining a semi-ordered lattice. Within lipidic mesophases, lipidic cubic phases (LCPs) fulfill a special role: LCPs are bicontinuous mesophases in which a curved lipid bilayer is interdigitated with two identical and not connected aqueous channels to form a minimal surface geometry (*2*). LCPs are unique nanostructured matrices that have been lauded for their advantageous characteristics such as biocompatibility, amphiphilicity and their "membrane-like" nature. These features have been utilized in several disciplines of science and technology from membrane biology (*3-7*), drug delivery (*8-10*), food emulsifiers (*11*) to biosensing devices (*12-14*). The most commonly studied amphiphilic lipids which form LCPs are the c*is*-unsaturated monoacylglycerols (MAGs), which are a distinctive class of lipids that can form various lyotropic liquid crystalline phases with different inverse geometries. These phases, and their transitions, can be affected by tuning hydration and temperature (*15*). Most importantly, they are known to form inverse bicontinuous LCPs in excess of water and room temperature.

Despite remarkable recent advances in the field, there are only a few lipids that are known to form LCPs. As discussed in **chapter 1** of this thesis, the conformation of the lipidic bilayer is the result of the sum of a large number of attractive and repulsive intermolecular and mesophase-level interactions. Due to this complexity, it is not trivial to establish a clear relationship between the molecular properties of the lipids and the macroscopic properties of the ensuing mesophases (*16*). The size and nature of the head group, together with the length and curvature of the chain, govern the packing arrangements of the molecules within the lipidic bilayer and therefore the phase transitions of amphiphilic aggregates in general. For the monoacylglycerols in particular, the chain splay (**Figure 1**) was shown to have an essential role in effecting the phase and structural behavior, with an increased stability of negatively curved phases increasing the chain splay (*17*). Thus, it is important to understand the polymorphism of lipidic nanostructures on a molecular level by investigating the driving forces of amphiphilic self-assembly, phase transitions and phase behavior. This can be achieved through the design and synthesis of novel amphiphilic lipids with small variations in the hydrophobic region.

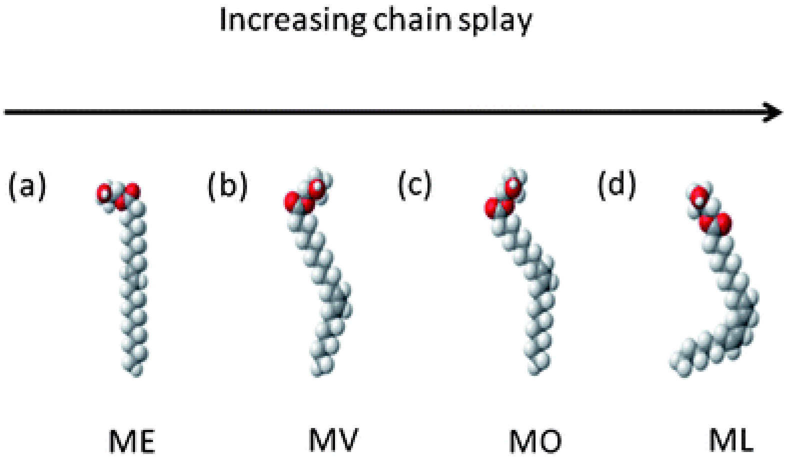

Figure 1. The molecular structure of the most common MAGs in increasing order of chain splay: (a) 1-monoelaidin (ME), (b) monovaccenin (MV), (c) monoolein (MO), (d) monolinolein (ML).

This study has taken inspiration from naturally occurring molecules, namely cyclopropanated phospholipids. These lipids are found with widespread distribution amongst bacteria. In the case of gram negative bacteria, cyclopropanated lipids have been found in both the inner and the outer membrane. This chemical phenomenon is highly conserved amongst various bacteria. Together with the high energetic cost of the cyclopropanation reaction this suggests that these lipids play an important biological role, which is still not completely understood. Significantly, it has been shown that the presence of cyclopropanated phospholipids improves the survival ability of bacterial pathogens like *M. tuberculosis* (*18*), and enhances the resistance of the *E. coli* cell membrane to acid and cold shock (*19*). They also appear to have an important role in regulating membrane fluidity and bilayer thickness (*20*).

In this thesis, the most intensely studied, naturally occurring *cis*-monoacylglycerols have been modified by replacing the olefin with a rigid cyclopropyl moiety, thereby obtaining a small library of novel target lipids that exhibit a subtle variation in the alkyl chain region, where the *cis*-double bonds of traditional MAGs have been replaced with a *cis*-cyclopropane moiety

(**Figure 2**). The cyclopropyl ring has chemical properties similar to a double bond due to its strained conformation and the distortion of its orbitals. Most importantly for our system, the general curvature of the target molecules is similar to that of the *cis*-MAGs due to the similar angle of the two functional groups, albeit the added methylene group protrudes out of the plane of the molecule, creating a kink on the molecular structure and consequently locking the *cis* geometry.

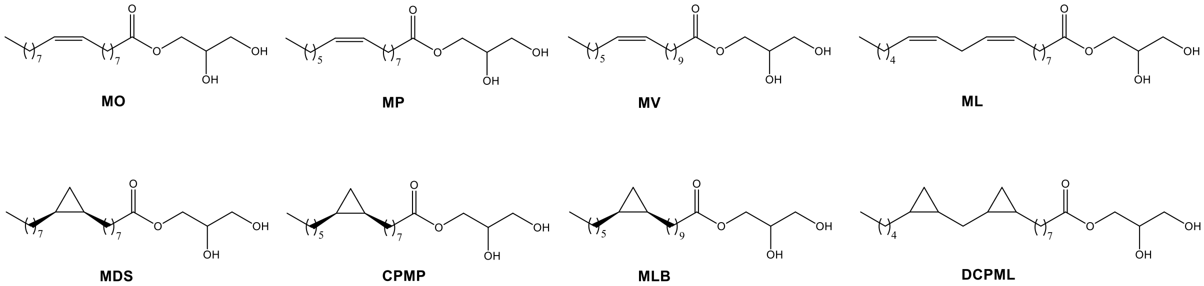

Figure 2. Designed cyclopropaneted analogous of the most common MAGs.

Lipidated ClC inhibitor

Chloride channels (ClC) are a class of membrane proteins essential for transport and diffusion of Cl^- ions across the cell membranes (*21*). This important class of membrane proteins will be described in greater detail in **chapter 5** of this thesis. ClCs are present in all kingdoms of life, and their highly conserved structure make this family interesting from structural and mechanistic point of view (*22-24*). Moreover, in the last 25 years, nine different ClC homologues were discovered in humans and subsequently linked to numerous hereditary diseases. Malfunction of different ClCs is related to myotonia congenita, osteoporosis, Dent's disease and Bartter's syndrome disease (*23*). Even though ClC proteins represent potentially important drug targets, there is a lack of selective, potent inhibitors or activators of these proteins (*25*). Few inhibitors are known to be active on several ClCs, for example, 5-nitro-2-(3-phenylpropylamino) benzoic acid (NPPB), propionic acid (CPP) and the general ClC blocker 4,4′-diisothiocyanostilbene2,2′-disulfonic acid (DIDS), which highlights the need to further investigate the mechanism of action of these membrane proteins in health and disease, and how they can be blocked. The high resolution structure of the medically important complexes between the ClC transporter and any of its inhibitors is unknown, as is the mode of binding and mechanism of inhibition. In order to understand, control and manipulate these vital proteins, a novel inhibitor was designed and synthesized with differing degrees of hydrophobicity, in order to utilize these lipophilic inhibitors, incorporated into LCPs, for the crystallization of the complex with EcClC.

The molecular design of the novel inhibitor is based on the well-established inhibitor, DIDS, which has been shown to be unstable in water (*26*), undergoing hydrolysis to 4,4′-diaminostilbene-2,2′-disulfonic acid (DADS), a molecule which does not have an effect on the activity of ClCs.

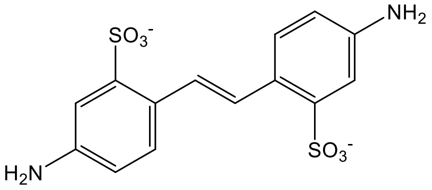

DADS

Figure 3. Chemical structure of diaminostilbene-2,2′-disulfonic acid (DADS).

However, its polymerization products are potent inhibitors, whose affinity to the protein increases with their molecular weight **(Figure 4)**. In a recent study, a novel inhibitor (4,4'-octanamidostilbene-2,2'-disulfonate, OADS) with higher affinity than DIDS was synthesized (*27*).

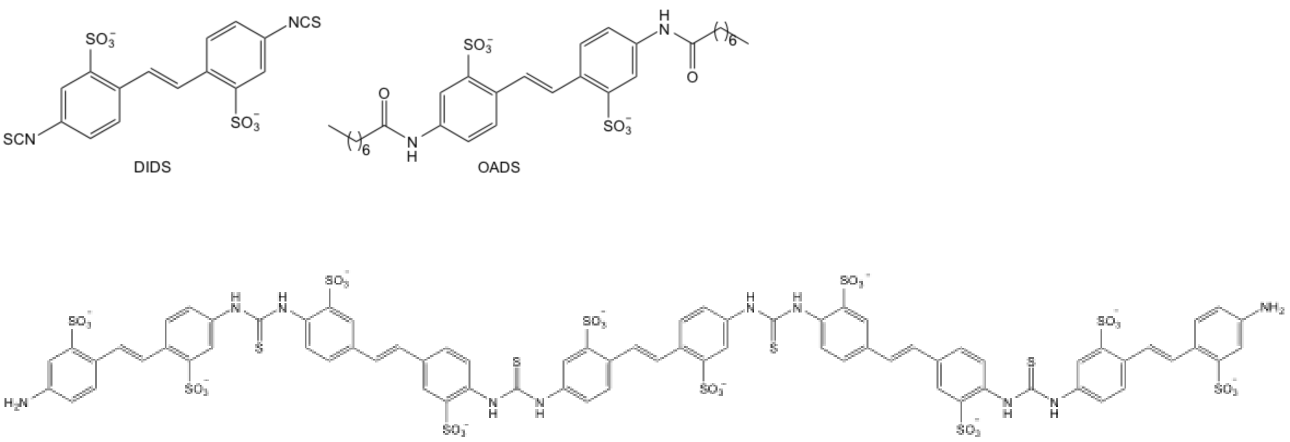

Figure 4. Chemical structures of ClC-ec1 inhibitors: DIDS, OADS, and the pentameric product of the hydrolysis and polymerization of DIDS.

The strategy taken in this study was to increase the molecular weight of DADS by anchoring lipidic tails to it (**Figure 5)**, thereby enhancing the lipophilicity of the molecule and consequently, its probability of partitioning into the bilayer of the mesophase. It was hypothesized that the immobilization of the alkylated inhibitor may have the additional advantage of improving the ability to crystalize the complex protein- inhibitor from the LCPs.

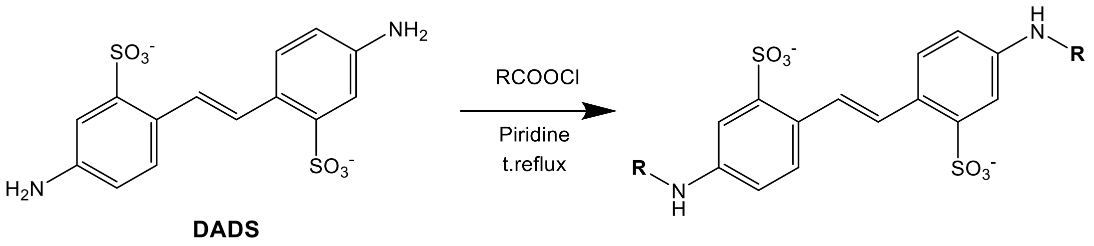

Figure 5. Lipidation of DADS to generate new, potential EcClC inhibitors able to be solubilized and incorporated in the lipidic bilayer of LCPs .

2.1 Results and discussion

2.1.1 Synthesis cyclopropanated lipids

Four different cyclopropanated lipids were designed and synthesized: monodihydrosterculin (MDS) (*28*), cyclopropyl monopalmitolein (CPMP), monolactobacillin (MLB), and dicyclopropyl monolinolein (DCPML) as shown in **Figure 2**. The hypothesis underlying these studies is that the rigidity of the lipidic tail can be modulated by changing the number and the position of the cyclopropyl group and the length of the hydrophobic chains, as shown schematically in **Figure 6.**

Starting from lipids that are known to form lipidic cubic phase, the *cis* double bond was systematically replaced by a geometrically confined cyclopropyl ring. The members of this synthesized family differ in terms of:

- the number of the cyclopropyl groups: one or two (corresponding to monoolein vs monolinolein),
- the position of the cyclopropanation: C_9 or C_{11} (corresponding to monoolein vs monovaccenin),
- and the chain length: C_{18} or C_{16} with a cyclopropyl group in the C_9 position (corresponding to monoolein vs monopalmitolein).

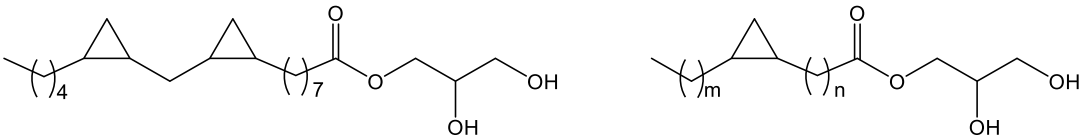

DCPML 4d

m=7 n=7 MDS 4a
m=5 n=7 CPMP 4b
m=5 n=9 MLB 4c

Figure 6. Designed cyclopropanated MAGs that have been synthesized.

Three synthetic routes were attempted for each one of the target lipids in order to optimize the yields for the different products starting from the commercially available corresponding acid **1** (**Figure 7**). Cyclopropanation of olefin **1** was carried out with diethyl zinc and diiodomethane in the presence of 2,4,6-trichlorophenol according to a method previously described in the literature (*29*) to afford the corresponding cyclopropanaated acid **2** in 65-75 % yield.

The acid **2** was subsequently used to obtain the corresponding desired product using three different routes as shown in **Figure 7.**

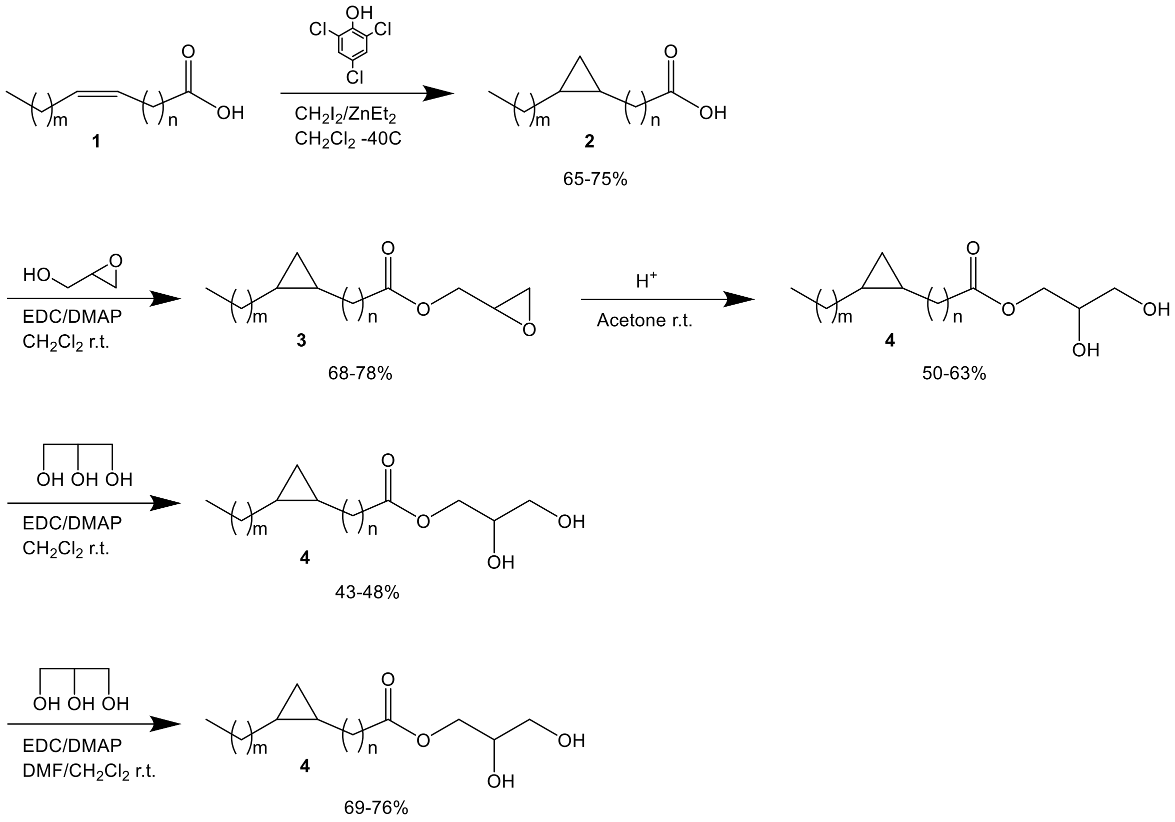

Figure 7. Various strategies employed to optimize the synthesis of cyclopropanated MAGs.

As a first attempt, the acid **2** was reacted with glycerol in the presence of *N*-(3-dimethylaminopropyl)-*N′*-ethylcarbodiimide hydrochloride (EDC) and 4-(dimethylamino)pyridine (DMAP) in dichloromethane to afford the desired ester **3** in 68-78% yield. The latter was then hydrolyzed in a solution of H_2SO_4 in acetone to obtain the desired product **4**.

Following the second approach, the acid **2** was reacted with a large excess of glycerol in the presence of EDC and DMAP in dichloromethane to afford the desired ester **4** in 43-48% yield.

Due the low solubility of glycerol in dichloromethane the second route was modified by changing the solvent to dimethylformamide (DMF), resulting in increase of the yield up to 69-76%.

2.1.2 Synthesis of DADS derivatives

The synthesis of OADS and the oleic derivative of DADS was accomplished in one step starting from commercially available DADS (**Figure 8**). Alkylation of DADS was carried out with octanoyl chloride or oleoyl chloride in dry pyridine according to a method previously described in the literature (*30, 31*), to afford the desired product in 90% yield. In the case of OADS, the product was solubilized in CH_3CN, and the filtrate solubilized again in CH_2Cl_2. In the case of the oleic derivative of DADS, the product was precipitated in CH_3CN, washed in CH_3CN and solubilized in CH_2Cl_2. The products were characterized by ^1H NMR.

Alternative strategies for the alkylation were attempted. Firstly, DADS was reacted with EDC, DMAP and the corresponding acid in Et_2O/CH_2Cl_2, but due the low solubility of DADS no product was formed. In addition, a reaction of DADS with $NaCO_3$ and the corresponding acyl chloride for 24h in a mixture of H_2O and dioxane was also attempted, obtaining a yield lower than 10%.

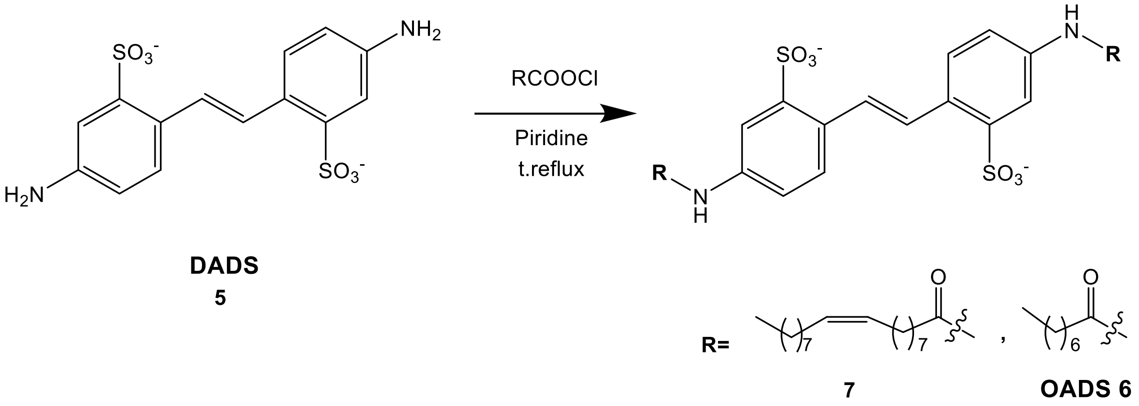

Figure 8. Synthesis of DADS derivatives with octanoyl chloride or oleoyl chloride in dry pyridine, 12 min, T reflux., 90%.

2.2 Materials and methods

Glycerol anhydrous was purchased from Fluka, diethyl zinc was purchased from Acros Organics, EDC was purchased from TCI, and all the other reagents and solvents were purchased from Sigma Aldrich or VWR. All chemicals and solvents were used as received, unless otherwise stated. Reactions were carried out under an inert atmosphere of argon in dry solvents. Dichloromethane was degassed with argon and purified by passage through activated alumina solvent column (MC Brown solvent system) prior to use. Column chromatography was performed using silica gel Merck 60 (particle size 0.040–0.063 mm). Analytical thin-layer chromatography (TLC) was performed using Merck pre-coated silica gel plates 60 F_{254};

visualization by UV absorption and/or by dipping in a solution of $KMnO_4$ (1 g), K_2CO_3 (2 g) in H_2O (100 mL) and subsequent heating. ^{1}H-NMR spectra were recorded on a Bruker AV2-500 (500MHz) spectrometer. Chemical shifts are given in parts per million (ppm) relative to the solvent residual peak: $CDCl_3$ = 7.26 ppm. Coupling constants *J* are expressed in Hz and multiplicities are abbreviated as follows: s (singlet), br (broad), d (doublet), t (triplet), q (quadruplet), quint (quintet), m (multiplet). ^{13}C-NMR chemical shifts are reported relative to the solvent residual peaks: $CDCl_3$ = 77.23 ppm. High-resolution electrospray mass spectra were performed on a Bruker maXis QTOF-MS instrument. A mass accuracy ≤2 ppm was obtained in the peak-matching acquisition mode.

Synthesis of 1-(*cis*-9,10-methylene-octadecanoyl)-*rac*-glycerol (compound 4a (MDS))

8-(2-octylcyclopropyl)octanoic acid (dihydrosterculic acid) (2a)

To a stirred solution of 2,4,6-trichlorophenol (8.60 g, 43.5 mmol) in 200 mL of dry CH_2Cl_2 at -40 °C under argon was added a 1 M hexane solution of diethyl zinc (44 mL, 44 mmol). The solution was stirred for 15 min at -40 °C and then diiodomethane (11.66 g, 3.50 mL, 43.5 mmol) was slowly added over a period of 10 min. After stirring for 15 min at the same temperature oleic acid **1a** (3.07 g, 3.47 mL, 10.88 mmol) was added. The reaction mixture was stirred at -40 ^{o}C for an additional 1 h and then allowed to warm to rt and stirred overnight. The mixture was washed with 300 mL of 10 % HCl. The organic phase was separated and the aqueous phase was extracted with CH_2Cl_2 (3 x 150 mL). The combined organic phases were washed with a saturated solution of NaCl and dried over $MgSO_4$. The solvent was removed under reduced pressure and the residue was purified by column chromatography on silica gel eluted with a mixture CH_2Cl_2/MeOH 95:5. The solvent was evaporated to afford a yellow oil (2.4 g), which was precipitated with cold acetonitrile to afford compound **2a** as a white solid (2.1 g, 65%).

HRMS (ESI $[M + Na]^+$) m/z: calcd for ($C_{19}H_{36}NaO_2$) 319.26074, found 319.26075.

1-(*cis*-9,10-methylene-octadecanoyl)-*rac*-glycerol (MDS) (4a)

To a stirred solution of acid **2a** (660 mg, 2.23 mmol) in 50 mL of dry CH_2Cl_2/DMF (3:1) was added EDC (556 mg, 2.90 mmol) followed by DMAP (27 mg, 0.223 mmol) at 0 °C under argon. The solution was stirred for 1 h at 0 °C and then was added dropwise over a period of 30 min to a solution of glycerol (1.23 g, 13.38 mmol) in 50 mL of dry DMF at 0 °C. The mixture was stirred for 12 h at room temperature and then washed with a saturated solution of $NaHCO_3$. . The organic phase was separated and the aqueous phase was extracted with CH_2Cl_2 (3 x 100 mL). The combined organic phases were washed with brine and dried over $MgSO_4$. The solvent was removed under reduced pressure and the residue was purified by column chromatography on silica gel and eluted with a mixture of cyclohexane/ethylacetate 8:2 to 4:6. The solvent was evaporated to afford a yellow oil (630 mg), which was precipitated with cold acetonitrile to afford a yellow solid which was then purified by low-temperature crystallization in acetonitrile (-20 °C to 4 °C) to yield 570 mg of 1-MDS **4a** as a white solid (69%), mp: 27 °C.

^{1}H NMR (500 MHz, $CDCl_3$) δ 4.22 (dd, *J* = 11.7, 4.6 Hz, 1H), 4.16 (dd, *J* = 11.7, 6.2 Hz, 1H), 3.94 (tt, *J* = 6.0, 4.3 Hz, 1H), 3.86 – 3.84 (m, 0H), 3.71 (dd, *J* = 11.4, 4.0 Hz, 1H), 3.61 (dd, *J* = 11.4, 5.8 Hz, 1H), 2.42 – 2.33 (m, 2H), 1.97 (br, 2H) 1.68 – 1.60 (m, 2H), 1.45 – 1.22 (m, 23H), 1.21 – 1.09 (m, 2H), 0.94 – 0.85 (m, 3H), 0.70 – 0.62 (m, 2H), 0.60 – 0.54 (m, 1H), -0.33 (td, *J* = 5.3, 4.0 Hz, 1H).

^{13}C NMR (125 MHz, $CDCl_3$) δ 174.40, 170.29, 70.29, 65.18, 63.33, 34.17, 31.94, 30.23, 30.14, 29.70, 29.45, 29.38, 29.31, 29.15, 28.73, 28.67, 24.92, 22.71, 15.77, 15.72, 14.14, 10.92; HRMS (ESI $[M + Na]^+$) m/z: calcd for ($C_{22}H_{42}NaO_4$) 393.29749, found 393.29753.

Synthesis of 1-(*cis*-9,10-methylene-esadecanoyl)-*rac*-glycerol (compound 4b (CPMP))

8-(2-hexylcyclopropyl)octanoic acid (CP-palmitoleic acid) (2b)

To a stirred solution of 2,4,6-trichlorophenol (8.60 g, 43.5 mmol) in 250 mL of dry CH_2Cl_2 at -40 °C under argon was added a 0.9 M hexane solution of diethyl zinc (49 mL, 44 mmol). The solution was stirred for 15 min at -40 °C and then diiodomethane (11.66 g, 3.50 mL, 43.5 mmol) was slowly added over a period of 10 min. After stirring for 15 min at the same temperature, palmitoleic acid **1b** (2.77 g, 3.10 mL 10.88 mmol) was added. The reaction mixture was stirred at -40 °C for an additional 1 h and then allowed to warm to r.t. and stirred overnight. The mixture was washed with 300 mL of 10 % HCl. The organic phase was separated and the aqueous phase was extracted with CH_2Cl_2 (3 x 150 mL). The combined organic phases were washed with a saturated solution of NaCl and dried over $MgSO_4$. The solvent was removed under reduced pressure and the residue was purified by column chromatography on silica gel eluted starting with CH_2Cl_2, and after elution of excess 2,4,6-trichlorophenol with CH_2Cl_2/MeOH 95:5 to get the product **2b** as a slightly yellow oil (2.13 g, 73%).

^1H NMR (500 MHz, $CDCl_3$) δ 2.28 (t, *J* = 7.5 Hz, 2H), 1.57 (q, *J* = 7.5 Hz, 2H), 1.14 – 1.36 (m, 18H), 1.01 – 1.12 (m, 2H), 0.82 (t, *J* = 7.0 Hz, 3H), 0.46 – 0.62 (m, 3H), - 0.39 - -0.42 (m, 1H).

^{13}C-NMR (125 MHz, $CDCl_3$) 179.22, 33.91, 31.95, 30.18, 30.12, 29.42, 29.34, 29.28, 29.07, 28.72, 28.66, 24.70, 22.69, 15.77, 15.73, 14.11, 10.91.

HRMS (ESI $[M - H]^-$) m/z: calcd for ($C_{17}H_{31}O_2$) 267.23295, found 267.23271.

1-(*cis*-9,10-methylene-esadecanoyl)-*rac*-glycerol (CPMP) (4b)

To a stirred solution of acid (600 mg, 2.23 mmol) in 50 mL of a mixture of dry CH_2Cl_2/DMF (3:1) was added EDC (556 mg, 2.90 mmol) followed by DMAP (27 mg, 0.223 mmol) at 0 °C under argon. The solution was stirred for 1 h at 0 °C and then was added dropwise over a period of 30 min to a solution of glycerol (1.23 g, 13.38 mmol) in 50 mL of dry DMF at 0 °C. The mixture was stirred for 12 h at room temperature and then washed with a saturated solution of $NaHCO_3$. The organic phase was separated and the aqueous phase was extracted with CH_2Cl_2 (3 x 100 mL). The combined organic phases were washed with brine and dried over $MgSO_4$. The solvent was removed under reduced pressure and the residue was purified by column chromatography on silica gel and eluted with a mixture of cyclohexane/ethylacetate 8:2 to 4:6. The solvent was removed to give colourless solid product **4c** (420 mg, 55%).

^{1}H-NMR (500 MHz, $CDCl_3$) δ 4.86 (quint, *J* = 4.7 Hz, 1H of 2-NMH), 4.13 (dd, *J* = 11.7, 4.6 Hz, 1H), 4.08 (dd, *J* = 11.6, 6.2 Hz, 1H), 3.84 – 3.89 (m, 1H), 3.76 (t, *J* = 5.2 Hz, 4H of 2-NMH), 3.59 – 3.68 (m, 1H), 3.50 – 3.56 (m, 1H), 2.64 (br d, OH), 2.26 – 2.34 (m, 2H), 2.18 – 2.25 (m, 1 H), 1.52 – 1.60 (m, 2H), 1.14 – 1.35 (m, 18H), 1.01 – 1.12 (m, 2H), 0.82 (t, *J* = 6.8 Hz, 3H), 0.46 – 0.62 (m, 3H), -0.40 (q, *J* = 5.1 Hz, 1H).

^{13}C-NMR (125 MHz, $CDCl_3$) δ 174.34, 70.27, 65.16, 63.35, 34.15, 31.94, 30.16, 30.11, 29.42, 29.33, 29.28, 29.13, 28.71, 28.65, 24.91, 22.68, 15.76, 15.71, 14.10, 10.91.

HRMS (ESI $[M + Na]^+$) m/z: calcd for ($C_{20}H_{38}O_4Na$) 365.26623, found 365.26647

Synthesis of 1-(*cis*-11,12-methylene-octadecanoyl)-*rac*-glycerol (compound 4c (MLB))

10-(2-hexylcyclopropyl)decanoic acid (Lactobacillic acid) (2c)

To a stirred solution of 2,4,6-trichlorophenol (8.60 g, 43.5 mmol) in 200 mL of dry CH_2Cl_2 at -40 °C under argon was added a 0.9 M hexane solution of diethyl zinc (49 mL, 44 mmol). The solution was stirred for 15 min at -40 °C and then diiodomethane (11.66 g, 3.50 mL, 43.5 mmol) was slowly added over a period of 10 min. After stirring for 15 min at the same temperature vaccenic acid **1c** (3.07 g, 3.46 mL, 10.88 mmol) was added. The reaction mixture was stirred at -40 ^{O}C for an additional 1 h and then allowed to warm to r.t. and stirred overnight. The mixture was washed with 300 mL of 10 % HCl. The organic phase was separated and the aqueous phase was extracted with CH_2Cl_2 (3 x 150 mL). The combined organic phases were washed with a saturated solution of NaCl and dried over $MgSO_4$. The solvent was removed under reduced pressure and the residue was purified by column chromatography on silica gel eluted starting with CH_2Cl_2, and after elution of excess 2,4,6-trichlorophenol with CH_2Cl_2/MeOH 95:5 to get the product **2c** as colourless solid (2.29 g, 71%).

^{1}H-NMR (500 MHz, $CDCl_3$) δ 2.28 (t, *J* = 7.5 Hz, 2H), 1.56 (quint, *J* = 7.4 Hz, 2H), 1.14 – 1.37 (m, 22H), 1.01 – 1.15 (m, 2H), 0.82 (t, *J* = 6.9 Hz, 3H), 0.47 – 0.61 (m, 3H), -0.40 (q, *J* = 5.1 Hz, 1H).

^{13}C-NMR (125 MHz, $CDCl_3$) δ 179.63, 33.97, 31.95, 30.19 (2C), 29.63 (2C), 29.44, 29.36, 29.25, 29.07, 28.73, 28.71, 24.69, 22.70, 15.77, 15.76, 14.12, 10.91.

HRMS (ESI $[M - H]^-$) m/z: calcd for ($C_{19}H_{35}O_2$) 295.26425, found 295.26394.

1-(*cis*-11,12-methylene-octadecanoyl)-*rac*-glycerol (MLB) (4c)

To a stirred solution of acid (660 mg, 2.23 mmol) in 50 mL of a mixture of dry CH_2Cl_2/DMF (3:1) was added EDC (556 mg, 2.90 mmol) followed by DMAP (27 mg, 0.223 mmol) at 0 °C under argon. The solution was stirred for 1 h at 0 °C and then was added dropwise over a period of 30 min to a solution of glycerol (1.23 g, 13.38 mmol) in 50 mL of dry DMF at 0 °C. The mixture was stirred for 12 h at room temperature and then washed with a saturated solution of $NaHCO_3$. The organic phase was separated and the aqueous phase was extracted with CH_2Cl_2 (3 x 100 mL). The combined organic phases were washed with brine and dried over $MgSO_4$. The solvent was removed under reduced pressure and the residue was purified by column chromatography on silica gel and eluted with a mixture of cyclohexane/ethylacetate 8:2 to 4:6. The solvent was removed to give the product **4c** (480 mg, 58%) as a slightly yellowish oil.

^{1}H-NMR (500 MHz, $CDCl_3$) δ 4.86 (quint, 1H of 2-MLB), 4.13 (dd, *J* = 11.7, 4.7 Hz, 1H), 4.09 (dd, *J* = 11.7, 6.1 Hz, 1H), 3.83 – 3.89 (m, 1H), 3.75 – 3.78 (m, 4H of 2-MLB), 3.62 (dd, *J* = 11.4, 4.0 Hz, 1H), 3.53 (dd, *J* = 11.5, 5.8 Hz, 1H), 2.24 – 2.35 (m, 2H), 2.04 (br s, 2H, OH), 1.52 – 1.61 (m, 2H), 1.15 – 1.37 (m, 22H), 1.01 – 1.12 (m, 2H), 0.82 (t, *J* = 7.8 Hz, 3H), 0.45 – 0.67 (m, 3H), -0.35 – -0.46 (m, 1H).

^{13}C-NMR (125 MHz, $CDCl_3$) δ 174.34, 70.26, 65.16, 63.32, 34.15, 31.94, 30.19, 30.17, 29.62 (2C), 29.45, 29.34, 29.24, 29.13, 28.71, 28.70, 24.91, 22.69, 15.76, 15.74, 14.12, 10.90.

HRMS (ESI $[M + Na]^+$) m/z: calcd for ($C_{22}H_{42}O_4Na$) 393.29753, found 393.29757.

Synthesis of 1-(*cis*-9,10,12,13-dimethylene-octadecanoyl)-*rac*-glycerol (compound 4d (DCPML))

8-(2-((2-pentylcyclopropyl)methyl)cyclopropyl)octanoic acid (CP-linoleic acid) (2d)

To a stirred solution of 2,4,6-trichlorophenol (8.60 g, 43.5 mmol) in 200 mL of dry CH_2Cl_2 at -40 °C under argon was added a 0.9 M hexane solution of diethyl zinc (49 mL, 44 mmol). The solution was stirred for 15 min at -40 °C and then diiodomethane (11.66 g, 3.50 mL, 43.5 mmol) was slowly added over a period of 10 min. After stirring for 15 min at the same temperature linoleic acid **1d** (1.53 g, 1.70 mL, 5.44 mmol) was added. The reaction mixture was stirred at -40 ^{o}C for an additional 1 h and then allowed to warm to r.t. and stirred overnight. The mixture was washed with 300 mL of 10 % HCl. The organic phase was separated and the aqueous phase was extracted with CH_2Cl_2 (3 x 150 mL). The combined organic phases were washed with a saturated solution of NaCl and dried over $MgSO_4$. The solvent was removed under reduced pressure and the residue was purified by column chromatography on silica gel eluted starting with CH_2Cl_2, and after elution of excess 2,4,6-trichlorophenol with CH_2Cl_2/MeOH 95:5 to get the product **2d** as a slightly yellow oil (1.16 g, 69%).

Mixture of diastereoisomers:

^{1}H-NMR (500 MHz, $CDCl_3$) δ 2.28 (t, *J* = 7.5 Hz, 1H), 1.51 – 1.62 (m, 2H), 1.17 – 1.46 (m, 17H), 0.91 – 1.15 (m, 3H), 0.82 (t, *J* = 6.8 Hz, 3H), 0.67 – 0.75 (m, 2H), 0.51 – 0.66 (m, 4H), -0.30 – -0.40 (m, 2H).

^{13}C-NMR (125 MHz, $CDCl_3$) δ 179.90, 34.06, 31.90, 30.13, 29.89, 29.42, 29.30, 29.08, 28.88, 28.87, 28.72, 28.70, 28.02, 27.87, 24.70, 22.72, 16.05, 15.93, 15.91, 15.88, 15.66, 15.61, 14.12, 11.02, 10.84.

HRMS (ESI $[M - H]^-$) m/z: calcd for ($C_{20}H_{35}O_2$) 307.26425, found 307.26407.

1-(*cis*-9,10,12,13-dimethylene-octadecanoyl)-*rac*-glycerol (DCPML) (4d)

To a stirred solution of acid (688 mg, 2.23 mmol) in 50 mL of a mixture of dry CH_2Cl_2/DMF (3:1) was added EDC (556 mg, 2.90 mmol) followed by DMAP (27 mg, 0.223 mmol) at 0 °C under argon. The solution was stirred for 1 h at 0 °C and then was added dropwise over a period of 30 min to a solution of glycerol (1.23 g, 13.38 mmol) in 50 mL of dry DMF at 0 °C. The mixture was stirred for 12 h at room temperature and then washed with a saturated solution of $NaHCO_3$. The organic phase was separated and the aqueous phase was extracted with CH_2Cl_2 (3 x 100 mL). The combined organic phases were washed with brine and dried over $MgSO_4$. The solvent was removed under reduced pressure and the residue was purified by column chromatography on silica gel and eluted with a mixture of cyclohexane/ethylacetate 8:2 to 4:6. The solvent was removed to give the product **4d** (605 mg, 71%) as a slightly yellowish oil.

^{1}H NMR (400 MHz, $CDCl_3$) δ 4.86 (quint, *J* = 4.8 Hz, 1H of 2-MBMO), 4.13 (dd, *J* = 11.7, 4.7 Hz, 1H), 4.09 (dd, *J* = 11.6, 6.1 Hz, 1H), 3.83 – 3.90 (m, 1H), 3.75 – 3.78 (m, 4H of 2-MBMO), 3.62 (dd, *J* = 11.5, 4.0 Hz, 1H), 3.54 (dd, *J* = 11.5, 5.8 Hz, 1H), 2.25 – 2.34 (m, 2H), 2.18 (br s, 2H, OH), 1.52 – 1.61 (m, 2H), 1.17 – 1.47 (m, 17H), 0.91 – 1.13 (m, 3H), 0.82 (t, *J* = 7.0 Hz, 3H), 0.68 – 0.77 (m, 2H), 0.51 – 0.65 (m. 4H) -0.29 – -0.39 (m, 2H).

^{13}C-NMR (125 MHz, $CDCl_3$) δ 174.34, 70.25, 65.13, 63.32, 34.14, 31.88, 30.11, 29.87, 29.41, 29.28, 29.12, 28.86, 28.84, 28.69, 28.68, 28.01, 27.85, 24.90, 22.70, 16.03, 15.91, 15.91, 15.89, 15.85, 15.64, 15.58, 14.10, 11.01, 10.82.

HRMS (ESI $[M + Na]^+$) m/z: calcd for ($C_{23}H_{42}O_4Na$) 405.29753, found 405.29715.

Synthesis of 4,4'-octanamidostilbene-2,2'-disulfonate, OADS

To a stirred solution of DADS (1g, 2.7 mmol) in 50 mL of dry pyridine at reflux temperature under argon was added oleoyl chloride (1.84 ml, 1.75g, 10.8 mmol) dropwise. The solution was stirred for 40 min, then transferred to a single neck flask and the solvent was evaporated under reduced pressure. The crude product was dissolved in hot CH_3CN and then twice precipitated at 4 °C. The precipitated red crystals were filtered, the solvent was removed under reduced pressure, and the product extracted with $CHCl_3$. The solvent was removed under reduced pressure to obtain the desired product OADS **6** as an orange solid (1.5g, 90%).

Synthesis of 4,4'-oleamidostilbene-2,2'-disulfonate

To a stirred solution of DADS (200 mg, 0.54 mmol) in 10 mL of dry pyridine at reflux temperature under argon was added oleoyl chloride (0.72 ml, 650mg, 2.16 mmol) dropwise, after which the solution becomes immediately transparent. The solution was stirred for 15 min, then transferred to a single neck flask and the solvent was evaporated under reduced pressure. The crude product was dissolved in hot CH_3CN and then twice precipitated at 4 ^{o}C. The resultant yellow oil was dissolved in CH_2Cl_2, the precipitate was removed by filtration. The solvent was removed under reduced pressure to obtain the desired product **7** as slightly yellowish solid (0.44g, 90%).

References

1. V. Luzzati, Biological significance of lipid polymorphism: The cubic phases - commentary. *Curr Opin Struc Biol* **7**, 661-668 (1997).
2. H. Delacroix, V. Luzzati, P. Mariani, The cubic phases of lipid systems - structure, physical-properties and biological relevance. *Abstr Pap Am Chem Soc* **198**, 146-Coll (1989).
3. E. M. Landau, J. P. Rosenbusch, Lipidic cubic phases: A novel concept for the crystallization of membrane proteins. *Proc Natl Acad Sci USA* **93**, 14532-14535 (1996).
4. V. Cherezov *et al.*, High-resolution crystal structure of an engineered human beta(2)-adrenergic g protein-coupled receptor. *Science* **318**, 1258-1265 (2007).
5. L. C. Johansson, A. B. Wohri, G. Katona, S. Engstrom, R. Neutze, Membrane protein crystallization from lipidic phases. *Curr Opin Struc Biol* **19**, 372-378 (2009).
6. K. Larsson, Cubic lipid-water phases - structures and biomembrane aspects. *J Phys Chem* **93**, 7304-7314 (1989).
7. G. Lindblom, L. Rilfors, Cubic phases and isotropic structures formed by membrane-lipids - possible biological relevance. *Biochim Biophys Acta* **988**, 221-256 (1989).
8. X. Mulet, B. J. Boyd, C. J. Drummond, Advances in drug delivery and medical imaging using colloidal lyotropic liquid crystalline dispersions. *J Colloid Interface Sci* **393**, 1-20 (2013).
9. S. Aleandri, C. Speziale, R. Mezzenga, E. M. Landau, Design of light-triggered lyotropic liquid crystal mesophases and their application as molecular switches in "on demand" release. *Langmuir* **31**, 6981-6987 (2015).
10. W. K. Fong, R. Negrini, J. J. Vallooran, R. Mezzenga, B. J. Boyd, Responsive self-assembled nanostructured lipid systems for drug delivery and diagnostics. *J Colloid Interface Sci* **484**, 320-339 (2016).
11. R. Mezzenga, P. Schurtenberger, A. Burbidge, M. Michel, Understanding foods as soft materials. *Nat Mater* **4**, 729-740 (2005).
12. E. Nazaruk, E. M. Landau, R. Bilewicz, Membrane bound enzyme hosted in liquid crystalline cubic phase for sensing and fuel cells. *Electrochim Acta* **140**, 96-100 (2014).
13. V. Razumas, J. Kanapienienė, T. Nylander, S. Engström, K. Larsson, Electrochemical biosensors for glucose, lactate, urea, and creatinine based on enzymes entrapped in a cubic liquid crystalline phase. *Anal Chim Acta* **289**, 155-162 (1994).
14. J. J. Vallooran *et al.*, Lipidic cubic phases as a versatile platform for the rapid detection of biomarkers, viruses, bacteria, and parasites. *Adv Funct Mater* **26**, 181-190 (2016).
15. V. Luzzati *et al.*, in *Curr top membr*. **44,** 3-24 (1997).
16. C. Fong, T. Le, C. J. Drummond, Lyotropic liquid crystal engineering-ordered nanostructured small molecule amphiphile self-assembly materials by design. *Chem Soc Rev* **41**, 1297-1322 (2012).
17. C. V. Kulkarni *et al.*, Engineering bicontinuous cubic structures at the nanoscale-the role of chain splay. *Soft Matter* **6**, 3191-3194 (2010).
18. V. Rao, N. Fujiwara, S. A. Porcelli, M. S. Glickman, Mycobacterium tuberculosis controls host innate immune activation through cyclopropane modification of a glycolipid effector molecule. *J Exp Med* **201**, 535-543 (2005).
19. Y. Y. Chang, J. E. Cronan, Membrane cyclopropane fatty acid content is a major factor in acid resistance of escherichia coli. *Mol Microbiol* **33**, 249-259 (1999).
20. D. Poger, A. E. Mark, A ring to rule them all: The effect of cyclopropane fatty acids on the fluidity of lipid bilayers. *J Phys Chem B* **119**, 5487-5495 (2015).

21. R. Dutzler, A structural perspective on clc chloride channel and transporter function. *Febs J* **274**, 47-47 (2007).
22. J. J. Garcia-Celma, A. Szydelko, R. Dutzler, Transport properties of a prokaryotic clc transporter assayed by solid-supported membrane electrophysiology. *Biophys J* **102**, 215a-215a (2012).
23. R. Dutzler, E. B. Campbell, R. MacKinnon, Gating the selectivity filter in clc chloride channels. *Science* **300**, 108-112 (2003).
24. C. Speziale, L. Salvati Manni, C. Manatschal, E. M. Landau, R. Mezzenga, A macroscopic h+ and cl- ions pump via reconstitution of ecclc membrane proteins in lipidic cubic mesophases. *Proc Natl Acad Sci USA* **113**, 7491-7496 (2016).
25. A. S. Verkman, L. J. V. Galietta, Chloride channels as drug targets. *Nat Rev Drug Discov* **8**, 153-171 (2009).
26. K. Matulef *et al.*, Inhibition of clc-ec1 by dids hydrolysis products. *Biophys J*, 347a-347a (2007).
27. A. E. Howery *et al.*, A designed inhibitor of a clc antiporter blocks function through a unique binding mode. *Chem Biol* **19**, 1460-1470 (2012).
28. L. Salvati Manni *et al.*, Phase behavior of a designed cyclopropyl analogue of monoolein: Implications for low-temperature membrane protein crystallization. *Angew Chem Int Ed* **54**, 1027-1031 (2015).
29. A. B. Charette, S. Francoeur, J. Martel, N. Wilb, New family of cyclopropanating reagents: Synthesis, reactivity, and stability studies of iodomethylzinc phenoxides. *Angew Chem Int Ed* **39**, 4539-4542 (2000).
30. D. W. Hein, E. S. Pierce, Optical bleaching agents .1. Derivatives of dichlorodiaminostilbenedisulfonic acid. *J Am Chem Soc* **76**, 2725-2731 (1954).
31. B. Jing, N. Tokutake, D. H. McCullough, 3rd, S. L. Regen, A quantitative assessment of the influence of permanent kinks on the mixing behavior of phospholipids in cholesterol-rich bilayers. *J Am Chem Soc* **126**, 15344-15345 (2004).

Chapter 3

Phase behavior of designed cyclopropyl analogues of the most commonly investigated monoacylglycerols.

Most nanostructured lipidic materials used in biomedical applications to date are based on naturally or commercially available lipids, mainly monoacylglycerols (MAGs). Monoacylglycerols are a unique class of lipids, which show a complex polymorphism upon hydration (**Figure 1**). By changing the ratio of lipid to water, they exhibit specific transitions between lyotropic liquid crystalline phases with various inverse geometries (*1*). With an increasing amount of water at ambient temperatures, the typical sequence of the most commonly studied MAGs, monoolein (MO) and monolinolein (MLO) is: lamellar crystalline (*Lc*), liquid crystalline lamellar (*Lα*), bicontinuous cubic (*Ia3d* and *Pn3m*), while at high temperatures (80-90°C) is inverse micellar phase (L_2) and inverse hexagonal phase (H_{II}) (*2*). In addition to the variation of hydration, environmental factors such as temperature and pressure affect phase stability and control the formation of various phases with defined material properties (*1, 3-5*). The geometry and the structure of these phases have been well-established (*2, 6*), and the curvature of the channel is a characteristic parameter of lipidic phases, with the highest curvature associated with the high-temperature phases.

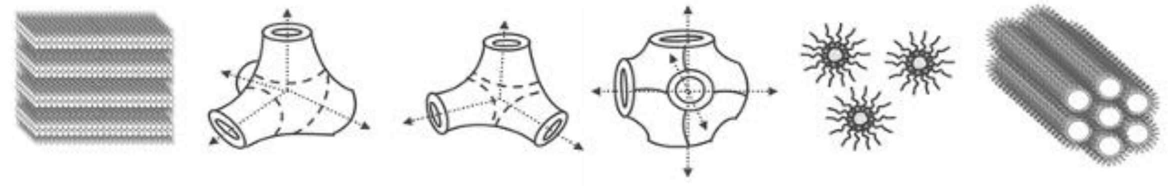

Figure 1. Sequence of phases generally formed by monoacylglicerols upon hydration. From left to right: lamellar *Lα*, bicontinuous cubic *Ia3d*, *Pn3m, Im3m*, inverse micellar phase L_2 and inverse hexagonal H_{II}.

Both the *Lc and Lα* phases consist of an alternation of a planar lipidic bilayer and a layer of water, but while *Lc* is a solid phase organized in a crystalline lattice, *Lα* is a liquid crystalline phase that flows like a viscous liquid albeit according to an internal crystalline order. Cubic phases are made out of one curved lipidic bilayer arranged in an infinite periodic minimal surface that encompasses two identical, but not interconnected water channels (*7*). The type of surface symmetry can vary forming different cubic phases with gyroid (*Ia3d*), double diamond (*Pn3m*), or primitive symmetry (*Im3m*). In the inverse hexagonal phase, the lipidic molecules assemble into inverse micellar cylinders that are packed in a hexagonal lattice. Among these geometries, the inverse bicontinuous cubic phases are of particular interest as bio-inspired matrices in several fundamental and applied scientific disciplines such as membrane biology (*3, 8-11*), drug delivery (*12-14*), food emulsifiers (*15*) and biosensing devices (*16-18*). This is due to their high interfacial surface area, three-dimensional continuous hydrophilic and hydrophobic regions and thermodynamic stability in excess of water.

The inverse hexagonal phase is also being intensively studied as intermediate in membrane fusion and as drug delivery system due its stability in excess of water, and its capacity to solubilize drugs in a similar manner to the cubic phases. Moreover, dispersed inverse hexagonal phases show a slower release profile than dispersed cubic phase (*19*). Unfortunately, the availability of pure lipids demonstrating a stable inverse hexagonal phase in excess water at physiological temperature is limited to few examples such as phosphatidylethanolamines (*20, 21*), 1-glyceryl monooleyl ether (*22*) and glycerate surfactants (*23*). Alternatively, they are formed by mixing MAGs or phytantriol with a hydrophobic additive (*24, 25*).

The increasing scope of applications of LCPs in various biomedical areas often requires the ability to tune the nanoscopic and macroscopic properties of LCPs to the required use. For instance, the mesophase geometry determines the release rate of encapsulated drugs (*13, 14, 19, 26-28*), as well as the thermostability (*29*). In addition to molecular geometry, the ability of the mesophase to incorporate different amounts of water and the thickness of the lipidic bilayer determines the utility of the mesophase for protein crystallization (*30, 31*). For membrane protein crystallization (*8*) in particular, the screening of alternative lipids has been shown to be a valid method for crystal optimization (*32*).

Clearly, control of the molecular features of the lipid determines the properties of the nanostructure and thus can empower numerous technological applications of lipidic mesoscopic materials. Consequently, the design and construction of a matrix with a specific geometry and phase behavior requires availability of new basic molecular motifs and rigorous phase characterization to elucidate the relationship between the structure and properties. The position of the *cis*-double bond in the chain, and head group modification, especially charged ones, are known to influence curvature and hence phase behavior (*33*). In this thesis, a family of novel lipids with discrete variations in the hydrophobic region has been designed and synthesized, and subsequently their phase behavior established in order to understand how subtle molecular changes of the lipid structure can be used to influence the balance of mesophases formed.

In this work we have modified the most intensely studied MAGs, monoolein (MO), monopalmitolein (MP), monovaccein (MV) and monolinolein (ML), replacing the olefin with a rigid cyclopropyl moiety to obtain a novel family of designed lipids: monodihydrosterculin (MDS), cyclopropyl monopalmitolein (CPMP), monolactobacillin (MLB), dicyclopropyl monolinolein (DCPML). Each one of these lipids shows a subtle variation in the alkyl chain, where the *cis*-double bond of a traditional monoacylglycerol has been replaced with a *cis*-cyclopropane. The ability of cyclopanated lipids to protect the bacterial membrane from acid and cold shock together with the chemical and geometrical effect of a cyclopropyl ring on the lipidic chain are described in **chapter 2** of this thesis together with the synthetic routes of these target lipids. Their structure and the structure of the corresponding unsaturated monoacylglicerols are depicted again in **Figure 2.**

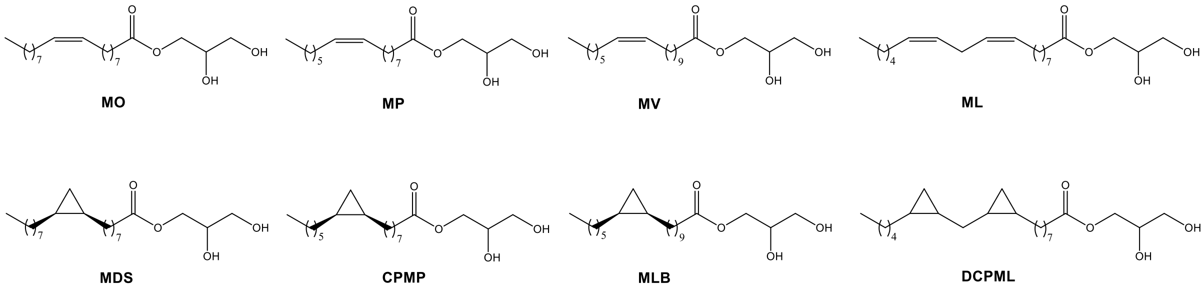

Figure 2. Top row: chemical structure of common unsaturated monoacylglycerols. From left to right: monoolein (MO), monopalmitolein (MP), monovaccein (MV) and monolinolein (ML). Bottom row: chemical structure of the synthesized cyclopropaneted monoacylglicerols. From left to right: monodihydrosterculin (MDS), cyclopropyl monopalmitolein (CPMP), monolactobacillin (MLB), dicyclopropyl monolinolein (DCPML).

In order to characterize the effect of the cyclopropyl moiety on the phase diagram of these novel lipids, their aqueous and thermal phase behavior were studied with small-angle X-ray scattering (SAXS).

3.1 Results and discussion

3.1.1 Phase diagrams

Full phase diagrams for the four target MAGs were established by SAXS, which is the method of choice to investigate the temperatures and compositions at which order-to-order transitions occur. The four phase diagrams (**Figures 3, 5-7**) of the cyclopropanated lipids are shown overlaid on the phase diagrams of the corresponding *cis*-olefinic MAGs.

The first cyclopropanated system studied was MDS (*29*). At temperatures below 30°C, the binary MDS:H_2O phase diagram features order-to-order transitions from the $L\alpha$ to *Ia3d*, and from *Ia3d* to *Pn3m* upon hydration, and finally formation of the fully hydrated *Pn3m* cubic phase above a characteristic boundary of full hydration (**Figure 3**). At high temperatures, all phases transform into the isotropic L_2 phase. The sequence of transitions between the mesophases is similar to that of MO, while the temperature and hydration range of the order-to-order transition differ. Significantly, the high-temperature H_{II} phase that appears in MO (*2, 6*) is absent in the corresponding cyclopropanated system. The highly curved H_{II} phase has the highest packing frustration energy, and its absence may be correlated with a difference in the chain stretching energy due to the new hydrophobic motif (*34*).

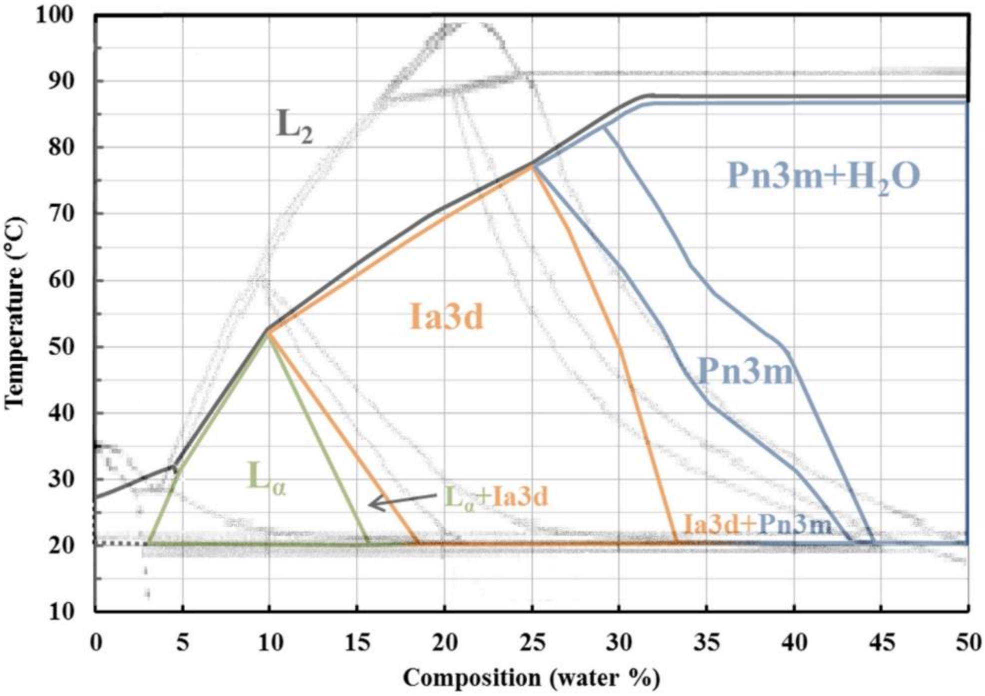

Figure 3. Overlay of the binary phase diagrams of MDS (solid lines) and MO (background, light grey) adapted from H. Qiu, M. Caffrey (*2*). Sample composition/temperature phase diagram of the MDS:water system was established by SAXS, taking into account evolution of the structural parameters in order to determine the mesophase and conditions of maximum hydration, and implicitly, the coexistence of the bulk phase with excess water. The phase diagram shows a series of order to order transitions with the following phase sequence: *Lα* (green)→ *Lα+Ia3d* (green+orange)→ *Ia3d* (orange)→ *Ia3d+Pn3m* (orange+blue)→ *Pn3m* (blue). Reproduced with permission from (*29*).

The overlay of the binary phase diagrams of MDS and MO (**Figure 3)** reveals that at a given composition the transition temperature of any phase to the high-temperature L_2 phase is lower in the MDS than in the MO system. The boundary lines between L_2 and the lower-temperature phases in these two systems are not parallel, and form a wedge that broadens with increasing hydration: at low water content (5 %) the transition from *Lα* to L_2 is isothermal (35 °C) in both systems. Upon increasing the water content, the MDS mesophases become increasingly less stable at high temperature, which is reflected in a relatively low transition temperature. Consequently, at 15 % water the *Ia3d* to L_2 transition temperatures are 65 °C and 85 °C for the MDS and MO systems, respectively.

The cubic-*Ia3d* is the most pronounced phase in both MO and MDS phase diagrams. For MDS, the *Lα-Ia3d* boundary is at lower water content than in MO, whereas the *Ia3d-Pn3m* boundary starts at lower hydration at a lower temperature, and ends at higher hydration at a higher temperature. At even higher water content, the fully hydrated *Pn3m* phase is shifted to higher water content in MDS. Thus, the existence of the cubic phase for MDS is larger in the composition space, and smaller in the temperature space when compared to MO.

The phase diagram of the MDS:H_2O system (**Figure 3**) demonstrates a number of novel features that can be directly related to the molecular geometry of the hydrophobic chain, and its packing arrangement within various mesophases. As can be seen from the broader existence range of the cubic phases, the MDS system can accommodate more molecules of water in the cubic phase. Most importantly, this system, which possesses a rigid and more restricted cyclopropyl geometry, was shown to form curved cubic phases at lower temperature than the corresponding MO system, analogous to observed differences between corresponding phosphatidylethanolamines (*35*, *36*).

For a given phase at constant temperature, an increase in water content results in swelling, i.e. increase of the lattice size (**Figure 4**). For the *Lα* phase, the latter corresponds to the inter-bilayer distance, that is, thickness of the aqueous compartment. For the cubic phases, this corresponds to the aqueous channel size. At a given temperature, there is a maximal hydration for a certain phase, above which coexistence with a maximally hydrated phase sets in. The coexistence region eventually transforms into the pure maximally hydrated phase upon further increase of water (**Figure 4**). In the coexistence region, the lattice parameter remains constant until a complete phase transition is accomplished (**Figure 4B**). Additionally, the curvature and the size variation of the lyotropic liquid crystalline unit cell are phase-dependent: the *Lα* and the cubic *Pn3m* have smaller lattice parameters, and the cubic *Ia3d* has larger lattice parameters (**Figure 4B**).

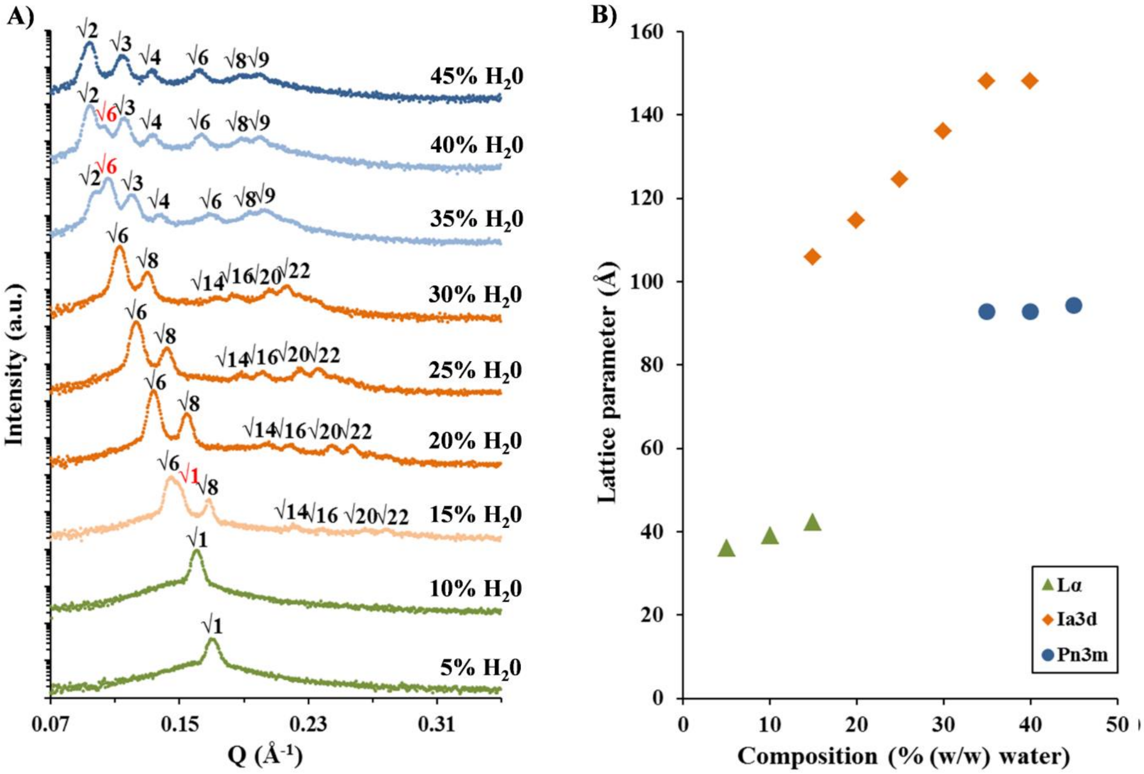

Figure 4. A) SAXS spectra of the scattered intensities versus scattering vector q, azimuthally averaged into 1D profiles, showing the structural evolution of the MDS:water system with increasing hydration at a constant temperature (30 °C). The spectra reveal a series of order to order transitions with the following phase sequence: *Lα* (green)→ *Lα+Ia3d* (beige)→ *Ia3d* (red)→ *Ia3d+Pn3m* (pale blue)→ *Pn3m* (blue), each phase being unequivocally characterized due to its unique diffraction peak ratios. B) Evolution of the lattice parameter size as a function of hydration for the different mesophases in the MDS:water system at 30 °C. Reproduced with permission from (*29*).

Following the finding that the cyclopropyl moiety had a profound impact on the phase behavior due to its effect on the packing arrangement of the MAGs, the studies were expanded to the other three synthetic systems: MLB, CPMP, and DCPML. The phase diagrams of the singly cyclopropanated lipids CPMP (**Figure 5**) and MLB (**Figure 6**) present a sequence of phase transitions which is similar to their corresponding monoacylglycerols: the characteristic *Lα* phase at low water content, a transition to the cubic *Ia3d*, and subsequently from *Ia3d* to the cubic *Pn3m* upon hydration. In both cases, the *Pn3m* cubic phase was found to be stable in excess of water, and it was possible to determine a full hydration line in which the *Pn3m* phase coexists with pure water through the analysis of the lattice parameters at each level of hydration.

In the case of CPMP the boundaries are similar at low amount of water, but at room temperature the transition to *Pn3m* phase occurs at higher hydration level than in the corresponding unsaturated lipid MP. The high temperature behavior of this lipid was difficult to interpret because of a number interferences on the SAXS spectra. Some peaks that do not belong to the *Pn3m* phase, are difficult to interpret and show low reproducibility were found in the temperature range above 80 °C. The phase behavior up to 80 °C is reported in **Figure 5**.

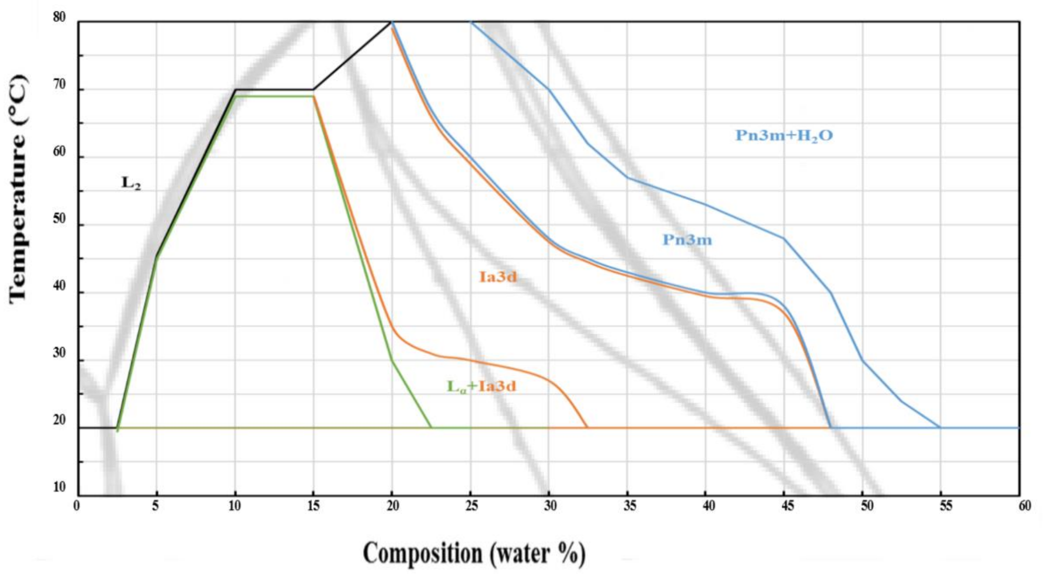

Figure 5. Overlay of the binary phase diagrams of CPMP (solid lines) and MP (background) adapted from J. Briggs' PhD thesis, (The Ohio State University, Columbus, Ohio 1994). Sample composition/temperature phase diagram of the CPMP:water system was established by SAXS, taking into account evolution of the structural parameters in order to determine the phase maximum hydration, and implicitly coexistence of the bulk phase with excess water. The phase diagram shows a series of order to order transitions with the following phase sequence: *Lα* (green)→ *Lα+Ia3d* (green+orange)→ *Ia3d* (orange)→ *Pn3m* (blue).

For the MLB system, the phase sequence is the same as that of the corresponding *cis*-unsaturated lipid MV, but the phase boundaries are shifted in most of the cases to lower water content (**Figure 6)**. Moreover, for MLB, the highly curved H_{II} phase is present at high temperature, which was not observed in the phase behavior of MV. However, since the phase behavior of MV was characterized only up to 80 °C (*37*), its presence at higher temperatures cannot be excluded.

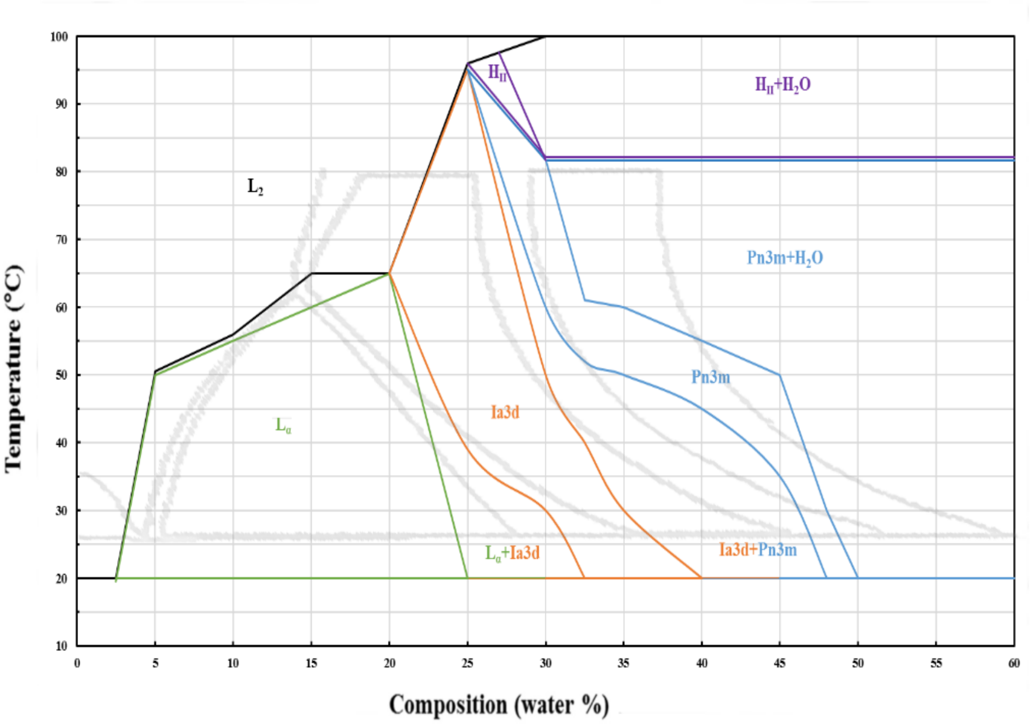

Figure 6. Overlay of the binary phase diagrams of MLB (solid lines) and MV (background) adapted from Kulkarni et al. (*37*). Sample composition/temperature phase diagram of the MLB:water system was established by SAXS, taking into account evolution of the structural parameters in order to determine the phase maximum hydration, and implicitly coexistence of the bulk phase with excess water. The phase diagram shows a series of order to order transitions with the following phase sequence: *Lα* (green)→ *Lα+Ia3d* (green+orange)→ *Ia3d* (orange)→ *Ia3d+Pn3m* (orange+blue)→ *Pn3m* (blue) and at high temperature the transition *Pn3m* (blue)→ H_{II} (violet).

In the case of the most curved lipid in the series, DCPML, a most remarkable and unusual phase behavior was observed: the *Ia3d* cubic phase had already formed at 22°C and at water content of 5% (w/w). Instead of the typical phase sequence upon hydration that was observed for most of the other MAGs, including the corresponding unsaturated lipid ML (*La* → *Ia3d* → *Pn3m*), hydrating the DCPML system resulted in an order-to-order phase transition from *Ia3d* to H_{II} (**Figure 7**).

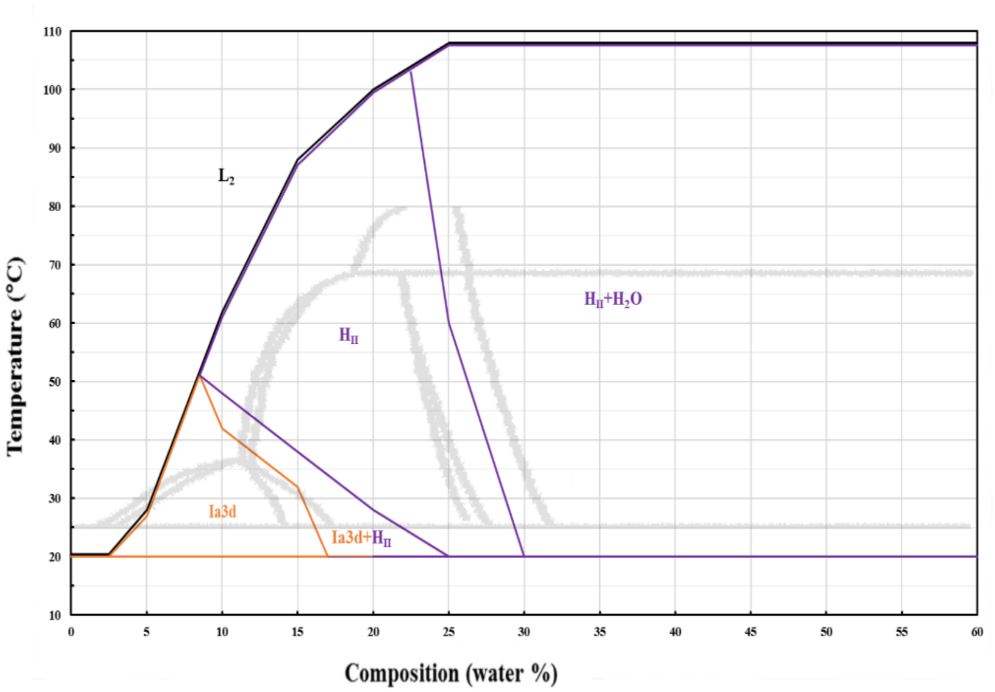

Figure 7. Overlay of the binary phase diagrams of DCPML (solid lines) and ML (background) adapted from Kulkarni et al. (*37*). The sample composition/temperature phase diagram of the DCPML:water system was established by SAXS, taking into account evolution of the structural parameters in order to determine the phase formed at maximum hydration, and implicitly, the coexistence of the bulk phase with excess water. The phase diagram shows a series of order to order transitions with the following phase sequence: *Ia3d* (orange)→ *Ia3d*+ H_{II} (orange+ violet) → H_{II} (violet).

The presence of a stable H_{II} at physiological and room temperature is a remarkable finding compared to the other MAGs. Previous studies have shown that it is only possible to obtain stable H_{II} phases with MAGs at room temperature by addition of hydrophobic molecules such as tetradecane or oleic acid (*19, 24*), or by having an ether bond instead the ester one linking the chain to the headgruop (*38*). The H_{II} phase has been successfully utilised in drug delivery (*26, 39*), and as a matrix for membrane protein reconstitution (*40*). The characteristic slower and prolonged release of hydrophilic molecule from H_{II} renders this geometry particularly appealing for several applications. However, the difficulties related to the complexity of ternary systems have thus far limited the practicality of this mesophase. The stability of the H_{II} phase at room temperature also suggested a shift of the phase behavior to lower temperatures and hydration.

In the case of MDS, it was hypothesized that absence of the H_{II} phase was due to the different chain stretching energy of the cyclopropanated lipid in combination with the high packing frustration energy required for the formation of such a highly curved phase. Considering the new results, especially the unprecedented phase behavior of DCPML, in which the H_{II} phase is stable in a large range of temperatures from 5°C to 105°C we can conclude that the rigidity of the cyclopropyl moiety doesn't constitute a limit for the formation of a highly packed phase. We can also deduce that in analogy with the degree of unsaturation (*37*), increasing the number of cyclopropyl groups lowers the transition temperature between different phases. Moreover, Kulkarni et al. (*37*) compared the phase diagram of 4 different lipids: ME (1-monoelaidin), MV, MO, and ML in increasing order of chain splay. They demonstrated that increase in the chain splay of the lipidic molecule results in the stabilization of phases with an increasing negative curvature, and in the relative destabilization of the primitive bicontinuous cubic phase with a lower transition temperature to the more curved inverse micellar and inverse hexagonal phases. Interestingly, in the cyclopropanated systems the classic sequence MV→MO→ML of increasing chain splay was inverted for the first two components. Considering the stability of the inverse hexagonal phase, with the transition to an inverse hexagonal phase at 85°C for the cyclopropanated analogous of MV (MLB), and assuming that this is stabilized by an increasing of chain splay we can propose a new chain splay sequence for the cyclopropanated lipids: MDS→MLB→DCPML. Because of the limited number of lipids that form LCPs and the complexity of the system it is hard to find general rules to predict the phase behavior and to design new morphologies able to form such phases.

3.1.2 Low temperature phase behavior

The hydrated MDS system forms a stable *Pn3m* cubic phase at 4°C (**Figure 8**). This observation is in accordance with the finding that the high-temperature boundaries of MDS phases are lower than those of MO.

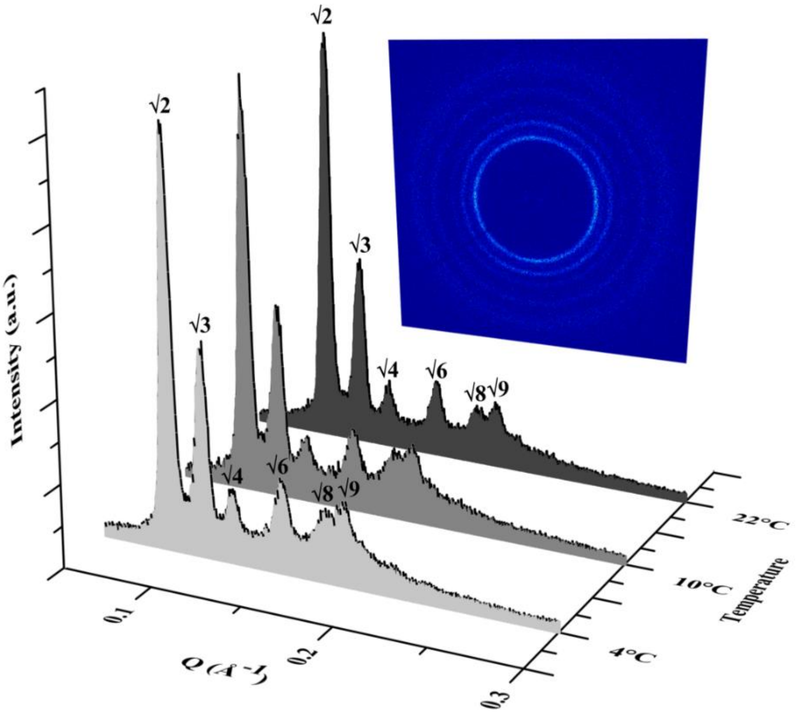

Figure 8. 1D SAXS spectra of the scattered intensities versus scattering vector, *q*, depicting the diffraction patterns of MDS mesophases containing 50 % (w/w) water at the selected temperatures. The double diamond *Pn3m* cubic phase exists in the temperature range of 4-22 °C, as revealed by the SAXS diffraction peaks in the ratio: √2:√3:√4:√6:√8:√9. Reproduced with permission from (*29*).

Currently available LCPs are often limited in the range of temperature over which they can be used, and are generally unstable at low temperatures (0–4 °C), undergoing phase transition into a lamellar crystalline phase (*2, 6*). One of the most important applications of LCPs has been their potential in generating well-diffracting 3-D crystals of membrane proteins. To date, LCP-generated crystals have yielded about 10 % of all membrane protein structures, but these crystals were obtained at room temperature. Although available LCPs, such as the widely used MO-based one, can form supercooled cubic systems that can be maintained to produce low-temperature crystals under certain conditions (*41*), they do not form thermodynamically stable LCPs at low temperature, and are therefore prone to phase transition. In addition, the handling of minute amounts of LCP is not trivial, and any additional component, such as the various additives needed for membrane protein crystallization, may affect phase stability. The same holds for surface effects, which are very pronounced when setting up small drops in the nanoliter range.

Thus the instability of LCPs at low temperature greatly limits its use, and calls for the design and development of stable low-temperature LCPs for biochemical and biophysical studies. The reasons for seeking low-temperature LCPs are manifold: Some membrane proteins are notoriously unstable at room temperature (*42*), requiring low temperature for structural and functional studies. In addition, diffusion is known to be a necessary and crucial process in nucleation and crystal growth: too fast a diffusion may lead to irreversible aggregation and precipitation, while a too slow one may never lead to mature crystals. To have at one's disposal LCPs in a very broad range of temperatures is a clear advantage for controlling diffusion in the lipidic bilayer and in the aqueous channels. Moreover, size of the aqueous channels of the LCPs is an important variable, and the larger the temperature range available, the more flexibility there is in terms of aqueous channel size. Lastly, recent advances in free electron laser (FEL) science and technology (*43*) offer novel prospects in structural biology. Specifically, the availability of LCP injectors makes is feasible to attempt to crystallize complexes of membrane proteins with other membrane proteins or with soluble proteins, which is at the frontier of membrane structural biology, requiring novel lipidic system that are thermodynamically stable at low temperature.

To test the applicability of MDS low-temperature LCPs for the crystallization of membrane proteins, the light-induced proton pump bacteriorhodopsin (bR) was crystallized from MO- and MDS-LCPs at 20 °C in comparative experiments, as well as from MDS-LCP at 4 °C. Results of these experiments are presented in **chapter 5**.

The peculiar low temperature behavior of MDS shows that the steric hindrance introduced with the kink of the cyclopropyl moiety may increase the ability of this family of lipids to maintain a more disordered liquid crystalline phase. This consideration was combined with the observation of a shift of the phase diagram of DCPML to lower temperatures and hydration, and the presence of the H_{II} phase at room temperature. Therefore, the phase behavior of DCPML at low temperature was investigated, which resulted in the observation of an unusual stability of the curved bicontinuous cubic phase at lower than expected temperatures. SAXS measurements of the DCPML mesophase containing 30 % (w/w) water revealed a stable H_{II} phase until 8°C. By lowering the temperature even further, the *Ia3d* cubic geometry was formed and was retained until 0°C. From the measured lattice parameter of the *Ia3d* phase at 0 °C (127.58 Å) it was possible to calculate the radius of the aqueous channel (24.83 Å) as is reported in **chapter 1** of this thesis. This complex phase behavior at low temperatures was further investigated using differential scanning calorimetry (DSC).

In order to resolve first-order transition peaks corresponding to the phase transitions of bound and free water in the hydrophilic domains of the lyotropic liquid crystalline phases, DSC measurements of samples with various water contents were carried out. Since the melting temperatures of the bound and free water are typically different, this technique can provide insight into the thermodynamics of the liquid crystalline phase transitions. In pure water, by increasing the temperature from -70°C, a sharp peak for the first-order transition appears at 0°C. In DCPML LCPs, the water is confined in the mesophase channels and the size of the channels changes with composition of the sample, increasing its radius at higher hydrations. From DSC measurements on DCPML mesophases reported in **Figure 9** it is possible to monitor how the peak for the freezing water changes according with the composition of the sample. Most importantly, the enthalpy peak is completely absent in the samples with 5 and 10% w/w of water. The sharp peak for the free water phase transition appears in the samples with 20% and 25% w/w of water. Lowing the water content results in the peak changing its shape, suggesting a different nature of the water in the channel, until the complete absence of the peak for the bound water. At lower hydration the aqueous channels of the *Ia3d* phase become small enough to entirely confine the water. The DSC measurements also confirmed the phase transition temperatures that were measured by SAXS. A possible deviation of a few degrees in the transition temperatures can be explained by different heating rate and subsequent equilibration time, as well as an error (±0.5%) in the sample composition.

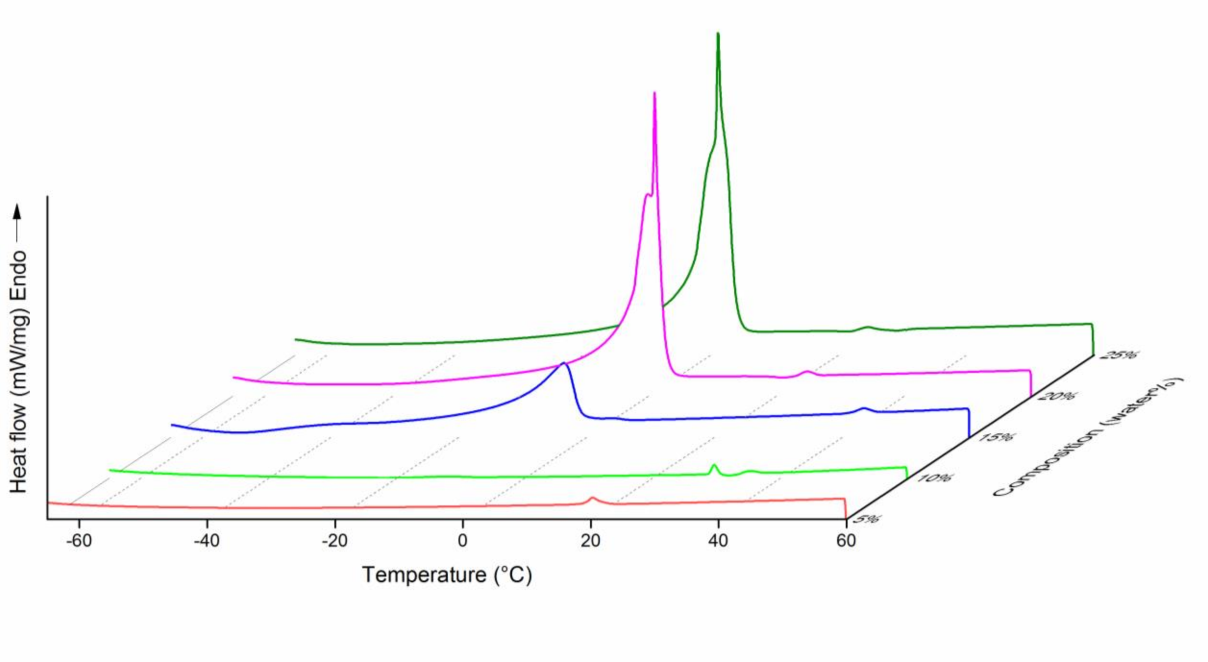

Figure 9. DSC traces of DCPML with water content ranging from 5 to 25% w/w. The peaks correspond to the first-order transitions of free and bound water in the samples with 25% w/w water (olive green), 20% w/w water (magenta), 15% w/w water (blue). The first order transition peaks are absent for the samples with 10% w/w water (green) and 5% w/w water (red). Samples were heated from -70°C to 60°C with a scanning rate of 5 °C/min in a heat/cool/heat cycle. The traces presented in the figure were obtained during the second heating process.

As a control experiment, samples of commercial Dimodan (monolinolein of 95% purity) with various water contents were studied with DSC. The first order transition peak appears at 0°C for both compositions (**Figure 10**). The lack of a first-order transition peak in the DSC suggests that the water in the channels of the *Ia3d* cubic phase in the low hydration regime, i.e. at 5% w/w and 10% w/w, is confined within the mesophase and therefore cannot freeze. It has been established that confinement of water in a range between 1 to 100 nm can prevent formation of the arrangement of water molecules in a tetrahedral ice structure, thereby preventing crystallization at any temperature, creating a state of supercooled water (*44*).

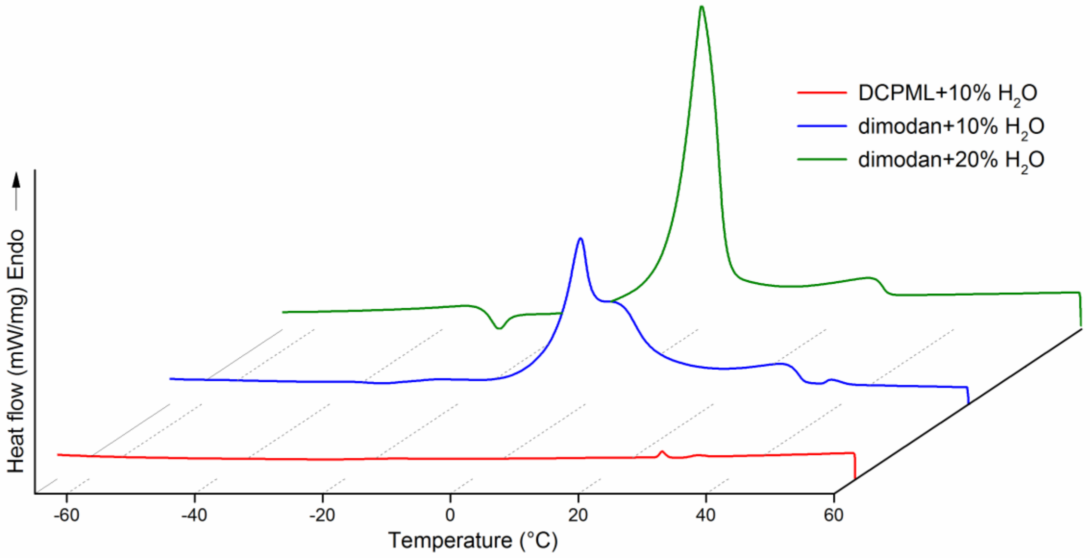

Figure 10. DSC traces of DCPML with 10% w/w water (red) and of Dimodan with 10% w/w water (blue) and 20% w/w water (olive green). The peaks correspond to the first-order transition of free and bound water in the Dimodan samples with 10% w/w water (pale blue) and 20% w/w water (green). Absence of the peak for the first order transition for the DCPML sample with 10% w/w water (red). Sample were heated from -70°C to 60°C with a scanning rate of 5 °C/min in a heat/cool/heat cycle. The curves presented in the figure are obtained during the second heating process.

In order to calculate the radius of the LCPs' aqueous channels, DCPML sample with 10% water was further investigated at low temperature by SAXS. The sample was cooled down to -7°C with a cooling rate of 0.5°C/min and kept at constant temperature for 36 hours. SAXS spectra were collected while increasing the temperature from -7 to 22 °C (**Figure 11)**.

Temperature °C	Lattice parameter Å	Water channel radius Å
22	94.19	7.08
10	95.65	7.19
0	96.50	7.24
-7	98.80	7.34

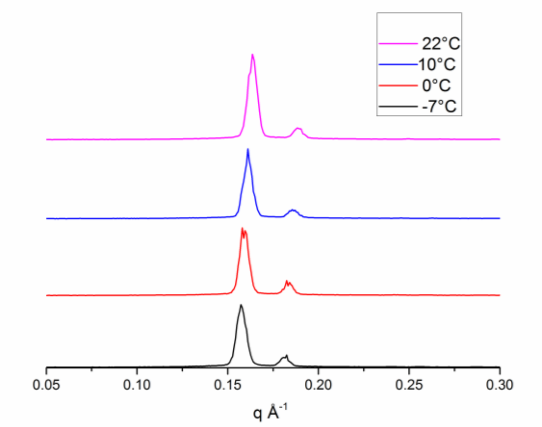

Figure 11. Lattice parameters and water channel radius of DCPML with 10% w/w water calculated from the SAXS spectra at various temperatures: 22 °C magenta, 10°C blue, 0°C red and -7°C black.

Supercooling behavior of confined water has been studied in the last decade and was shown in systems such as carbon nanotubes (*45*) or porous silica hydrogels (*46*). It was also theoretically predicted that inverted micelles could induce supercooling (*47*), but this behavior has never been directly observed. It was already known that the dynamics of water in LCPs is dramatically altered relative to bulk water (*48*), affecting nearly all other kinetic phenomena, including small-molecule and ion transport (*49*).

The discovery reported herein of a LCP system that is able to confine water and avoid its crystallization down to -70°C is directly related to the atypical phase behavior of DCPML. In fact, the presence of an *Ia3d* phase already at low water content is crucial for the formation of small aqueous channels able to confine the water in a cylindrical geometry. Moreover, the transition to a L_c phase of commercially available lipids at low temperature prevented the finding of supercooled bounded water in LCPs.

3.2 Materials and methods

Cyclopropanated lipids were synthetized according to the procedure previously reported by Salvati Manni et al. (*29*) and as reported in **chapter 2** of this thesis. Purity of the lipids was confirmed by ^{1}H-NMR, ^{13}C-NMR and mass spectroscopy.

Mesophase sample preparation

Liquid-crystalline mesophases were prepared by mixing weighed quantities of desired lipid and water (to achieve the desired composition of each sample of the phase diagram) inside sealed Pyrex glass tubes, followed by melting to a fluid isotropic state by gentle heating, mixing by vortex and centrifugation until a homogenous mixture was obtained. The prepared mesophases were then allowed to cool to room temperature over a period of 24 h in order for them to reach a state of thermodynamic equilibrium before SAXS measurements were performed.

An alternative method using two 100 µL Hamilton syringes loaded with the weighed quantities of lipid and water, respectively was also employed. After homogenization with the Hamilton coupled syringe setup, the obtained mesophases were transferred to 2mm quartz glass capillaries (Hilgenberg) between two layers of Teflon and sealed with a solvent free 2-component epoxy resin adhesive (UHU plus). The sample was then melted to form an isotropic fluid, and subsequently equilibrated at room temperature for at least 24 h before measurements.

Small-angle X-ray scattering (SAXS) measurements

SAXS measurements were used to determine phase identity, identify the symmetry and unit cell parameters of the mesophases at the different conditions. Experiments were performed on a Rigaku SAXS instrument with MicroMax-002+ microfocused beam, operating at voltage and filament current of 45 kV and 0.88 mA, respectively. The Ni-filtered Cu Kα radiation (λCu K_{α}=1.5418 Å) was collimated by three pinhole (0.4, 0.3 and 0.8 mm) collimators and the data were collected with a two-dimensional argon-filled Triton detector. An effective scattering-vector range of $0.03\ \text{Å}^{-1} < q < 0.45\ \text{Å}^{-1}$ was probed, where q is the scattering wave vector defined as $q=4\pi\ \sin(\theta)/\lambda$ Cu Kα, with a scattering angle of 2θ, calibrated using silver behenate. 2 mm quartz glass capillaries containing the sample were placed into a stainless steel holder. Additional measurements were performed on a Bruker AXS Micro, with a microfocused X-ray source, operating at voltage and filament current of 50 kV and 1,000 µA, respectively. The Cu Kα radiation (λCu Kα = 1.5418 Å) was collimated by a 2D Kratky collimator, and the data were collected by a 2D Pilatus 100K detector.

An effective scattering-vector range of 0.04 $Å^{-1} < q < 0.5$ $Å^{-1}$ was probed. Samples were placed inside a stainless steel cell between two thin replaceable mica sheets and sealed by an O-ring, with a sample volume of 10 μL and a thickness of ∼1 mm. Measurements were performed at different temperatures, and samples were equilibrated for 30 minutes prior to measurements, while scattered intensity was collected over 30 minutes. For the low-temperature experiments special care was taken to exclude supercooling.

Mesophases were identified by their specific Bragg peak positions. For the double diamond cubic phase (*Pn3m*) the relative positions in q of the Bragg reflections are at $\sqrt{2}:\sqrt{3}:\sqrt{4}:\sqrt{6}:\sqrt{8}:\sqrt{9}\ldots$, whereas for the gyroid bicontinuous cubic phase (*Ia3d*) the Bragg peaks are at $q = \sqrt{6}:\sqrt{8}:\sqrt{14}:\sqrt{16}:\sqrt{20}\ldots$. The H_{II} phase is identified by reflections at $1:\sqrt{3}:\sqrt{4}\ldots$, the bilayer lamellar ($L\alpha$) phase exhibits Bragg peaks in the ratio of 1:2:3:4… and the L_2 phase is identified by a singular characteristic broad peak. The mean lattice parameter, a, was deduced from the corresponding set of observed interplanar distances, d ($d = 2\pi/q$), using the appropriate scattering law for the phase structure. For cubic phases:

$$a = d\sqrt{h^2 + k^2 + l^2} \qquad (1)$$

while for the H_{II} phase:

$$a = \frac{4\Pi}{q\sqrt{3}}\sqrt{h^2 + hk + k^2} \qquad (2)$$

For the L_2 phase, which shows only one broad peak, d is termed the characteristic distance.

Differential scanning calorimetry (DSC)

DSC experiments were performed on a Thermal Advantage DSC from TA Instruments. The samples were loaded in aluminium capsules contained in a steel sample pan of known mass and thermal conductivity. The experiments were carried out with an empty sample pan as the reference. Samples were allowed to equilibrate for at least 48h before the experiment, and were then scanned for a temperature range starting from −70 to 60 °C with a scanning rate of 5 °C/min in a heat/cool/heat cycle.

References

1. V. Luzzati *et al.*, in *Curr top membr*. (1997), vol. 44, pp. 3-24.
2. H. Qiu, M. Caffrey, The phase diagram of the monoolein/water system: Metastability and equilibrium aspects. *Biomaterials* **21**, 223-234 (2000).
3. G. Lindblom, L. Rilfors, Cubic phases and isotropic structures formed by membrane-lipids - possible biological relevance. *Biochim Biophys Acta* **988**, 221-256 (1989).
4. H. M. Barriga *et al.*, Temperature and pressure tuneable swollen bicontinuous cubic phases approaching nature's length scales. *Soft Matter* **11**, 600-607 (2015).
5. T. Y. Tang *et al.*, Hydrostatic pressure effects on the lamellar to gyroid cubic phase transition of monolinolein at limited hydration. *Langmuir* **28**, 13018-13024 (2012).
6. J. Briggs, H. Chung, M. Caffrey, The temperature-composition phase diagram and mesophase structure characterization of the monoolein/water system. *J Phys II* **6**, 723-751 (1996).
7. S. T. Hyde, Bicontinuous structures in lyotropic liquid crystals and crystalline hyperbolic surfaces. *Curr Opin Solid State Mater Sci* **1**, 653-662 (1996).
8. E. M. Landau, J. P. Rosenbusch, Lipidic cubic phases: A novel concept for the crystallization of membrane proteins. *Proc Natl Acad Sci USA* **93**, 14532-14535 (1996).
9. V. Cherezov *et al.*, High-resolution crystal structure of an engineered human beta(2)-adrenergic g protein-coupled receptor. *Science* **318**, 1258-1265 (2007).
10. L. C. Johansson, A. B. Wohri, G. Katona, S. Engstrom, R. Neutze, Membrane protein crystallization from lipidic phases. *Curr Opin Struc Biol* **19**, 372-378 (2009).
11. K. Larsson, Cubic lipid-water phases - structures and biomembrane aspects. *J Phys Chem* **93**, 7304-7314 (1989).
12. X. Mulet, B. J. Boyd, C. J. Drummond, Advances in drug delivery and medical imaging using colloidal lyotropic liquid crystalline dispersions. *J Colloid Interface Sci* **393**, 1-20 (2013).
13. S. Aleandri, C. Speziale, R. Mezzenga, E. M. Landau, Design of light-triggered lyotropic liquid crystal mesophases and their application as molecular switches in "on demand" release. *Langmuir* **31**, 6981-6987 (2015).
14. W. K. Fong, R. Negrini, J. J. Vallooran, R. Mezzenga, B. J. Boyd, Responsive self-assembled nanostructured lipid systems for drug delivery and diagnostics. *J Colloid Interface Sci* **484**, 320-339 (2016).
15. R. Mezzenga, P. Schurtenberger, A. Burbidge, M. Michel, Understanding foods as soft materials. *Nat Mater* **4**, 729-740 (2005).
16. E. Nazaruk, E. M. Landau, R. Bilewicz, Membrane bound enzyme hosted in liquid crystalline cubic phase for sensing and fuel cells. *Electrochim Acta* **140**, 96-100 (2014).
17. V. Razumas, J. Kanapieniené, T. Nylander, S. Engström, K. Larsson, Electrochemical biosensors for glucose, lactate, urea, and creatinine based on enzymes entrapped in a cubic liquid crystalline phase. *Anal Chim Acta* **289**, 155-162 (1994).
18. J. J. Vallooran *et al.*, Lipidic cubic phases as a versatile platform for the rapid detection of biomarkers, viruses, bacteria, and parasites. *Adv Funct Mater* **26**, 181-190 (2016).
19. R. Negrini, R. Mezzenga, Ph-responsive lyotropic liquid crystals for controlled drug delivery. *Langmuir* **27**, 5296-5303 (2011).
20. D. Marsh, J. M. Seddon, Gel-to-inverted hexagonal (l beta-hii) phase transitions in phosphatidylethanolamines and fatty acid-phosphatidylcholine mixtures, demonstrated by 31p-nmr spectroscopy and x-ray diffraction. *Biochim Biophys Acta* **690**, 117-123 (1982).
21. J. M. Seddon, G. Cevc, R. D. Kaye, D. Marsh, X-ray diffraction study of the polymorphism of hydrated diacyl- and dialkylphosphatidylethanolamines. *Biochemistry* **23**, 2634-2644 (1984).

22. J. Barauskas *et al.*, Synthesis and aqueous phase behavior of 1-glyceryl monooleyl ether. *Colloids Surf. B Biointerf* **41**, 49-53 (2005).
23. B. J. Boyd, D. V. Whittaker, S. M. Khoo, G. Davey, Hexosomes formed from glycerate surfactants - formulation as a colloidal carrier for irinotecan. *Int J Pharmaceut* **318**, 154-162 (2006).
24. M. Nakano *et al.*, Dispersions of liquid crystalline phases of the monoolein/oleic acid/pluronic f127 system. *Langmuir* **18**, 9283-9288 (2002).
25. Y. D. Dong, I. Larson, T. Hanley, B. J. Boyd, Bulk and dispersed aqueous phase behavior of phytantriol: Effect of vitamin e acetate and f127 polymer on liquid crystal nanostructure. *Langmuir* **22**, 9512-9518 (2006).
26. S. Phan, W. K. Fong, N. Kirby, T. Hanley, B. J. Boyd, Evaluating the link between self-assembled mesophase structure and drug release. *Int J Pharmaceut* **421**, 176-182 (2011).
27. N. Rahanyan-Kagi, S. Aleandri, C. Speziale, R. Mezzenga, E. M. Landau, Stimuli-responsive lipidic cubic phase: Triggered release and sequestration of guest molecules. *Chemistry* **21**, 1873-1877 (2015).
28. W. K. Fong, T. Hanley, B. J. Boyd, Stimuli responsive liquid crystals provide 'on-demand' drug delivery in vitro and in vivo. *J Control Release* **135**, 218-226 (2009).
29. L. Salvati Manni *et al.*, Phase behavior of a designed cyclopropyl analogue of monoolein: Implications for low-temperature membrane protein crystallization. *Angew Chem Int Ed* **54**, 1027-1031 (2015).
30. V. Cherezov, J. Clogston, M. Z. Papiz, M. Caffrey, Room to move: Crystallizing membrane proteins in swollen lipidic mesophases. *Journal of Molecular Biology* **357**, 1605-1618 (2006).
31. A. Zabara, R. Mezzenga, Plenty of room to crystallize: Swollen lipidic mesophases for improved and controlled in-meso protein crystallization. *Soft Matter* **8**, 6535-6541 (2012).
32. D. F. Li, J. Lee, M. Caffrey, Crystallizing membrane proteins in lipidic mesophases. A host lipid screen. *Cryst Growth Des* **11**, 530-537 (2011).
33. C. Fong, T. Le, C. J. Drummond, Lyotropic liquid crystal engineering-ordered nanostructured small molecule amphiphile self-assembly materials by design. *Chem Soc Rev* **41**, 1297-1322 (2012).
34. P. M. Duesing, R. H. Templer, J. M. Seddon, Quantifying packing frustration energy in inverse lyotropic mesophases. *Langmuir* **13**, 351-359 (1997).
35. B. Perly, I. C. Smith, H. C. Jarrell, Acyl chain dynamics of phosphatidylethanolamines containing oleic acid and dihydrosterculic acid: 2h nmr relaxation studies. *Biochemistry* **24**, 4659-4665 (1985).
36. E. J. Dufourc, I. C. Smith, H. C. Jarrell, A 2h-nmr analysis of dihydrosterculoyl-containing lipids in model membranes: Structural effects of a cyclopropane ring. *Chem Phys Lipids* **33**, 153-177 (1983).
37. C. V. Kulkarni *et al.*, Engineering bicontinuous cubic structures at the nanoscale-the role of chain splay. *Soft Matter* **6**, 3191-3194 (2010).
38. S. Engstrom, P. Wadsten-Hindrichsen, B. Hernius, Cubic, sponge, and lamellar phases in the glyceryl monooleyl ether-propylene glycol-water system. *Langmuir* **23**, 10020-10025 (2007).
39. T. H. Nguyen, T. Hanley, C. J. Porter, B. J. Boyd, Nanostructured reverse hexagonal liquid crystals sustain plasma concentrations for a poorly water-soluble drug after oral administration. *Drug Deliv Transl Res* **1**, 429-438 (2011).
40. A. Zabara, R. Negrini, P. Baumann, O. Onaca-Fischer, R. Mezzenga, Reconstitution of ompf membrane protein on bended lipid bilayers: Perforated hexagonal mesophases. *Chem Commun* **50**, 2642-2645 (2014).
41. D. Li, S. T. Shah, M. Caffrey, Host lipid and temperature as important screening variables for crystallizing integral membrane proteins in lipidic mesophases. Trials with diacylglycerol kinase. *Cryst Growth Des* **13**, 2846-2857 (2013).
42. S. H. White, W. C. Wimley, Membrane protein folding and stability: Physical principles. *Annu Rev Biophys Biomol Struct* **28**, 319-365 (1999).

43. U. Weierstall *et al.*, Lipidic cubic phase injector facilitates membrane protein serial femtosecond crystallography. *Nat Commun* **5**, 3309 (2014).
44. R. Bergman, J. Swenson, Dynamics of supercooled water in confined geometry. *Nature* **403**, 283-286 (2000).
45. G. Hummer, J. C. Rasaiah, J. P. Noworyta, Water conduction through the hydrophobic channel of a carbon nanotube. *Nature* **414**, 188-190 (2001).
46. M. Cammarata *et al.*, Structure and dynamics of water confined in silica hydrogels: X-ray scattering and dielectric spectroscopy studies. *Eur Phys J E Soft Matter* **12 Suppl 1**, S63-66 (2003).
47. N. E. Levinger, Water in confinement. *Science* **298**, 1722-1723 (2002).
48. P. O. Eriksson, G. Lindblom, Lipid and water diffusion in bicontinuous cubic phases measured by nmr. *Biophys J* **64**, 129-136 (1993).
49. L. M. Antognini, S. Assenza, C. Speziale, R. Mezzenga, Quantifying the transport properties of lipid mesophases by theoretical modelling of diffusion experiments. *J. Chem. Phys.* **145**, (2016).

Chapter 4

Digestion of monoacylglycerols and their cyclopropanated derivatives: molecular structure and nanostructure determine rate of digestion.

As fully hydrated mesophases (*Pn3m*, H_{II}, etc.) can coexist with excess of water, they can be dispersed to form nanostructured particles in the presence of a surface stabilizer. They are named in accordance with the geometry of their internal nanostructure: dispersed cubic phases are called cubosomes (*1*) and hexagonal phases are called hexosomes (*2*), analogous to dispersed lamellar particles, liposomes (*3*). Important physicochemical properties like thermotropicity, biodegradability and amphiphilicity of the bulk lipidic cubic phase (LCP) are correspondingly preserved in the dispersion (*4*), while retention of the geometry depends on the nature and the amount of the stabilizer (*5*). Such colloidal particles constitute a potential solution to the a number of issues associated with the size and complexity of the bulk systems and the difficulties in handling a viscous, sticky bulk mesophase (*6*). Because of their unique set of properties and their stability in aqueous environments, cubosomes have been largely studied as drug delivery systems for small hydrophilic (*7*) and hydrophobic (*8*) molecules. Since different geometries present different release rate upon dilution, on-demand manipulation of dispersed nanostructured particles that change their phase behavior has been developed as a method to control this release. For instance, dispersed cubic systems – cubosomes - exhibit burst release upon dilution, while liposomes and hexosomes are known to be slower releasing mesophases (*4*). The dynamic phase behavior alteration from a mesophase which is slow releasing to a mesophase that displays fast release with an external stimulus has been conceived as the trigger mechanism for the dynamic release of encapsulated drug (*9*). This has led recently to the development of stimuli responsive lipidic particles that respond to photothermal, magnetic, ultrasound stimuli as well as pH variation (*4*).

Upon ingestion, lipid metabolism and absorption takes place in the gastrointestinal tract which is regulated by enzymatic hydrolysis (*10, 11*). A first digestion takes place in the stomach with the action of the gastric lipase (*12*), followed by a second and more efficient digestion in the small intestine by water soluble pancreatic lipase at the oil-water interface (*13*). This enzyme is responsible for the cleavage of the ester bonds that connect the glycerol head group to the lipidic chain(s). In the last few years, it has been shown that ester hydrolysis results in the complex dynamic transformation of the phase behavior of the digested lipid (*14-16*). These phase transitions from various lamellar and non-lamellar nanostructures, which were observed for the first time during digestion of olive oil (*14*) were recently characterized using synchrotron SAXS in animal (*17*) and human milk (*18*). This discovery has reinvigorated the search for synthetic and mixed lipid formulations, opening up the possibility of using enzymatic hydrolysis (*19*) as a stimulus to achieve the desired phase transitions in lipidic nanocarriers for a better assimilation of drugs, lipophilic vitamins and nutrients (*20-24*).

Despite the fast development of basic research on cubosomes and the increasing popularity of these dispersed particles in last few years, few lipids have been engineered and tested for the development of new formulations. Additionally, few studies have systematically investigated absorption, metabolism and toxicity of these nanoparticles upon administration to the body, as this is one of the main limiting factors in the applicability of such materials. Interestingly, of the two most studied lipids that form LCP dispersions, phytantriol (PT) and MO, the former has shown higher toxicity *in vitro*, suggesting that monoacylglycerols are more biocompatible for drug delivery formulations (*25*). Since the phase behavior of the dispersed mesophases can be different from that of the original bulk phase, physicochemical characterization of new dispersed systems is essential for the development of novel smart stimuli-responsive materials.

Cyclopropanated lipids have been found to be an important component of several bacterial membranes, different seed oils, plants and in a smaller amount within lipids produced by animals (*26*) and in mammalian tissues, including humans (*27*). Although cyclopropyl fatty acids are widely spread between different species and have been detected in several dairy products like milk and cheese (*28*), in nuts (*29*) and in wine (*30*), not much is known about the toxicity of these lipids to humans and the way they are processed and assimilated during digestion (*27*). Their interesting phase behavior in bulk makes them potential candidates for novel formulations. In this work, the dynamic digestion of three synthesized designer cyclopropanated lipids that are able to form nanostructured colloidal particles have been studied, and their digestion is compared with that of the corresponding *cis*-unsaturated commercially available lipids. Time resolved SAXS measurements are used to monitor the phase changes during the digestion combined with kinetic data from the titration of the produced acid.

4.1 Results and discussion

The cyclopropanated lipids MDS (1-(*cis*-9,10-methylene-octadecanoyl)-*rac*-glycerol), CPMP (1-(*cis*-9,10-methylene-hexadecanoyl)-*rac*-glycerol) and DCPML (1-(*cis*-*cis*-9,10-12,13-*bis*-methylene-octadecanoyl)-*rac*-glycerol), and their corresponding unsaturated lipids MO (monoolein), MP (monopalmitolein) and ML (monolinolein) were used to form dispersed nanostructured particles at 37 °C and their digestion behavior was studied with time-resolved synchrotron SAXS. Each lipid was dispersed (5% w/w) in a 0.5% Pluronic F108 in milliQ water and the initial phase was determined by SAXS, as shown in **Figure 1**, **2** and **3** as a red spectrum.

The initial phases are different for the different lipids and the nanostructure was not always conserved in comparison with the bulk phase. For example, MP (**Figure 2)** forms a *Pn3m* phase in excess of water at 37°C, while in dispersion it forms a *Im3m* phase. In contrast, the corresponding cyclopropanated lipid CPMP (**Figure 2)** retains the *Pn3m* geometry upon dispersion, like in the bulk system. Studies on the phase retention of MO cubosomes show that the phase behavior can be strongly influenced by the stabilizer, and that Pluronic F108 is the most effective stabilizer in retaining the cubic geometry. In accordance with our data this phase retention is strongly dependent on the nature of the lipid, and stability tests have to be performed for the different formulations. Interestingly, MO and its corresponding cyclopropanated lipid, MDS (**Figure 1)**, reveal a coexistence of *Pn3m* and *Im3m* phases with similar lattice parameters for the two different lipids, even though the two systems show different phase behaviors in bulk as is shown in the previous chapter of this thesis. Thus MO forms cubosomes of *Pn3m* and *Im3m* geometries with lattice parameters of 96 Å and 135 Å, respectively. Similarly, MDS forms *Pn3m* and *Im3m* dispersed particles with lattice parameters of 95 Å and 141 Å, respectively. As expected from the bulk phase diagram studies, pure ML forms a *Pn3m* phase, while the corresponding cyclopropanated lipid DCPML forms an H_{II} phase at 37 °C as well as in bulk (**Figure 3)**. This particular resistance of DCPML hexosomes to phase transition, together with the possibility to be still digested and eventually assimilated makes this novel lipid extremely appealing for several applications that require a slow release phase which is stable at physiological temperature (*31*).

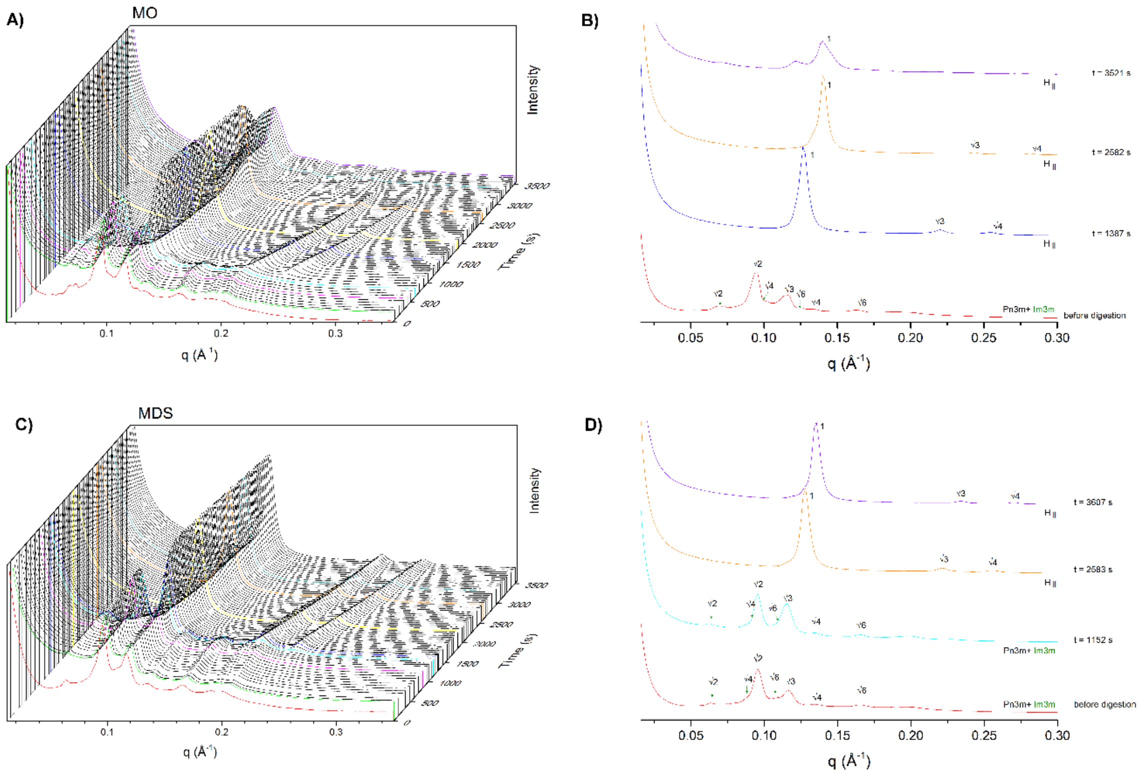

Figure 1. SAXS profiles showing time-resolved intensity vs scattering vector q during the lipase digestion of a dispersion of MO (A) and MDS (C). SAXS spectra of the various phases that occur during the lipase-induced transformations are depicted for MO (B) and MDS (D). For both lipids the initial dispersion forms a coexistence of *Im3m* and *Pn3m* cubic phases, while subsequent digestion leads to the formation of pure *Pn3m* and eventually to the H_{II} phase. The digestion of MO shows the final *FI* structure at 3500s, while MDS still presents a sharp H_{II} signal at the same time.

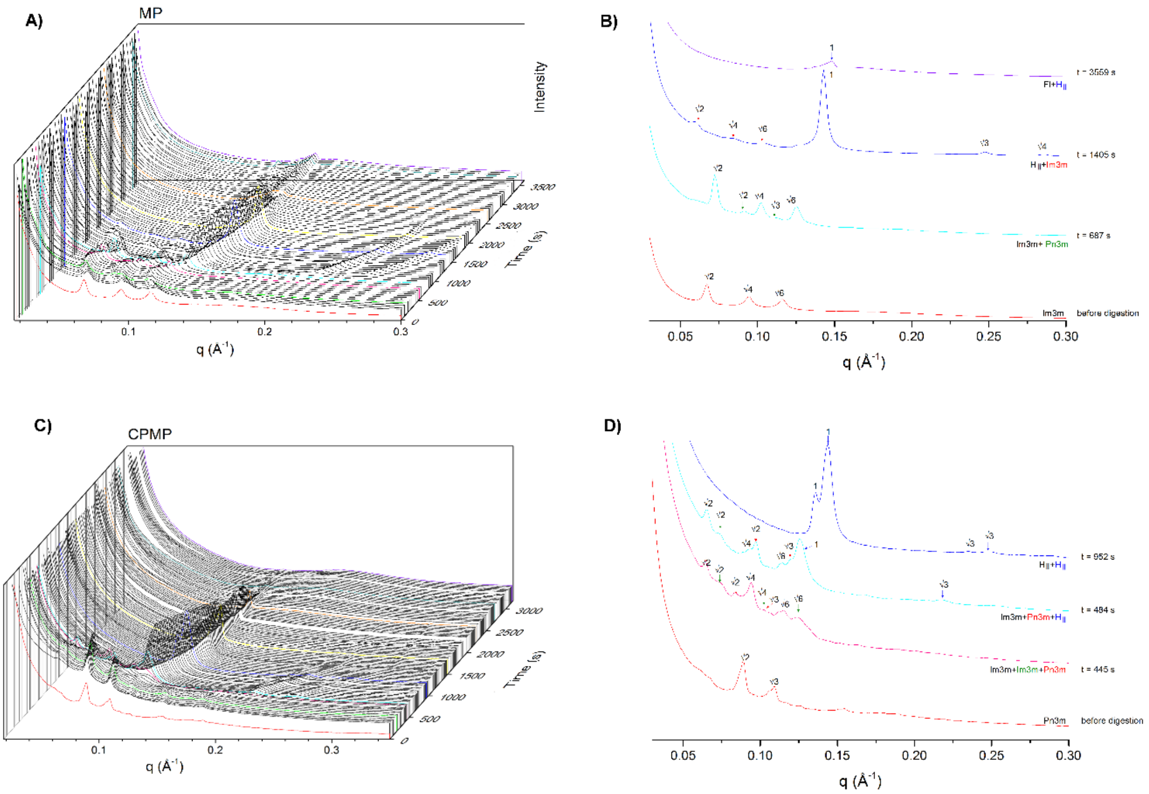

Figure 2. SAXS profiles showing time-resolved intensity vs scattering vector q during the lipase digestion of a dispersion of MP (A) and CPMP (C). SAXS spectra of the various phases that occur during the lipase-induced transformations are depicted for MP (B) and CPMP (D). For MP the initial dispersion forms a *Im3m* phase, subsequent digestion leads to the formation of the *Pn3m* phase in coexistence with the initial *Im3m*. Further digestion leads to a coexistence of *Im3m* and H_{II} phases and finally the system is digested to *FI*. For CPMP the initial dispersion forms a *Pn3m* phase, after 400s a complex phase coexistence with two different *Im3m* phases and a *Pn3m* has been characterized. Further digestion leads to a coexistence of *Im3m*, *Pn3m* and H_{II} phases, followed by two different H_{II} phases and a final dissolution of the structure at ca. 2500s.

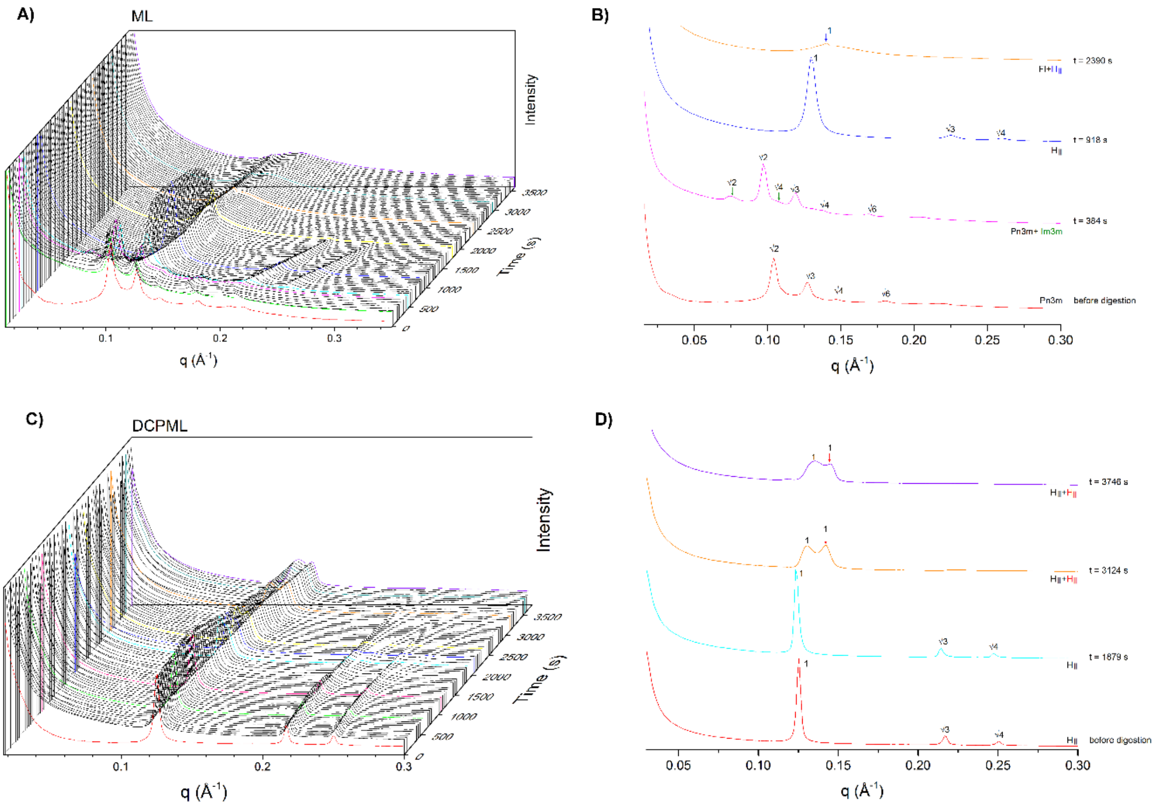

Figure 3. SAXS profiles showing time-resolved intensity vs scattering vector q during the lipase digestion of a dispersion of ML (A) and DCPML (C). SAXS spectra of the various phases that occur during the lipase-induced transformations are depicted for ML (B) and DCPML (D). For ML the initial dispersion forms a *Pn3m* phase, subsequent digestion leads to the formation of the *Im3m* phase in coexistence with the initial *Pn3m*. Further digestion leads to H_{II} phase and finally to *FI*. For DCPML the initial dispersion forms a H_{II} phase, after 2500s the system evolves to a coexistence of two different H_{II} phases that are stable for more than 3500s.

Once digested, all the cubosomes are converted into hexosomes, but the transition between the two different cubic geometries (*Pn3m*-*Im3m*) can be inverted.

The digestion of cyclopropanated lipids was found to be generally slower than that of the corresponding *cis*-unsaturated lipids. In the case of ML and DCPML the different rates could be rationalized by the different geometries and the slower diffusion of hydrophilic molecules in the H_{II} phase than in a *Pn3m* cubic phase (*32*, *33*), explaining the slower action of the enzyme that is confined in the aqueous channel. This approach cannot be considered for the MO-MDS systems that show similar initial phase behavior, but a different digestion rate.

This suggests that the packing arrangement of the lipidic chain influences the availability of the polar head group even if the geometry and the lattice parameters of the two phases are similar, resulting in a greater resistance to digestion for the cyclopropanated lipid.

Time resolved NMR studies were performed in order to establish the relative amounts of sn1 and sn2 hydrolysis during the digestion of MP. **Figure 4** shows the ^{1}H-NMR spectra at t=0 when the only two lipid molecules in the mixture are 1-MP and 2-MP. After 1h digestion (**Figure 5)** the peaks of the digested lipids and the two esters are still present in the mixture. The ratio between 1-MP and 2-MP was calculated using the integral of the H2' of both esters (the signal of H1'of 1-MP has the same chemical shift as that of the stabilizer), indicating that no significant change occurred. The total digestion was calculated using the ratio between the integral of the ^{1}H of the olefin (H 9,10) and the signals from both esters: After 1h, 50% of both 1-MP and 2-MP were hydrolyzed to acid. Kinetic experiments by acid titration were carried out to establish the rate of the reaction for the different lipids. After testing by NMR that both esters (sn1 and sn2) are hydrolyzed by the considered enzyme, with no remarkable selectivity for one of the two glycerol position, and considering that NMR kinetic measurements are less sensitive and did not show any substantial difference with the titration data, they were not performed on the synthetic lipids.

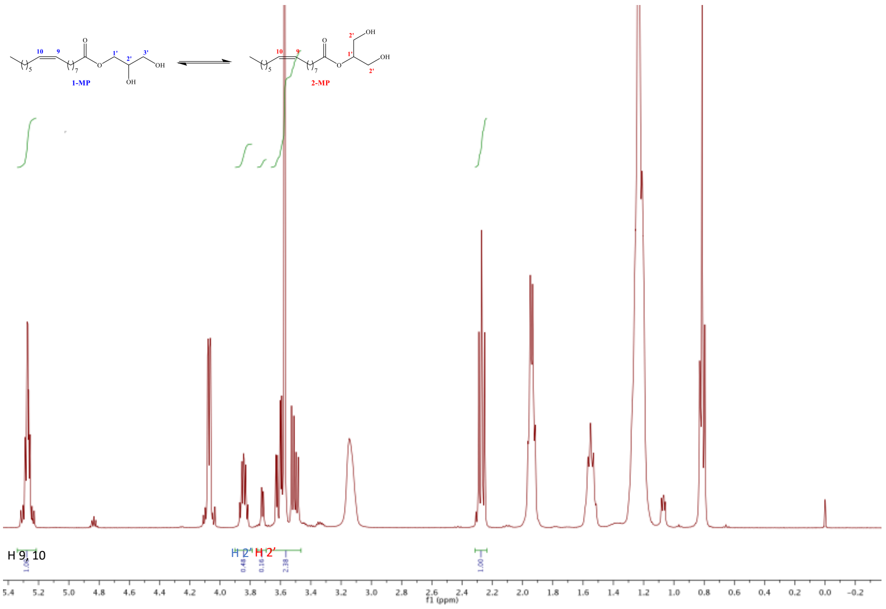

Figure 4. ^{1}H-NMR spectrum of the MP digestion mixture before lipase addition (t=0). The natural equilibrium of 1-MP and 2-MP is shown at the top of the figure. Signals related to 1-MP are reported in blue, signals related to 2-MP in red and the signal of the mixture in black.

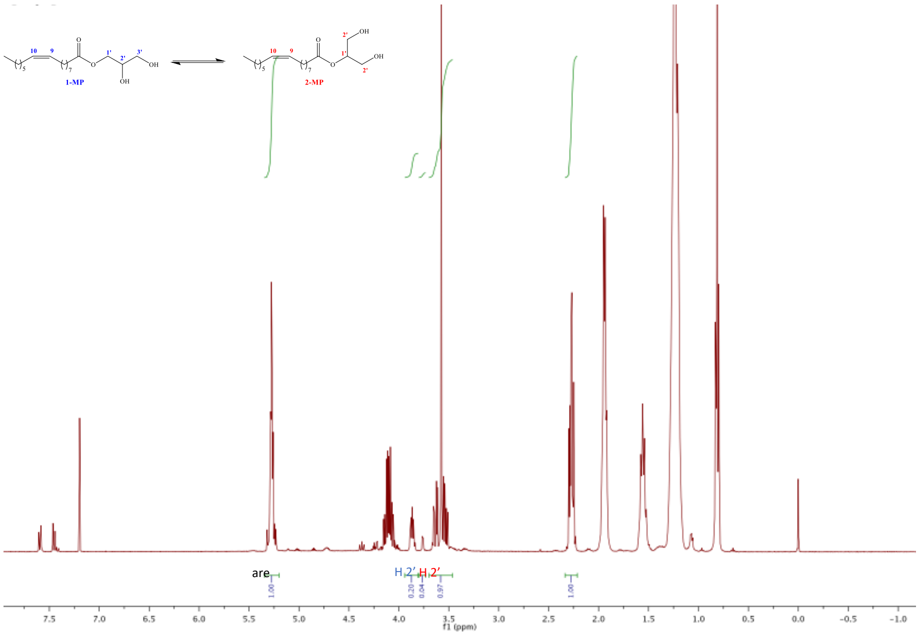

Figure 5. ^{1}H-NMR spectrum of the MP digestion mixture at t=3600s after lipase addition. The natural equilibrium of 1-MP and 2-MP is shown at the top of the figure. Signals related to 1-MP are reported in blue, signals related to 2-MP in red and the signal of the mixture acid/ester in black.

4.2 Materials and methods

Cyclopropanated lipids were synthetized according to the procedure previously reported by Salvati Manni et al. (*34*) and as reported in **chapter 2** of this thesis. Purity of the lipids was confirmed by ^{1}H-NMR, ^{13}C-NMR and mass spectroscopy. Monoolein (MO), Monopalmitolein (MP) and Monolinolein (ML) were purchased from Nu-Check. 4- bromophenylboronic acid (4-BPBA, >95%) was purchased from Sigma Aldrich (St. Louis, MO, USA). Lipase USP grade pancreatin extract was purchased from Southern Biologicals (Nunawading, Victoria, Australia), the enzyme was reconstituted by dissolving 340mg of dry extract in 1.8 ml of digestion buffer (50 mM Tris maleate, 5 mM CaCl2·2H2O, 150 mM NaCl, 6 mM NaN3 as anti-microbial agent, pH adjusted with NaOH to 6.5)

Preparation of nanostructured dispersions

Nanostructured dispersions were produced by hydrating each lipid with 0.5% Pluronic F108 in milliQ water to prepare a 5% (w/w) lipid dispersion. The coarse dispersion was further processed with a probe sonicator with pulsed sonication for 10 min at 20% amplitude. Digestion buffer was added to obtain a 3% (w/w) lipid dispersion.

Small Angle X-ray Scattering (SAXS)

Time resolved SAXS (TRSAXS) data for the enzymatic studies were collected on the SAXS/WAXS beamline at the Australian Synchrotron. *In vitro* digestion experiments were conducted in a thermostated glass digestion vessel at 37 °C (*15*). 10 mL of the dispersion was equilibrated in the digestion vessel before the remote addition of 1 mL of lipase solution (10 mg/mL) to initiate digestion. The digestion medium was pumped (10 mL/min) through a 1.5 mm quartz capillary flow cell using a peristaltic pump and the quartz capillary was placed in the X-ray beam (*35*).

The scattering profiles were acquired for 5 s every 10 s at an energy of 10 keV using a Pilatus 1 M detector (active area 169×179 mm^2 with a pixel size of 172 μm) with a sample-to-detector distance of 1015 mm, providing a q range of $0.01\ \text{Å}^{-1} < q < 0.7\ \text{Å}^{-1}$. The scattering images were integrated into the one-dimensional scattering function I(q) using the in-house-developed software package ScatterBrain. The q range calibration was made using silver behenate as the standard. The cubic and hexagonal phase space groups and lattice parameters were determined by the relative positions of the Bragg peaks in the scattering curves, which correspond to the reflections on planes defined by their (hkl) Miller indices (*36*).

Dispersed LLC phases in excess water are readily identified using SAXS, where each phase can be identified by its specific Bragg peak positions. For the double diamond cubic phase (V_2, *Pn3m*) the Bragg reflections occur at relative position in q at √2:√3:√4:√6:√8:√9… and for the primitive bicontinuous cubic phase (V_2, *Im3m*) the Bragg peaks occur at q = √2:√4:√6:√8:√10…. The H_{II} phase is identified by reflections at 1:√3:√4…, and the L_2 phase is identified by a singular characteristic broad peak. The mean lattice parameter, a, was deduced from the corresponding set of observed interplanar distance, d ($d = 2\pi/q$), using the appropriate scattering law for the phase structure. For cubic phases:

$$a = d\sqrt{h^2 + k^2 + l^2} \tag{1}$$

while for the H_2 phase:

$$a = \frac{4\Pi}{q\sqrt{3}}\sqrt{h^2 + hk + k^2} \tag{2}$$

For the L_2 phase, which shows only one broad peak, d is termed the characteristic distance.

NMR studies

Nanostructured dispersions for NMR studies were prepared following the same procedure as described above. At t=0 a solution of pancreatin in digestion buffer was added to the lipidic dispersion. 2ml samples of the mixture were taken at different times and the enzymatic reaction was stopped by adding 200µl of the 4-BPBA solution (0.5M in MeOH). The dispersion was then freeze-dried to remove methanol, and the water phase was extracted with CH_2Cl_2. The organic layer was dried on $NaSO_4$, filtered and evaporated. The lipid was then dissolved in $CDCl_3$ and analyzed by ^{1}H-NMR.

References

1. S. Andersson, M. Jacob, S. Lidin, K. Larsson, Structure of the cubosome - a closed lipid bilayer aggregate. *Z Kristallogr* **210**, 315-318 (1995).
2. B. J. Boyd, D. V. Whittaker, S. M. Khoo, G. Davey, Hexosomes formed from glycerate surfactants - formulation as a colloidal carrier for irinotecan. *Int J Pharmaceut* **318**, 154-162 (2006).
3. A. Yaghmur, L. de Campo, L. Sagalowicz, M. E. Leser, O. Glatter, Control of the internal structure of mlo-based isasomes by the addition of diglycerol monooleate and soybean phosphatidylcholine. *Langmuir* **22**, 9919-9927 (2006).
4. W. K. Fong, R. Negrini, J. J. Vallooran, R. Mezzenga, B. J. Boyd, Responsive self-assembled nanostructured lipid systems for drug delivery and diagnostics. *J Colloid Interface Sci* **484**, 320-339 (2016).
5. J. Y. T. Chong, X. Mulet, L. J. Waddington, B. J. Boyd, C. J. Drummond, Steric stabilisation of self-assembled cubic lyotropic liquid crystalline nanoparticles: High throughput evaluation of triblock polyethylene oxide-polypropylene oxide-polyethylene oxide copolymers. *Soft Matter* **7**, 4768-4777 (2011).
6. S. Aleandri, D. Bandera, R. Mezzenga, E. M. Landau, Biotinylated cubosomes: A versatile tool for active targeting and code livery of paclitaxel and a fluorescein-based lipid dye. *Langmuir* **31**, 12770-12776 (2015).
7. Z. Karami, M. Hamidi, Cubosomes: Remarkable drug delivery potential. *Drug Discov Today* **21**, 789-801 (2016).
8. B. J. Boyd, Characterisation of drug release from cubosomes using the pressure ultrafiltration method. *Int J Pharmaceut* **260**, 239-247 (2003).
9. M. Kang, G. Huang, C. Leal, Role of lipid polymorphism in acoustically sensitive liposomes. *Soft Matter* **10**, 8846-8854 (2014).
10. J. Borovicka *et al.*, Regulation of gastric and pancreatic lipase secretion by cck and cholinergic mechanisms in humans. *Am J Physiol Gastrointest Liver Physiol* **273**, G374-G380 (1997).
11. H. Moreau *et al.*, Immunocytolocalization of human gastric lipase in chief cells of the fundic mucosa. *Histochemistry* **91**, 419-423 (1989).
12. M. Hamosh *et al.*, Fat digestion in the newborn - characterization of lipase in gastric aspirates of premature and term infants. *J Clin Invest* **67**, 838-846 (1981).
13. A. B. R. Thomson, M. Keelan, M. L. Garg, M. T. Clandinin, Intestinal aspects of lipid absorption - in review. *Can J Physiol Pharmacol* **67**, 179-191 (1989).
14. J. S. Patton, M. C. Carey, Watching fat digestion. *Science* **204**, 145-148 (1979).
15. D. B. Warren, M. U. Anby, A. Hawley, B. J. Boyd, Real time evolution of liquid crystalline nanostructure during the digestion of formulation lipids using synchrotron small-angle x-ray scattering. *Langmuir* **27**, 9528-9534 (2011).
16. S. Salentinig, L. Sagalowicz, M. E. Leser, C. Tedeschi, O. Glatter, Transitions in the internal structure of lipid droplets during fat digestion. *Soft Matter* **7**, 650-661 (2011).
17. S. Salentinig, S. Phan, J. Khan, A. Hawley, B. J. Boyd, Formation of highly organized nanostructures during the digestion of milk. *ACS Nano* **7**, 10904-10911 (2013).
18. S. Salentinig, S. Phan, A. Hawley, B. J. Boyd, Self-assembly structure formation during the digestion of human breast milk. *Angew Chem Int Ed* **54**, 1600-1603 (2015).
19. R. de la Rica, D. Aili, M. M. Stevens, Enzyme-responsive nanoparticles for drug release and diagnostics. *Adv Drug Deliv Rev* **64**, 967-978 (2012).

20. W. K. Fong *et al.*, Generation of geometrically ordered lipid-based liquid-crystalline nanoparticles using biologically relevant enzymatic processing. *Langmuir* **30**, 5373-5377 (2014).
21. L. D. Hong, S. Salentinig, A. Hawley, B. J. Boyd, Understanding the mechanism of enzyme-induced formation of lyotropic liquid crystalline nanoparticles. *Langmuir* **31**, 6933-6941 (2015).
22. J. Borne, T. Nylander, A. Khan, Effect of lipase on monoolein-based cubic phase dispersion (cubosomes) and vesicles. *J Phys Chem B* **106**, 10492-10500 (2002).
23. S. Phan, S. Salentinig, C. A. Prestidge, B. Boyd, Self-assembled structures formed during lipid digestion: Characterization and implications for oral lipid-based drug delivery systems. *Drug Deliv Transl Res* **4**, 275-294 (2014).
24. S. Phan *et al.*, Structural aspects of digestion of medium chain triglycerides studied in real time using ssaxs and cryo-tem. *Pharm Res* **30**, 3088-3100 (2013).
25. T. M. Hinton *et al.*, Bicontinuous cubic phase nanoparticle lipid chemistry affects toxicity in cultured cells. *Toxicol Res* **3**, 11-22 (2014).
26. S. Shah, J. M. White, S. J. Williams, Total syntheses of cis-cyclopropane fatty acids: Dihydromalvalic acid, dihydrosterculic acid, lactobacillic acid, and 9,10-methylenehexadecanoic acid. *Org Biomol Chem* **12**, 9427-9438 (2014).
27. T. Sledzinski *et al.*, Identification of cyclopropaneoctanoic acid 2-hexyl in human adipose tissue and serum. *Lipids* **48**, 839-848 (2013).
28. A. Caligiani, A. Marseglia, G. Palla, An overview on the presence of cyclopropane fatty acids in milk and dairy products. *J Agr Food Chem* **62**, 7828-7832 (2014).
29. L. O. Hanus, P. Goldshlag, V. M. Dembitsky, Identification of cyclopropyl fatty acids in walnut (juglans regia l.) oil. *Biomed Pap* **152**, 41-45 (2008).
30. H. Teixeira, M. G. Goncalves, N. Rozes, A. Ramos, M. V. San Romao, Lactobacillic acid accumulation in the plasma membrane of oenococcus oeni: A response to ethanol stress? *Microbial Ecol* **43**, 146-153 (2002).
31. T. H. Nguyen, T. Hanley, C. J. Porter, B. J. Boyd, Nanostructured reverse hexagonal liquid crystals sustain plasma concentrations for a poorly water-soluble drug after oral administration. *Drug Deliv Transl Res* **1**, 429-438 (2011).
32. L. M. Antognini, S. Assenza, C. Speziale, R. Mezzenga, Quantifying the transport properties of lipid mesophases by theoretical modelling of diffusion experiments. *J. Chem. Phys.* **145**, 084903 (2016).
33. R. Negrini, R. Mezzenga, Ph-responsive lyotropic liquid crystals for controlled drug delivery. *Langmuir* **27**, 5296-5303 (2011).
34. L. Salvati Manni *et al.*, Phase behavior of a designed cyclopropyl analogue of monoolein: Implications for low-temperature membrane protein crystallization. *Angew Chem Int Ed* **54**, 1027-1031 (2015).
35. N. M. Kirby *et al.*, A low-background-intensity focusing small-angle x-ray scattering undulator beamline. *J Appl Crystallogr* **46**, 1670-1680 (2013).
36. S. T. Hyde, *Handbook of applied surface and colloid chemistry*. (John Wiley & Sons, 2002).

Chapter 5

Membrane protein crystallization.

In this thesis, four different membrane proteins have been studied with the purpose of investigating the utilization of lipidic cubic phases (LCPs) formed by tailor-made cyclopropanated lipids for membrane protein crystallization (exemplified by bacteriorhodopsin, bR) and for membrane protein structural studies (*Escherichia coli* chloride channel EcClC, *Ralstonia metallidurans* Rm1ClC, and the lipopolysaccharide transporter LptD-LptE). These membrane proteins will first be introduced, and subsequently their crystallization within LCPs and their diffraction resolution using synchrotron X-ray diffraction will be presented and discussed.

Bacteriorhodopsin

Bacteriorhodopsin (bR) is an integral membrane protein composed of the apoprotein bacterioopsin with its seven transmembrane α-helices, and the chromophore *trans*-retinal in the center of the structure connected through a Schiff base linkage to lysine 216 on helix G (*1*). bR is the best known light driven proton pump, it is powered by wavelengths of green light and it is the main component of the purple membrane (PM) of *Halobacterium salinarum* (*2*). The bacterial rhodopsin family is highly conserved among species especially in oceanographic bacteria, suggesting that rhodopsin mediated phototrophy is the most widespread mechanism to convert sunlight into chemical energy in biological systems (*3*). The structure of bR was the first structure of a membrane protein that was elucidated already in 1975: the presence of 2D crystals of bR clusters in the PM made it possible to get structural information via electron diffraction with a resolution of 7 Å (*4*). In the last four decades, bR has been extensively characterized and numerous structures have been deposited in the protein data bank: 84 by X-ray diffraction, 6 by electron diffraction and 3 by NMR (*1*).

Most importantly for the purpose of this thesis, bR was also the first membrane protein that was crystallized, and whose high resolution X-ray structure elucidated using the LCP method (*5*). The crystal habit and diffraction limit of bR was shown to critically depend on the identity of the hosting LCP-lipid (*5*), albeit the molecular determinants of this dependency are still elusive. In a recent work (*6*) an atomic resolution movie of the conformational changes that occur in the nanoseconds to milliseconds after photoactivation of bR was elucidated using time resolved serial femtosecond crystallography at an x-ray free electron laser. One of the 13 structural snapshots recorded is presented in **Figure 1**.

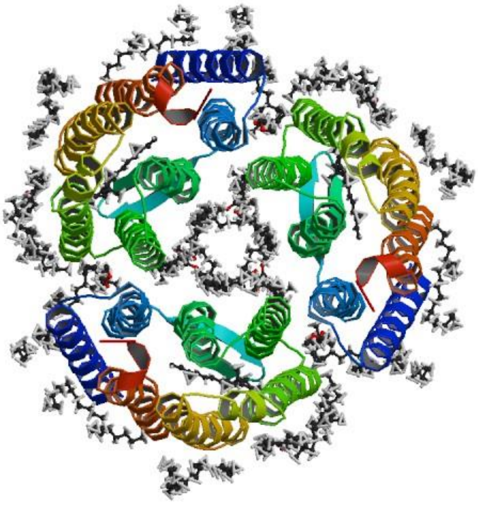

Figure 1. Resting state structure at 2.0 Å resolution of bacteriorhodopsin. The 10 ligands reported in the structure are molecules of native lipids, lipidic metabolites and retinal. PDB **5B6V.**

Due its high stability and the ability to reproduce well known crystallization conditions, bR was chosen as a model membrane protein to test the applicability of cubic phases formed with cyclopropanated lipids for crystallization of membrane proteins, and to study the effect of a different lipidic environment on the protein crystal morphology.

Lipopolysaccharide transporter

The lipopolysaccharide transporter (Lpt) is a machinery which consists of 7 different proteins: LptA, LptB, LptC, LptD, LptE, LptF and LptG. This machinery spans the bacterial membrane and is responsible for the transport of lipopolysaccharides (LPS) from the cytoplasm to the cell surface (*7*). LPS are complex glycolipids that form an integral component of the outer leaflet of the outer membrane (OM) of gram-negative bacteria. The presence of LPS on the OM is essential for the stability of the OM and for the survival of the bacteria in harsh conditions, and constitute one of the main factors in the development of bacterial resistance to antibiotics (*8*). The synthesis of LPS occurs on the surface between the inner membrane (IM) and the cytoplasm, and these amphiphilic molecules are then transported to the OM by Lpt (*9*). Recent research into antimicrobial peptides has unearthed a new family of antibiotics that presents a new mechanism of antibacterial action by targeting the outer membrane protein, LptD, in *Pseudomonas aeruginosa* (*10*). LptD is involved in the final step of the transport of the LPS from the IM to the OM; its main function being the insertion of the LPS into the outer leaflet of the OM (*11*). The ability of the peptidomimetic antibiotics to bind LptD results in the inhibition of the transport of LPS to the cell surface, and therefore an increase in the permeability of the OM and consequently a decrease in bacterial viability (*12*).

The most studied peptidomimetic antibiotic active on LptD is L27-11, a cyclic peptide that contains a 12-residue loop folded in an β-hairpin conformation (**Figure 2**).

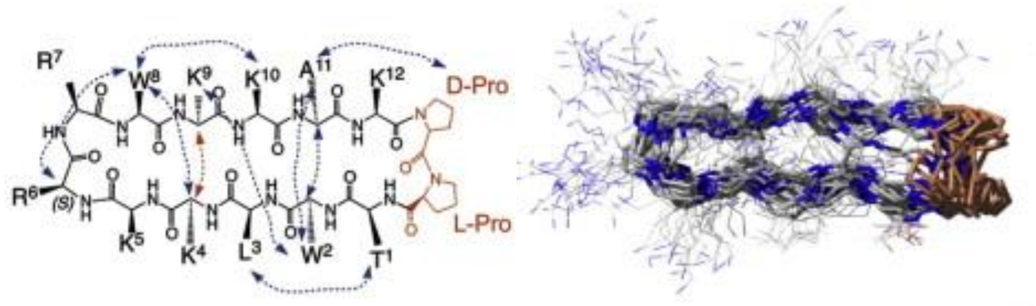

Figure 2. β-hairpin structure of the cyclic peptide L27-11 obtained by NMR. Dotted arrows indicate long range NOEs. Reproduced with permission from (*12*).

L27-11 shows antimicrobial activity against many *Pseudomonas* strains in nanomolar concentration, while it is almost completely inactive against other gram-negative bacteria (*12*). Although the LptD sequence and structure has been shown to be highly conserved for different gram-negative bacteria, LptD in *Pseudomonas* strains has an N-terminal domain that is ~90 amino acids longer than LptD in *E. coli* and *S. flexneri*. The C-terminal domain of LptD creates a transmembrane β-barrel pore composed of 26 antiparallel β-strands that is linked to the N-terminal domain by two pairs of non-consecutive disulfide bonds. An interesting feature of the periplasmic N-terminal domain is the β-jellyroll which consists of two β-sheets with eleven antiparallel β-strands each (*8, 13, 14*).

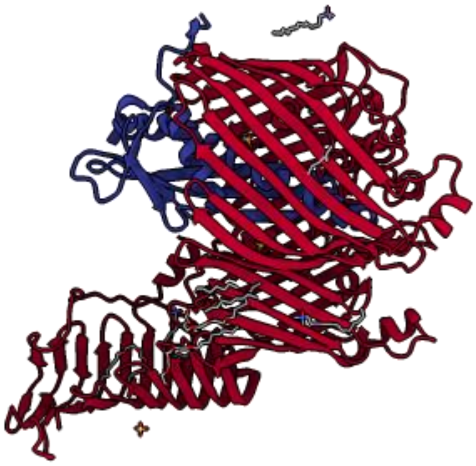

Figure 3. Crystal structure at 2.39 Å resolution of LptD/E from *S. flexneri*. PDB **4Q35.**

In order to determine the mechanism of action of the transporter and the role of the different Lpt proteins, they are being studied separately. In particular, in this thesis, we have attempted to crystallize LptD from *P. aeruginosa* in the absence and in the presence of the peptidomimetic antibiotic L27-11 in order to understand the structure and the inhibition mechanism of this protein. These crystallization experiments were carried out in LCPs.

LptD is purified in a complex together with the lipoprotein LptE. The structure of LptE is essential in forming a stable LptD-LptE complex, where the lipoprotein is attached to the N-terminus of LptD and resides within the LptD β-barrel. Its location is necessary for the correct folding of LptD, and at the same time, the LptE lipidic tail is embedded in the OM anchoring the machinery into the lipidic bilayer (*11*). LptE has also an essential role in the selective binding of LPS, and in the prevention of the passage of various compounds across the LptD β-barrel pore. Recently, high resolution crystal structures of the LptD-LptE complex from *S. typhimurium* and *S. flexneri* have been solved (**Figure 3)** (*13, 14*). However, the mechanism of action of L27-11 is still unresolved. The crystal structure of the complex LptD-LptE from

Pseudomonas aeruginosa could provide important information on the special conformation of the N-terminal domain of this protein and on the specific mechanism of action of the antibiotic.

Chloride channel and transporters

Chloride channels and transporters (ClCs) are membrane proteins abundant in eukaryotic and prokaryotic organisms. ClCs are atypical membrane proteins as they are made up of a dimer with distinct molecular architecture that catalyzes chloride movement across membranes in two distinct mechanisms: chloride-selective passive channels and secondary active chloride/proton antiporters. Since their first discovery in 1979 (*15*), ClCs have been identified in all kingdoms of life, including nine ClC homologues in humans (*16*-*20*). These nine ClC proteins can be found in the plasma membrane as gated chloride channels and play four essential roles: the maintenance of the membrane potential, epithelial ion transport, chloride-proton antiporters in membranes of intracellular vesicles of the endosomal-lysosomal pathway, and regulation of vesicular acidification. They play a diverse role in a variety of physiological processes and their malfunction can lead to several diseases such as myotonia congenita, osteoporosis, and Bartter's syndrome (*21*). However, several of their functions are not yet known and thus a better understanding of their behavior on a molecular level is necessary.

The structural determination of two bacterial homologs (*Salmonella typhimurium* StClC and *Escherichia coli* EcClC) (**Figure 4**) (*22*, *23*), combined with results of functional studies, shed light for the first time on the mechanism of the chloride-proton antiporters and revealed that the chloride movement is coupled to proton translocation with a 2:1 stoichiometry (*24*).

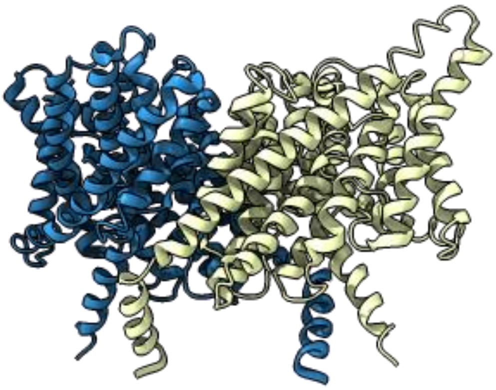

Figure 4. Crystal structure at 3.5 Å resolution of EcClC and Fab Complex. PDB **1KPK**.

Currently, it is believed that approximately half of the ClC family consists of transporters and it is debated how the dualism channel-transporter appeared during the course of evolution (*25*). The structure of EcClC represented a breakthrough in our understanding of this protein family, and subsequently the crucial characterization of the architecture of the well-conserved transmembrane transport domain was achieved. This membrane protein is a homodimer with two identical subunits, each consisting of 18 α-helices and an independent ion translocation pore. The two subunits are organized in an antiparallel architecture. In contrast to eukaryotic ClCs, which are equipped with cytoplasmic domains, EcClC consists only of the catalytic transmembrane domain.

The cytoplasmic domain, when present, is well conserved amongst the ClC family and it was shown to be important for the regulation of function. The high resolution structure is available for several ClC homologues and each constitutes of a tandem repeat of two CBS (cystathionine *β* synthase) subdomains. The ClC homologue from *Ralstonia metallidurans* (RmClC) is one of the few prokaryotic ClCs that contain cytoplasmic domains. The cytoplasmic domain of RmClC was crystallized and the structure solved and described in the dissertation of Dr. Sandra Markovic (University of Zurich, 2010), however, the transmembrane domain structure is still unknown. Crystallization of the full length protein and of the transmembrane domain segment was attempted during this PhD thesis. In addition, the family of ClC channels and transporters is of great importance in physiology and medicine, and structural information of full length homologues containing a cytoplasmic domain are not yet available. Because EcClC crystals were previously obtained from detergent solution but not from LCPs, an LCP-based methodology towards their crystallization was developed.

5.1 Results and discussion

5.1.1 Bacteriorhodopsin

To test the applicability of the cyclopropanated analogous of monoolein, MDS (1-(*cis*-9,10-methylene-octadecanoyl)-*rac*-glycerol) for the crystallization of membrane proteins in low and room temperature LCPs, the light-induced proton pump bacteriorhodopsin (bR) was crystallized from MO- and MDS-LCPs at 20 °C in comparative experiments, as well as from MDS-LCP at 4 °C.

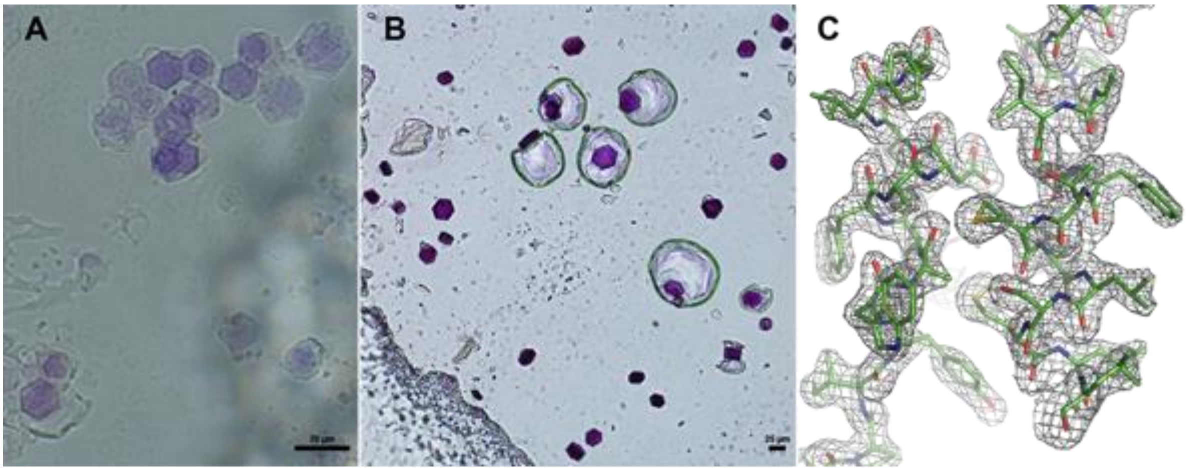

Figure 5. Comparison of bR crystals grown in MDS at 4 °C (A) and 20 °C (B). BR crystals in MDS constitute the first reported crystals of an integral membrane protein (IMP) grown at 4 °C from LCP. (C) Quality of σ_A-weighted $2mF_o$-DF_c electron density map of bR crystallized in MDS at 20 °C, contoured at 1.5 σ. Reproduced with permission from (*26*)

Plate-like hexagonal crystals with an average size of ~18 x 18 x 7 μm were observed after 3 days in MDS at 20 °C, and grew to the full size (~40 x 40 x 20 μm) in 10 days (**Figure 5b**). In contrast, crystallization in monoolein (MO) was slower, yielding fewer initial crystals (sized ~20 x 20 x 7 μm) under identical conditions after 10 days. These crystals grew to the full size in 28 days but remained smaller (~30 x 30 x 12 µm) than in the MDS case. Moreover, using the same crystallization screen, crystals appeared in a much broader range of conditions in MDS than in MO. The best crystals observed at 4 °C were obtained from MDS after 28 days (**Figure 5a**). Crystals were subjected to X-ray crystallographic analyses using synchrotron radiation. They belonged to space group $P6_3$, with one protein molecule in the asymmetric unit. The best diffraction was obtained from crystals grown from MDS-LCP at 20 °C, and the structure was refined at 1.83 Å resolution (**Figures 6 and 7**).

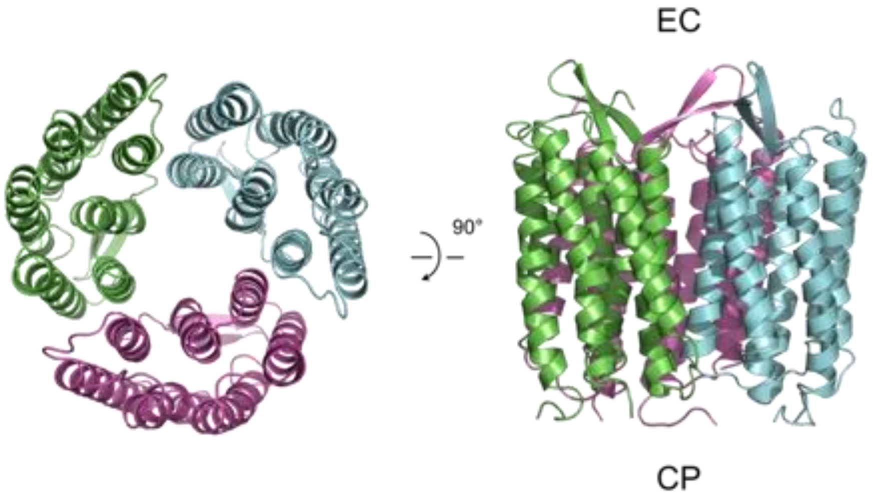

Figure 6. Crystal structure of bR in MDS at 20 °C, shown as a physiological trimer. Left: view perpendicular to the plane of the membrane from the cytoplasmic side. Right: view along the plane of the membrane depicting the extracellular (EC) and cytoplasmic (CP) sides. Reproduced with permission from (*26*).

The packing arrangement of unit cells was found to be lamellar as expected for protein crystals grown in LCP. (**Figure 7**)

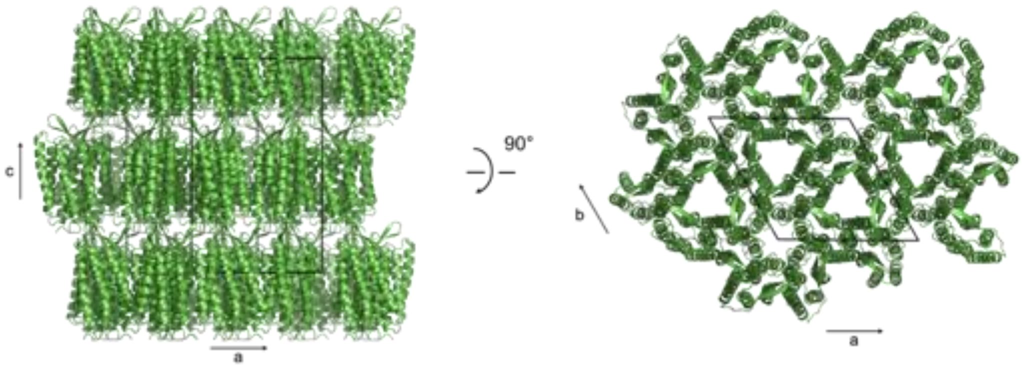

Figure 7. Crystal packing of bR crystallized from MDS LCP at 20 °C. Unit cell axes are indicated.

Reproduced with permission from (*26*)

The quality of σ_A-weighted $2mF_o$-DF_c electron density map is shown in **Figure 5C**. bR crystals grown from MDS LCP at 4 °C were very small (~15 x 15 x 5 µm), yet the crystal structure could be solved at 4.2 Å resolution (**Figure 8**), with identical unit cell parameters as those of the structure generated 20 °C, confirming the validity of the approach at low temperature.

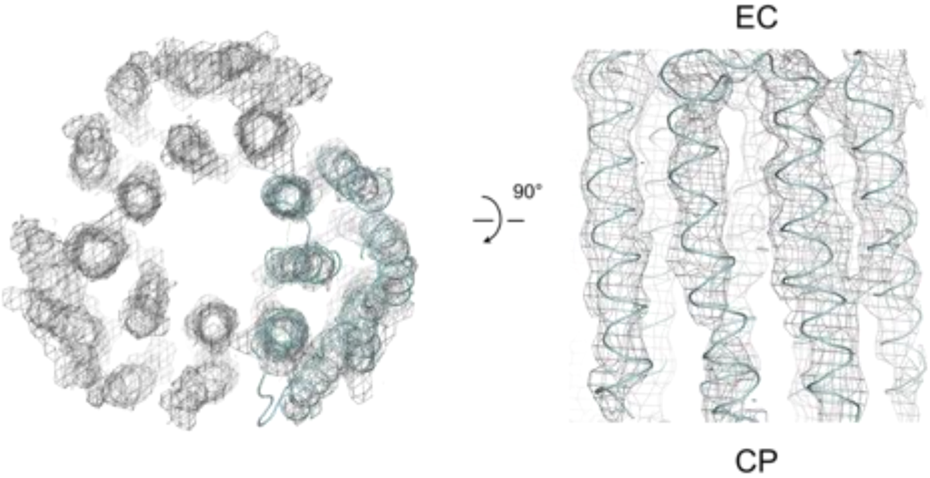

Figure 8. σ_A-weighted $2mF_o$-DF_c electron density map of bR crystallized from MDS LCP at 4 °C, contoured at 1.5 σ. Left: view perpendicular to the plane of the membrane from the cytoplasmic side. Right: view along the plane of the membrane depicting the extracellular (EC) and cytoplasmic (CP) sides. Reproduced with permission from (*26*).

Interestingly, the c axis in the MDS-grown crystals is unusually short (100 Å vs. 110 +/- 2 Å in the MO-grown crystals). This may be due to the smaller thickness of the lipid bilayer formed by the geometrically confined and kinked MDS, resulting in shorter c axis in the crystal, which is parallel to the transmembrane helices.

Crystals grown from MDS-LCP at 20 °C

Crystals belonged to space group $P6_3$, with one protein molecule in the asymmetric unit. X-ray diffraction data were collected from several crystals cryo-cooled to 100 K at beamline X06DA (Swiss Light Source, Villigen, Switzerland) with the PILATUS 2M high-resolution diffractometer at a wavelength $\lambda = 1$ Å. Data were processed and scaled with XDS (*27*). Resolution of the data crossed $I/\sigma(I) = 2.0$ at ~2.1 Å and the data were finally cut at 1.83 Å with $CC_{1/2}$= 10.2% (*28*). As previously reported (*29, 30*) , the crystals exhibited merohedral twinning with a twin fraction of 30% - 40%.

The structure was determined by molecular replacement in Phaser (*31*) using the highest-resolution bR structure (Protein Data Bank accession code 1M0L, 1.47 Å, crystals grown in the LCP) as a search model. The search model was prepared by removing all non-protein atoms except the retinal. Model building was done in Coot (*32*) and refinement was performed with REFMAC5 (*33*) and Phenix (*34*). The final R/R_{free} of the model is 0.1824 / 0.2120, with Ramachandran favored 99% and Ramachandran outliers 0%. Data collection and refinement statistics are shown in **Table 1** and were generated with Phenix Graphical Tools (*35*).

Crystals grown from MDS-LCP at 4 °C

Crystals belonged to space group $P6_3$, with one protein molecule in the asymmetric unit and with identical unit cell parameters to those of the crystals grown from MDS-LCP at 20 °C. X-ray diffraction data were collected from a single crystal cryo-cooled to 100 K at beamline X06SA (Swiss Light Source, Villigen, Switzerland) with the PILATUS 6M high-resolution diffractometer at a wavelength λ = 1 Å. Data were processed and scaled with XDS (*27*). Resolution of the data crossed I/σ(I) = 2.0 at ~7.1 Å and the data were finally cut at 4.2 Å with $CC_{1/2}$ = 66.7% (*28*) and with completeness = 92.5% in the highest resolution shell.

The structure was determined by 5 cycles of rigid-body refinement in REFMAC5 (*33*) with the high-resolution 20 °C-generated bR structure as a starting model, and due to the relatively low resolution of the data was not refined further. Data collection and merging statistics are shown in **Table 1**.

	bR 20 °C	**bR 4 °C**
Wavelength (Å)	1	1
Resolution range (Å)	46.69 - 1.83 (1.895 - 1.83)	36.36 - 4.04 (4.318 - 4.174)
Space group	$P6_3$	$P6_3$
Unit cell (Å)	60.94 60.94 100.13	61.05 61.05 100.15
	90° 90° 120°	90° 90° 120°
Total reflections	238704 (24408)	7304 (722)
Unique reflections	18616 (1862)	1296 (144)
Multiplicity	12.8 (13.1)	4.9 (5.0)
Completeness (%)	99.99 (100.00)	80.80 (92.31)
Mean I/sigma(I)	9.22 (0.59)	1.06 (0.98)
R-merge	0.2502 (4.378)	1.068 (1.697)

R-meas.	0.2607	1.198
$CC_{1/2}$	0.998 (0.102)	0.909 (0.667)
CC*	0.999 (0.372)	0.976 (0.786)
R-work	0.1824	N/A
R-free	0.212	N/A
Number of non-hydrogen atoms	1988	N/A
macromolecules	1760	N/A
ligands	217	N/A
water	11	N/A
Protein residues	226	N/A
RMS(bonds) (Å)	0.002	N/A
RMS(angles) (°)	1.1	N/A
Ramachandran favored (%)	99	N/A
Ramachandran outliers (%)	0	N/A
Clashscore	6.03	N/A
Average B-factor	48.1	N/A
macromolecules	45.4	N/A
ligands	69.4	N/A
solvent	51.9	N/A

Table 1. Data collection and refinement statistics. Statistics for the highest-resolution shell are shown in parentheses.

5.1.2 Lipopolysaccharide transport machinery

Crystals of LptD/E-His6 were obtained in the presence of $Zn(OAc)_2$ 0.01 M, MES buffer 100mM, pH 6.0 and PEG 200 40%. Tetragonal bipyramidal microcrystals were observed after 4 days in MO at 20 °C, and grew to the full size (∼20 x 10 µm) in 15 days (**Figure 9**). Resolution of the data crossed $I/\sigma(I) = 2.0$ at ~6Å which was not high enough to proceed further in structure elucidation. However, it provides a very interesting starting point for fine-tuning for optimal crystallization conditions.

Figure 9. LptD/E-His6 crystals grown at 20 °C for 15 days in MO-LCP. These crystals diffract to a resolution of 6 Å.

In order to optimize the crystal growth special screening of precipitant conditions was designed, varying systematically the pH (from 5.5 to 6.5), salt concentration (from 0.01 to 0.05 M of $Zn(OAc)_2$) and the nature and the concentration of the PEG (PEG 200 and 400 from 35 to 45%). The concentration of the protein was also varied and plates were set up with protein concentration of 10 mg/ml and 15 mg/ml. Crystallization plates were incubated at 20 °C for 30 days but no protein crystals were observed.

The same screening was made with a protein solution (10 mg/ml) that was previously mixed with the synthetic peptide L27-11. The LCP were formed directly with the solution peptide-protein. The concentration of the peptide was calculated in order to have 2 equivalents of peptide (calculated on a volume of 850 nl) for each equivalent of protein (calculated in 50 nl).

Crystals were observed (**Figure 10**) in several conditions and X-ray diffraction data were collected but none of them resulted in protein crystals.

Figure 10. Crystals of a small molecule (most probably L27-11) grown in MO at 20°C in presence of L27-11 in the protein solution.

Despite being unsuccessful in the optimization of crystal growth and determination of the structure of the target protein, it was shown that the LCP method is suitable for the crystallization and structural analysis of a large, transmembrane complex of proteins. It is noteworthy that the published structure of a LptD-LptE complex was obtained from crystals grown from a detergent solution (*13*, *14*).

5.1.3 *Escherichia coli* chloride channels EcClC

EcClC was crystallized in LCPs in order to find similarities and differences with crystals previously obtained from vapor diffusion experiments (*22*). LCP boli were set up screening different conditions and different protein concentrations. Crystals were obtained in the following conditions: KCl 0.5 M, PEG 400 35%, sodium acetate 0.05M, pH 4.5, protein concentrations: 15 and 25 mg/ml; potassium sodium tartrate 0.1 M, PEG 400 35%, ADA 0.05 M, pH 4.5, protein concentration: 15 mg/ml; ammonium sulfate 0.2 M, PEG 400 45%, TRIS 0.05 M, pH 8.4, protein concentration: 25 mg/ml.

X-ray diffraction data were collected, but only crystals grown in ammonium sulfate 0.2 M, PEG 400 45%, TRIS 0.05 M, pH 8.4 showed a protein diffraction pattern. Data were processed and scaled with XDS (*27*). Resolution of the data crossed $I/\sigma(I) = 2.0$ at ~9Å.

Crystallization experiments were set up in the conditions defined above, screening protein concentration from 15 to 25 mg/ml. Protein crystals were obtained with a protein concentration of 22 mg/ml (**Figure 11**). They grew to full size of 50 x 40 x 10 µm and diffracted to a resolution of ~6 Å.

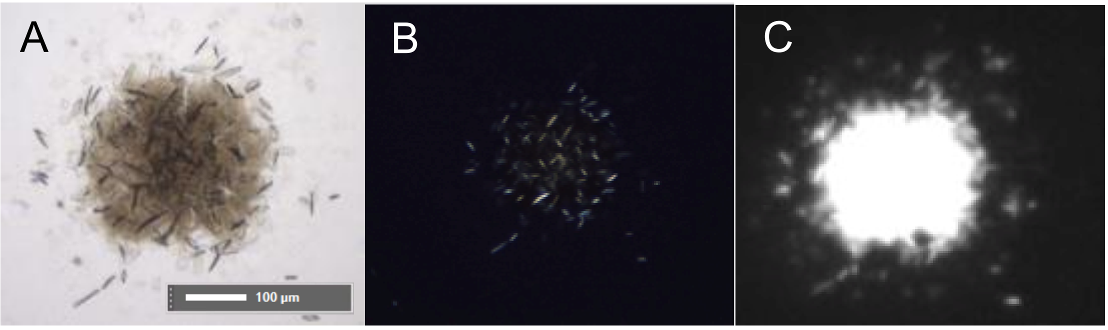

Figure 11. EcClC crystals grown in MO-LCP at 20 °C diffracting to 6 Å. A) image observed with normal light, B) corresponding image recorded between cross polarizers and C) with UV-fluorescence microscopy.

In order to optimize crystal growth of the protein after His-tag cleavage, special screening protocol of precipitant conditions was designed by systematically varying the pH (from 7.5 to 9.5), ammonium sulfate concentration (from 0.1 to 0.2 M) and the concentration of the PEG (PEG 400 from 33% to 57%). Crystallization experiments were set up at protein concentration of 22 mg/ml and using two different LCPs: MDS and MP (**Figure 12**).

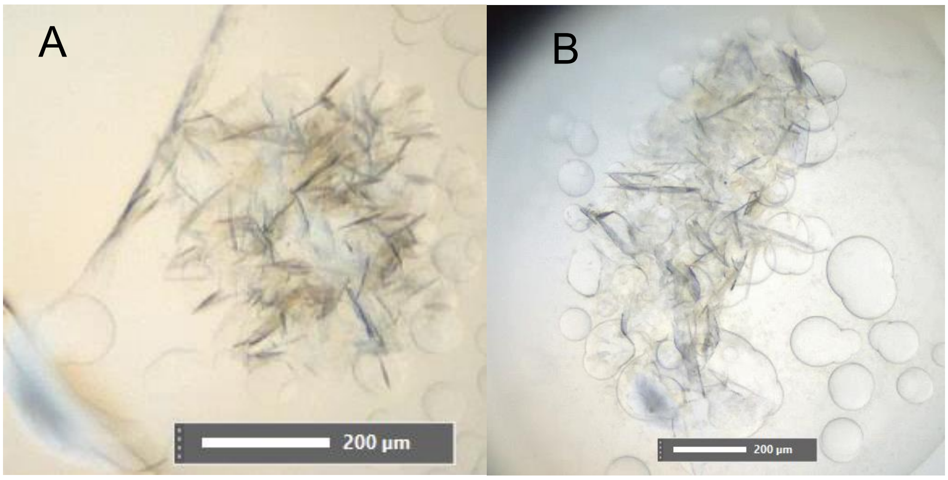

Figure 12. EcClC crystals grown in LCPs of A) MDS, diffracting up to 7 Å and B) MP, diffracting up to 4 Å at 20 °C. Image observed with normal light

X-ray diffraction data were collected on crystals from various setups. The crystals grown from MO-LCP at 20 °C with protein concentration 22 mg/ml in the presence of ammonium sulfate 0.2 M, PEG 400 40%, TRIS 0.05 M, pH 8.4 (**Figure 13**) showed the best diffraction.

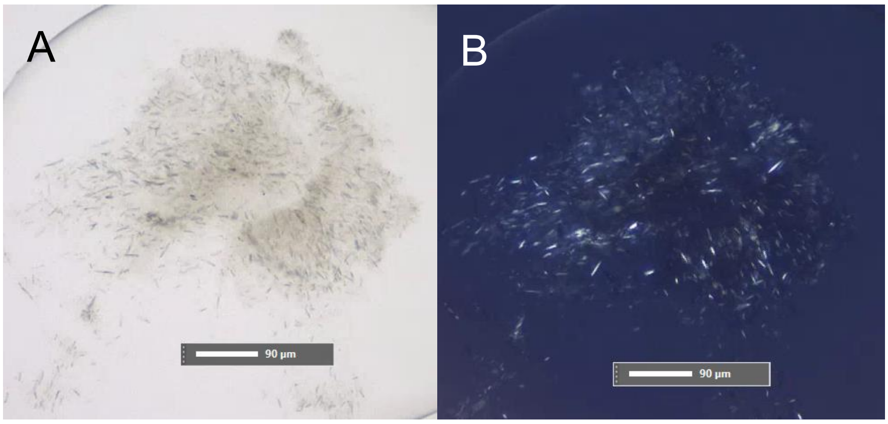

Figure 13. EcClC crystals grown in MO-LCP at 20 °C and diffracting to 3.4 Å. A) Image observed with normal light, B) corresponding image recorded between cross polarizers.

The structure of EcClC was solved by molecular replacement and refined up to 3.4 Å. (**Figure 14-16**).

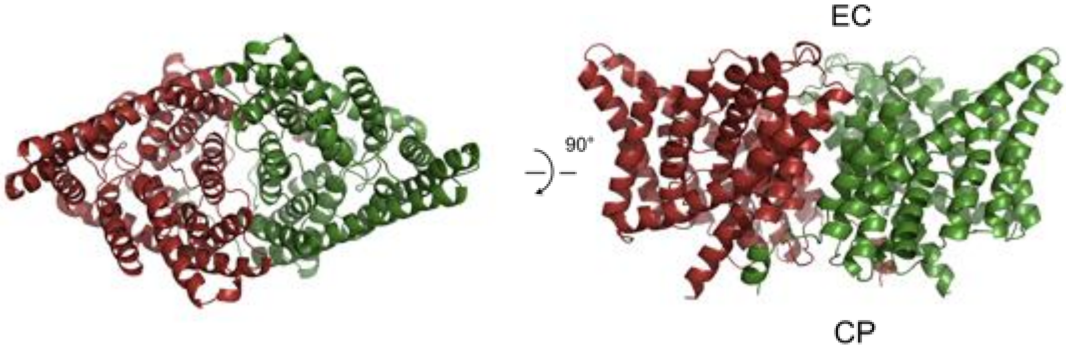

Figure 14. Crystal structure of EcClC in MO at 20 °C, shown as a dimer.

Packing arrangement of the proteins was found to be lamellar, as expected for membrane protein grown in LCP. (**Figure 15**)

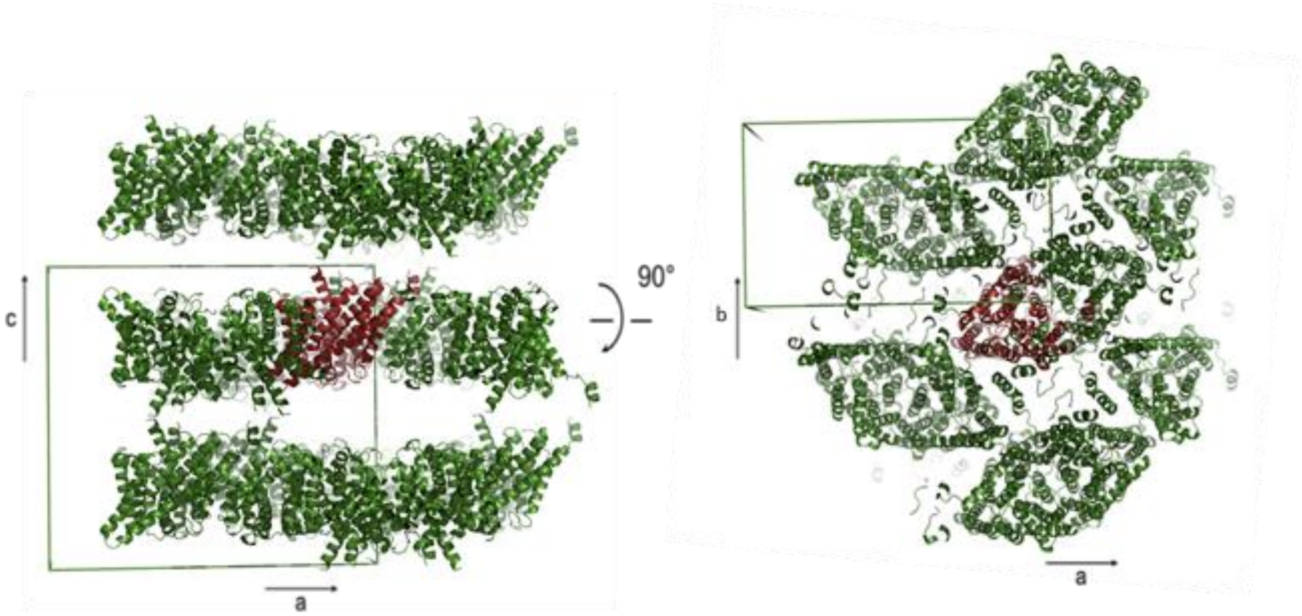

Figure 15. Crystal packing of EcClC crystallized from MO-LCP at 20 °C. Unit cell axes are indicated.

In the structure solved for the LCP-grown EcClC, the protein exhibits an identical conformation to that in the structure obtained from vapor diffusion crystals, which was used as a model for the molecular replacement (*22*).

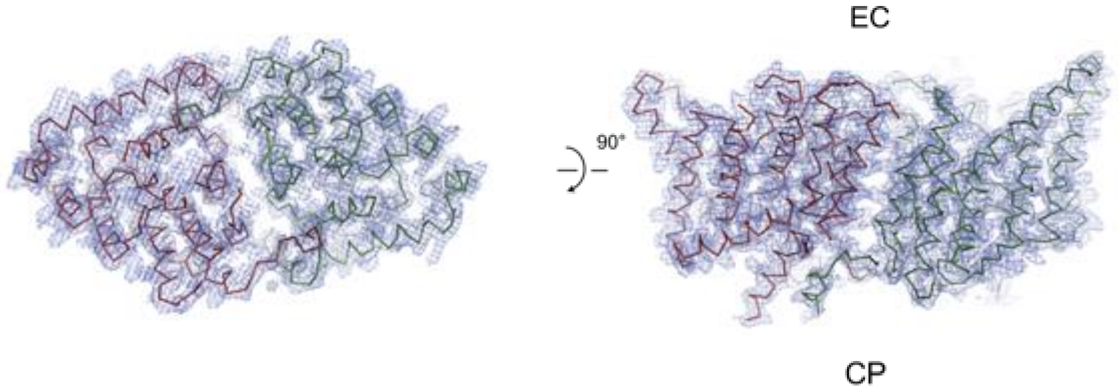

Figure 16. σ_A-weighted $2mF_o$-DF_c electron density map of EcClC dimer crystallized from MO-LCP at 20 °C, contoured at 1 σ.

Interesting details emerge from the analysis of the difference electron density map (F_O-F_C). From the map it was possible to build additional residues in the N and C termini that were not resolved in the structure obtained from the vapor diffiusion crystallization (*22*).

5.1.4 *Ralstonia metallidurans* chloride channels Rm1ClC

Crystallization screens of the full length Rm1ClC and of its transmembrane domain alone were set up in parallel, with protein concentrations of 15, 20, and 25 mg/ml in MO-LCP. While the full length protein did not crystallize, crystals of Rm1ClC TM were obtained in the presence of 0.2 M $(NH_4)_2SO_4$, 0.05 M NaOAc, 4.5 pH buffer, PEG 400 35%. Rod-like microcrystals were observed after 9 days in MO-LCP at 20 °C, grew to the full size (∼7 x 2 x 2 µm) in 20 days (**Figure 17**), and diffracted to low resolution. These crystallization conditions were used as a starting point for fine-tuning in search for optimal crystallization conditions.

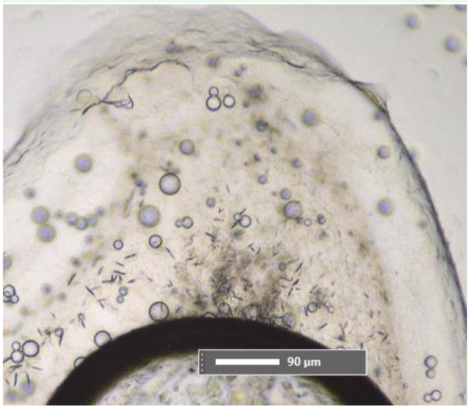

Figure 17. Rm1ClC crystals grown at 20 °C for 20 days in MO-LCP, diffracting to a resolution of 12 Å.

In order to optimize the crystal growth, special screening protocol of precipitant conditions was set up, varying systematically the pH (from 4 to 5), NaOAc concentration (from 0.01 to 0.1 M) and the PEG concentration (PEG 400 from 30 to 40%). The concentration of the protein was kept at 22 mg/ml. Crystallization plates were set up with LCP formed from MO and MP and were incubated at 20 °C. Crystals appeared in MO-LCPs in several conditions after 7 days, and grew to full size (∼15 x 2 x 2 µm) in 20 days (**Figure 18**). Resolution of the data crossed $I/\sigma(I) = 2.0$ at ~6Å, which was not high enough to proceed further in structure determination. However, it provides a very interesting starting point for fine-tuning en route to optimal crystallization conditions. Interestingly, no crystals were obtained from MP-LCPs.

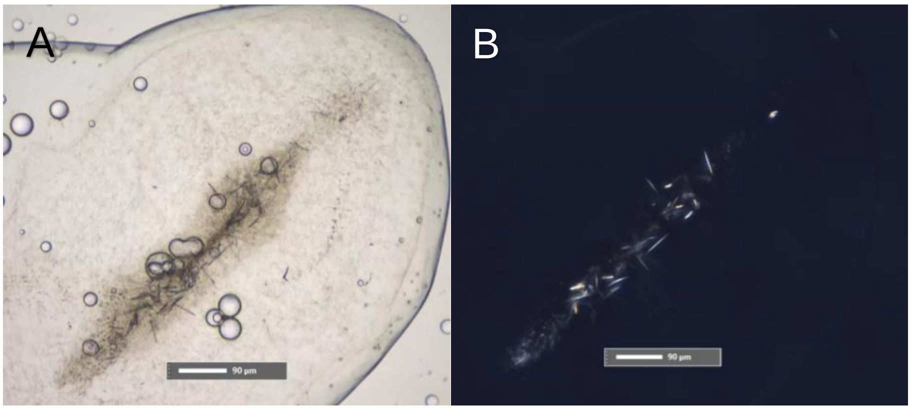

Figure 18. Rm1ClC crystals grown at 20 °C for 20 days in MO-LCP. Diffracting resolution was 6 Å. A) image observed with normal light, B) the corresponding image recorded between cross polarizers

Further crystal optimization was attempted by changing lipid for the formation of LCPs. Monooelaidin (ME) and a mixture of MO with 10% cholesterol were mixed with the protein solution to form the LCPs. After 7 days at 20 °C microcrystals appeared in both LCP set ups, but only the crystals in the MO-cholesterol mixture grew further after 20 days to size of ~7 x 2 x 2 µm, and diffracted up to ~7Å resolution.

Despite being unsuccessful in the optimization of crystal growth and determination of the high-resolution structure of the target protein, it was shown that the LCP method is suitable for the crystallization and structural analysis of chloride channels, and that changing lipid can be an essential step in crystal growth and optimization.

EcClC Crystals grown from MO LCP at 20 °C

Crystals belonged to space group $C222_1$, with one protein molecule in the asymmetric unit. X-ray diffraction data were collected from several crystals cryo-cooled to 100 K at beamline X06DA (Swiss Light Source, Villigen, Switzerland) with the PILATUS 6M high-resolution diffractometer at a wavelength $\lambda = 1$ Å. Data were processed and scaled with XDS (*27*). Resolution of the data crossed $I/\sigma(I) = 1.8$ at 3.4 Å and the data were finally cut at 3.4 Å with $CC_{1/2}$= 71.2% (*28*).

The structure was determined by molecular replacement in Phaser (*31*) using the EcClC structure (Protein Data Bank accession code 1OTS, 2.5 Å, crystals grown in vapor diffusion) as a search model. Model building was done in Coot (*32*) and refinement was performed with Phenix (*34*). The R/R_{free} of the model is 0.2469 / 0.2770, with Ramachandran favored 95%.

5.2 Materials and methods

Cyclopropanated lipids were synthetized according to the procedure previously reported by Salvati Manni et al. (*26*) and as reported in **chapter 2** of this thesis. Purity of the lipids was confirmed by ^{1}H-NMR, ^{13}C-NMR and mass spectroscopy.

Monoolein (MO), Monopalmitolein (MP) and Monooelaidin (ME) were purchased from Nu-Check.

5.2.1 Bacteriorhodopsin

Purification of bR from purple membranes

Lyophilized *Halobacterium salinarum* purple membranes (PM) were purchased from Sigma-Aldrich (product No. B0184). Bacteriorhodopsin (bR) was purified from PM according to an established procedure (*36*).

Briefly, 2 mg of lyophilized PM were resuspended in 2 ml of an aqueous solution of 150 mM KCl and collected by centrifugation (30 min, 20,000 *g*, 4 °C). The pellet was resuspended in 6 ml of 25 mM sodium phosphate buffer, pH 6.9. Subsequently, 2 ml of an aqueous 10% (w/v) n-octyl-β-D-glucopyranoside (OG, Anatrace) were added, the sample was sonicated for 1 min and incubated overnight in the dark. Prior to ultra-centrifugation (45 min, 120,000 g, 4 °C), the pH was adjusted to 5.5 with 0.1 N HCl. The supernatant was concentrated to 500 µl with an Amicon ultra centrifugal concentrator (30 kDa cutoff, Millipore) and subjected to size-exclusion chromatography on a Superdex 200 Increase 10/300GL column (GE Healthcare) pre-equilibrated with a 25 mM sodium phosphate buffer, pH 5.5, 1.2% OG at 4 °C. Pooled peak fractions were concentrated with an Amicon ultra centrifugal concentrator (30 kDa cutoff) to 10.2 mg/ml as judged by the absorption peak at 560 nm. The final absorbance ratio A_{280}/A_{560} was 1.51.

Data collection and structure determination

Crystals were grown from MO and MDS LCPs as described previously (*5*), and appeared as thin hexagonal plates. The crystals were mounted on the Dual-Thickness MicroMounts (MiTeGen) directly from the lipidic mesophase and were flash-frozen in liquid nitrogen.

Lipidic cubic phase crystallization of bR

Detergent-solubilized bR was reconstituted into the LCP by mixing with molten MO or MDS in a 2:3 (v/v) ratio (protein solution:lipid) using a syringe lipid mixer as previously described (*37*). Following formation of a transparent, uniformly colored purple LCP, 50-70 nl LCP boli were dispensed onto 96-well plastic plates (Swissci) and overlaid with 800 nl precipitant solution using the Gryphon LCP robot (Art Robbins Instruments). A specific screening protocol of precipitant conditions was made, varying systematically the pH (from 5.2 to 7.7) and Na/K-Pi concentration (from 1.5 to 3 M). Crystallization plates were incubated either at 20 °C (MO, MDS) or at 4 °C (MDS).

Plate-like hexagonal crystals with an average size of ~18 x 18 x 7 µm were observed after 3 days in MDS at 20 °C, and grew to the full size (~40 x 40 x 20 µm) in 10 days. In contradistinction, crystallization in MO was slower, yielding fewer initial crystals (~20 x 20 x 7 µm) under identical conditions (2.1 M Na/K-Pi, pH 5.3) after 10 days. These crystals grew to the full size in 28 days but were smaller (~30 x 30 x 12 µm). Moreover, using the same crystallization screen, crystals appeared in many more conditions in MDS than in MO. The best crystals (~15 x 15 x 5 µm) obtained at 4 °C could be observed in MDS after 28 days using the following conditions: saturated Na/K-Pi, pH 6.9.

A Zeiss Axioskop 2 MOT optical microscope and a Nikon Eclipse TE300 inverted microscope were used for observations with brightfield and cross polarized light. Images were captured by a Hamamatsu C5810 CCD camera.

5.2.2 LptD-LptE

Lipidic cubic phase crystallization of the LptD-LptE complex

The purified LptD-LptE complex was obtained from Dr. Gloria Andolina from the group of Prof. John A. Robinson, Department of Chemistry, University of Zurich. Expression and purification of the LPtD-LptE complex was part of Dr. Andolina's PhD thesis (2016), and crystallization trials were set up together as a collaborative project. The detergent-solubilized heterodimeric protein complex of LptD and LptE-His_6 from *P. Aeruginosa* was reconstituted into the LCP by mixing a protein solution with protein concentration of 10 mg/ml (20 mM NaH_2PO_4, 500 mM NaCl, pH 7.4, 0.015% LDAO and 10% glycerol) with molten MO in a 2:3 (v/v) ratio (protein solution:lipid) using a syringe lipid mixer as previously described (*37*).

Following formation of a uniformly transparent LCP, 50 nl LCP boli were dispensed onto 96-well plastic plates (*Swissci*) and overlaid with 800 nl precipitant solution using the Gryphon LCP robot (*Art Robbins Instruments*). Six commercially available screens were set up to probe different crystallization conditions, whereby four were based on the conditions reported in the literature for the crystallization from detergent solution of the analogue LptD-LptE complex from E.coli (*13, 14*).

The pH was fixed at 8.5 using a TRIS/HCl buffer system, the PEG 1000 and PEG 400 concentration was varied from 15% to 5%. The precipitation salt was changed from NaBr to KBr, and both the systems were tried at two different concentrations (500mM and 200mM).

Crystals were obtained for the commercial screening MenMeso (*Molecular Dimensions*) in the presence of $Zn(OAc)_2$ 0.01 M, MES buffer 100mM, pH 6.0 and PEG 200 40%. A Zeiss Axioskop 2 MOT optical microscope and a Nikon Eclipse TE300 inverted microscope were used for observations with brightfield and cross polarized light. Images were captured by a Hamamatsu C5810 CCD camera.

The crystals were mounted on the Dual-Thickness MicroMounts (*MiTeGen*) directly from the lipidic mesophase and were flash-frozen in liquid nitrogen.

Synchrotron X-ray diffraction data were collected from several crystals cryo-cooled to 100 K at beamline X06DA (Swiss Light Source, Villigen, Switzerland) with the PILATUS 2M high-resolution diffractometer at a wavelength $\lambda = 1$Å. Data were processed and scaled with XDS (*27*). Resolution of the data crossed $I/\sigma(I) = 2.0$ at ~6Å .

5.2.3 Chloride channels and transporters

EcClC Expression

The purification and expression of EcClC was described in the dissertation of Dr. Adrian Szydelko in the group of Prof. Raimund Dutzler, Department of Biochemistry, University of Zurich (2014). All EcClC expression plasmids used in this work were provided by Prof. Raimund Dutzler. For crystallization trials EcClC plasmids were freshly transformed into the BL21(DE3) *E. coli* strain. The bacteria were grown in a Luria Broth (LB) medium containing 50 µg/ml of kanamycin in baffled flasks, shaking at 90 RPM. The temperature was maintained at 37 °C until cell growth reached OD_{600} of 1.0, then the cultures were cooled to 20 °C and 0.2 mM isopropyl β-D-thiogalactopyranoside (IPTG) was added to the medium to induce the expression. The expression was carried out for 14 h at 20 °C. The typical large-scale expression culture of EcClC was carried out in 32 l of total culture volume. The cultures were harvested by centrifugation for 15 min at 5000 RPM (Sorvall SLC-6000 rotor), and the pellets were used immediately.

Membrane preparation and purification of EcClC

A buffer with 50 mM Tris-HCl at pH 7.4 and 150 mM sodium chloride, 20 µg/ml DNase, 1 mg/ml lysozyme, 1 µg/ml leupeptin, 1 µg/ml pepstatin was used to resuspend the pellets. The solution was homogenized and then run 3 times at >10000 psi in an EmulsiFlex-C3 (Avestin) pressure homogenizer to mechanically lyse the cells. After addition of 1 mM PMSF inhibitor, the solution was centrifuged for 45 min at 10 000 g, the supernatant collected and centrifuged for 90 min at 45 000 RPM (Ti70 rotor, Beckman Coulter). Using a Potter homogenizer, the resultant pelleted were resuspended in a buffer composed of 100 mM sodium chloride and 50 mM HEPES at pH 7.4. Membrane vesicles suspension was frozen in liquid nitrogen and subsequently stored at -80 °C.

EcClC was purified at room temperature. The frozen membranes were extracted with 50 mM *n*-decyl-β-D-maltoside (DM) SOL-grade (Affymetrix) for 2 h at room temperature. The extract was centrifuged for 40 min at 45,000 RPM (Ti70 rotor, Beckman Coulter) and the supernatant loaded onto a TALON affinity resin (Clontech) for immobilized metal affinity chromatography (IMAC). The column was washed with 40 mM imidazole and the desired protein eluted with 400 mM imidazole. LysC endoproteinase (Roche) 0.3 U per 5 mg of protein was added to the eluted protein and incubated for 1.5 h to cleave the His-tag. The protein was concentrated to 15±20 mg ml^{-1} with the Amicon MWCO 30 kDa centrifugal filtration unit (Millipore) and then run on a Superedex 200 10/300 GL column (GE Healthcare) in 45 mM DM, 150 mM NaCl and 10 mM TrisHCl at pH 7.5. The fractions corresponding to the monodisperse elution peak at 12.3 ml were collected and the protein concentrated using an Amicon MWCO 30 kDa centrifugal filtration unit. A_{280} was measured and protein concentration was calculated considering 1 mg/ml=1.0 AU.

Lipidic cubic phase crystallization of EcClC

Detergent-solubilized EcClC was reconstituted into the LCP by mixing a protein solution with concentration of 15 and 25 mg/ml with molten MO in a 2:3 (v/v) ratio (protein solution:lipid) using a syringe lipid mixer as previously described (*37*). Following formation of a uniformly transparent LCP, 50 nl LCP boli were dispensed onto 96-well plastic plates (Swissci) and overlaid with 800 nl precipitant solution using the Gryphon LCP robot (Art Robbins Instruments). 20 commercially available screens were set up to probe different crystallization conditions.

A Rock Imager 1000, Formulatrix key features was used for observation and imaging with brightfield, cross polarized and UV light.

The crystals were mounted on the Dual-Thickness MicroMounts (MiTeGen) directly from the lipidic mesophase and were flash-frozen in liquid nitrogen.

Synchrotron X-ray diffraction data were collected from several crystals cryo-cooled to 100 K at beamline X06DA (Swiss Light Source, Villigen, Switzerland) with the PILATUS 6M high-resolution diffractometer at a wavelength $\lambda = 1$ Å.

RmClC Expression

The purification and expression of RmClC was described in the dissertation of Dr. Sandra Markovic in the group of Prof. Raimund Dutzler, Department of Biochemistry, University of Zurich (2010). All RmClC expression plasmids used in this work were provided by Prof. Raimund Dutzler. For RmClC crystallization trials the expression plasmids were freshly transformed into the MC1061 *E. coli* strain. The bacteria were grown in a Terrific Broth (TB) medium containing 50 µg/ml ampicillin in baffled flasks, shaking at 90 RPM. The temperature was maintained at 37 °C until cell growth reached OD_{600} of 0.6, the cultures were then cooled to 25 °C and 0.001 % (w/v) arabinose (Sigma-Aldrich) was added to the medium to induce the expression. The expression was carried out for 15 h at 25 °C. The typical large-scale expression culture of full length (FL) protein RmClC FL and its transmembrane (TM) domain was carried out in 32 l of total culture volume. The cultures were harvested by centrifugation for 15 min at 5000 RPM (Sorvall SLC-6000 rotor) and the pellets were used immediately.

Membrane preparation and purification of Rm1ClC FL and its TM domain.

A buffer with 50 mM Tris-HCl at pH 7.4 and 150 mM sodium chloride, 20 µg/ml DNase, 1 mg/ml lysozyme, 1 µg/ml leupeptin, 1 µg/ml pepstatin was used to resuspend the pellets. The solution was homogenized and then run 3 times at >10000 psi in an EmulsiFlex-C3 (Avestin) pressure homogenizer to mechanically lyse the cells. After addition of 1 mM PMSF inhibitor, the solution was centrifuged for 45 min at 10 000 g, the supernatant collected and centrifuged for 90 min at 45 000 RPM (Ti70 rotor, Beckman Coulter). Using a Potter homogenizer, the resultant pellets were resuspended in a buffer composed of 150 mM sodium chloride, 50 mM Tris-HCl at pH 7.4 and 5% (v/v) glycerol. Suspension of membrane vesicles were frozen in liquid nitrogen and stored at -80 °C.

RmClC FL and TM were purified at 4 °C. The frozen membranes were extracted with 50 mM *n*-decyl-β-D-maltoside (DM) SOL-grade (Affymetrix) for 1.5 h. The extract was centrifuged for 40 min at 45,000 RPM (Ti70 rotor, Beckman Coulter) and the supernatant loaded onto a TALON affinity resin (Clontech) for immobilized metal affinity chromatography (IMAC). The column was washed with 20 mM imidazole and the desired protein eluted with 300 mM imidazole. In order to cleave the His-tag and remove imidazole HRV 3C protease (GE Healthcare) was added at a 1:10 (w/w) ratio to the eluted protein and incubated for 2 h in a 8000 MWCO dialysis membrane (Spectrum Laboratories), dialyzing against 40 volumes of the purification buffer supplemented with 2.5 mM DM SOL-grade. After cleavage the deca-His tag and green fluorescent protein (GFP) encoded with RmClC TM were removed from the protein sample with a second IMAC. This step was not required for the RmClC FL because its expression construct did not encode GFP molecule. 2 ml of NiNTA resin (Qiagen) was incubated with the protein solution for 15 min to bind the impurities, the flow-through fraction was collected and concentrated to 15±20 mg ml^{-1} with the Amicon MWCO 50 kDa centrifugal filtration unit (Millipore), and then run on a Superedex 200 10/300 GL column (GE Healthcare) in 150 mM sodium chloride, 10 mM Tris-HCl pH 7.4, 5 mM DM and 5 % (v/v) glycerol. The fractions corresponding to the monodisperse elution peak at 12.2 ml for the FL and 12.6 for the TM were collected and the protein concentrated using an Amicon MWCO 50 kDa centrifugal filtration unit. A_{280} was measured and protein concentration was calculated considering 1 mg/ml=1.0 AU for RmClC FL and 0.595 AU for RmClC TM.

Lipidic cubic phase crystallization of Rm1ClC

Detergent-solubilized Rm1ClC was reconstituted into the LCP by mixing a protein solution with concentration of protein of 22 mg/ml with molten MO in a 2:3 (v/v) ratio (protein solution:lipid) using a syringe lipid mixer as previously described (*37*). Following formation of a uniformly transparent LCP, 50 nl LCP boli were dispensed onto 96-well plastic plates

(Swissci) and overlaid with 800 nl precipitant solution using the Gryphon LCP robot (Art Robbins Instruments). Best diffracting crystals of Rm1ClC TM were grown in MO at 20 °C for 21 days. The LCP boli were incubated with an overlay of a precipitant solution with 0.2 M $(NH_4)_2SO_4$, 0.02 M NaOAc pH 5 buffer , PEG 400 30 %.

A Rock Imager 1000, Formulatrix key features was used for observation and imaging with brightfield, cross polarized and UV light.

The crystals were mounted on the Dual-Thickness MicroMounts (MiTeGen) directly from the lipidic mesophase and were flash-frozen in liquid nitrogen.

X-ray diffraction data were collected from several crystals cryo-cooled to 100 K at beamline X06DA (Swiss Light Source, Villigen, Switzerland) with the EIGER 16M X high-resolution diffractometer at a wavelength $\lambda = 1$ Å.

References

1. C. Wickstrand, R. Dods, A. Royant, R. Neutze, Bacteriorhodopsin: Would the real structural intermediates please stand up? *Biochim Biophys Acta* **1850**, 536-553 (2015).
2. U. Haupts, J. Tittor, D. Oesterhelt, Closing in on bacteriorhodopsin: Progress in understanding the molecule. *Annu Rev Bioph Biom* **28**, 367-399 (1999).
3. O. M. Finkel, O. Beja, S. Belkin, Global abundance of microbial rhodopsins. *ISME J* **7**, 448-451 (2013).
4. R. Henderson, P. N. T. Unwin, 3-dimensional model of purple membrane obtained by electron-microscopy. *Nature* **257**, 28-32 (1975).
5. E. M. Landau, J. P. Rosenbusch, Lipidic cubic phases: A novel concept for the crystallization of membrane proteins. *Proc Natl Acad Sci USA* **93**, 14532-14535 (1996).
6. E. Nango *et al.*, A three-dimensional movie of structural changes in bacteriorhodopsin. *Science* **354**, 1552-1557 (2016).
7. S. Okuda, D. J. Sherman, T. J. Silhavy, N. Ruiz, D. Kahne, Lipopolysaccharide transport and assembly at the outer membrane: The pez model. *Nature Reviews Microbiology* **14**, 337-345 (2016).
8. P. F. Muhlradt, J. Menzel, Outer membrane of salmonella - sites of export of newly synthesized lipopolysaccharide on bacterial surface. *Eur J Biochem* **35**, 471-481 (1973).
9. T. Wu *et al.*, Identification of a protein complex that assembles lipopolysaccharide in the outer membrane of escherichia coli. *Proc Natl Acad Sci USA* **103**, 11754-11759 (2006).
10. N. Srinivas *et al.*, Peptidomimetic antibiotics target outer-membrane biogenesis in pseudomonas aeruginosa. *Science* **327**, 1010-1013 (2010).
11. S. S. Chng, N. Ruiz, G. Chimalakonda, T. J. Silhavy, D. Kahne, Characterization of the two-protein complex in escherichia coli responsible for lipopolysaccharide assembly at the outer membrane. *Proc Natl Acad Sci USA* **107**, 5363-5368 (2010).
12. J. Schmidt, K. Patora-Komisarska, K. Moehle, D. Obrecht, J. A. Robinson, Structural studies of beta-hairpin peptidomimetic antibiotics that target lptd in pseudomonas sp. *Bioorgan Med Chem* **21**, 5806-5810 (2013).
13. H. Dong *et al.*, Structural basis for outer membrane lipopolysaccharide insertion. *Nature* **511**, 52-56 (2014).
14. S. Qiao, Q. Luo, Y. Zhao, X. C. Zhang, Y. Huang, Structural basis for lipopolysaccharide insertion in the bacterial outer membrane. *Nature* **511**, 108-111 (2014).
15. M. M. White, C. Miller, Voltage-gated anion channel from the electric organ of torpedo-californica. *J Biol Chem* **254**, 161-166 (1979).
16. K. Steinmeyer, C. Ortland, T. J. Jentsch, Primary structure and functional expression of a developmentally regulated skeletal-muscle chloride channel. *Nature* **354**, 301-304 (1991).
17. A. Thiemann, S. Grunder, M. Pusch, T. J. Jentsch, A chloride channel widely expressed in epithelial and nonepithelial cells. *Nature* **356**, 57-60 (1992).
18. S. Kieferle, P. Y. Fong, M. Bens, A. Vandewalle, T. J. Jentsch, 2 highly homologous members of the clc chloride channel family in both rat and human kidney. *Proc Natl Acad Sci USA* **91**, 6943-6947 (1994).
19. S. Brandt, T. J. Jentsch, Clc-6 and clc-7 are two novel broadly expressed members of the clc chloride channel family. *Febs Letters* **377**, 15-20 (1995).
20. K. Steinmeyer, B. Schwappach, M. Bens, A. Vandewalle, T. J. Jentsch, Cloning and functional expression of rat clc-5, a chloride channel related to kidney disease. *J Biol Chem* **270**, 31172-31177 (1995).

21. A. S. Verkman, L. J. V. Galietta, Chloride channels as drug targets. *Nat Rev Drug Discov* **8**, 153-171 (2009).
22. R. Dutzler, E. B. Campbell, R. MacKinnon, Gating the selectivity filter in clc chloride channels. *Science* **300**, 108-112 (2003).
23. R. Dutzler, E. B. Campbell, M. Cadene, B. T. Chait, R. MacKinnon, X-ray structure of a cic chloride channel at 3.0 angstrom reveals the molecular basis of anion selectivity. *Nature* **415**, 287-294 (2002).
24. R. Dutzler, E. B. Campbell, R. Mackinnon, Structural basis for ion conduction and gating in clc chloride channels. *J Gen Physiol* **122**, 1a-2a (2003).
25. A. Accardi, A. Picollo, Clc channels and transporters: Proteins with borderline personalities. *Biochim Biophys Acta Biomembr* **1798**, 1457-1464 (2010).
26. L. Salvati Manni *et al.*, Phase behavior of a designed cyclopropyl analogue of monoolein: Implications for low-temperature membrane protein crystallization. *Angew Chem Int Ed* **54**, 1027-1031 (2015).
27. W. Kabsch, Xds. *Acta Crystallogr D* **66**, 125-132 (2010).
28. P. A. Karplus, K. Diederichs, Linking crystallographic model and data quality. *Science* **336**, 1030-1033 (2012).
29. H. Luecke, H. T. Richter, J. K. Lanyi, Proton transfer pathways in bacteriorhodopsin at 2.3 angstrom resolution. *Science* **280**, 1934-1937 (1998).
30. A. Royant *et al.*, Detection and characterization of merohedral twinning in two protein crystals: Bacteriorhodopsin and p67(phox). *Acta Crystallogr D Biol Crystallogr* **58**, 784-791 (2002).
31. A. J. McCoy *et al.*, Phaser crystallographic software. *J Appl Crystallogr* **40**, 658-674 (2007).
32. P. Emsley, B. Lohkamp, W. G. Scott, K. Cowtan, Features and development of coot. *Acta Crystallogr D Biol Crystallogr* **66**, 486-501 (2010).
33. G. N. Murshudov *et al.*, Refmac5 for the refinement of macromolecular crystal structures. *Acta Crystallogr D Biol Crystallogr* **67**, 355-367 (2011).
34. P. V. Afonine *et al.*, Towards automated crystallographic structure refinement with phenix.Refine. *Acta Crystallogr D Biol Crystallogr* **68**, 352-367 (2012).
35. N. Echols *et al.*, Graphical tools for macromolecular crystallography in phenix. *J Appl Crystallogr* **45**, 581-586 (2012).
36. N. A. Dencher, M. P. Heyn, Preparation and properties of monomeric bacteriorhodopsin. *Method Enzymol* **88**, 5-10 (1982).
37. M. Caffrey, V. Cherezov, Crystallizing membrane proteins using lipidic mesophases. *Nat Protoc* **4**, 706-731 (2009).

Conclusions

In this thesis, novel lipids that demonstrate a complex polymorphism for the formation of alternative lipidic mesophases were successfully designed, synthesized, characterized and applied. These molecules were engineered and synthesized by replacing the central structural element of the commonly used monoacylglycerols (MAGs)- the *cis* double bond along the hydrophobic chain- with a cyclopropyl group. This project focused on four different commercially available MAGs, MO, MP, MV and ML. Repacement of the *cis* double bonds with cyclopropyl moieties resulted in the following designer lipids: MDS, CPMP, MLB, DCPML respectively. The molecules were systematically varied by altering the number of the cyclopropyl groups, the position of the cyclopropanation, and the chain length, in order to create a new family of lipids with similar properties. Various synthetic routes were explored in order to optimize the yields, which allowed for the production of grams of material necessary for the characterization and the application of the novel lipids.

The binary phase diagrams of these systems were studied by mixing lipid and water at precise compositions, and SAXS measurements at different temperatures were recorded in order to establish the phase identity and geometry, as well as the lattice parameters as a function of temperature and water content. The phase boundaries were defined and the resultant phase diagrams were built in accordance with the data.

Of particular interest were the low temperature behavior of the two systems MDS and DCPML. MDS exhibits a stable *Pn3m* bicontinuous cubic phase at 4 °C opening up the intriguing possibility of applying for the first time LCP crystallization of thermally unstable membrane proteins at low temperature.

In the case of DCPML, the unusual chain splay played a determinant role in the phase transitions, obtaining an uncommon and unique phase behavior at both room and low temperature. This system reveals a stable H_{II} phase at room temperature at high level of hydration (30%), and an *Ia3d* cubic phase already at 5% of water content. Most remarkably, the low water content (5-10%) *Ia3d* cubic phase confined the incorporated water molecules in the bicontinuous aqueous channels, preventing water reorganization into a crystalline structure even at temperatures down to -30 °C. DSC measurements combined with self-diffusion NMR experiments were carried out in order to determine the nature of the water in the channel. The absence of an enthalpy peak in the DSC around 0°C confirmed the lack of a first order transition, which corresponds to the freezing of water. Preliminary NMR studies show the diffusion of water until -30 °C leading to the conclusion that the water confined in the channel retains its liquid characteristics even at low temperature.

In order to test the capacity of these systems to switch phase on demand, and establish their applicability as drug carriers, enzymatic digestion of MDS, CPMP and DCPML dispersions were investigated. Phase changes during digestion were characterized with dynamic SAXS and the digestion behavior compared to that of the commercially available natural MAGs MO, MP and ML. Differences in phase formations and in digestion time were taken under considerations.

Crystallization of the model system bR was attempted in LCPs made up of all the four cyclopropanated lipids in order to test their applicability as membrane protein crystallization matrixes. To show the applicability of MDS for membrane protein crystallization at low temperatures, bR was successfully crystallized at room temperature and at 4 °C.

To determine protein structure in native-like environments, three additional membrane proteins were investigated: The two chloride channels EcClC and Rm1ClC, and the lipopolysaccharide transporter LptD-E. For all the proteins studied, it was possible to obtain low resolution diffracting crystals (6 Å) in LCPs. Whereas for Rm1ClC and LptD-E it was not possible to obtain better diffracting crystals, optimization of the LCP crystal growth led to successful determination of the structure of EcClC.

In conclusion, in this work four new designer cyclopropanated lipids were synthesized, their phase behavior was characterized and possible applications of the ensuing nanomaterials as drug delivery systems and membrane protein crystallization matrices were explored.

Appendix 1

Abbreviations

4-BPBA	4- bromophenylboronic acid
bR	bacteriorhodopsin
br	broad
CBS	cystathionine β synthase
ClC	chloride channel
CP	cytoplasmic
CPMP	cyclopropyl monopalmitolein
CPP	critical packing parameter
CPP	propionic acid
d	doublet
DADS	4,4’-diaminostilbene2,2’-disulfonic acid
DCPML	dicyclopropyl monolinolein
DIDS	4,4’-diisothiocyanostilbene2,2’-disulfonic acid
DMAP	4-(dimethylamino)pyridine
DMF	dimethylformamide
DSC	differential scanning calorimetry
EC	extracellular
EcClC	*Escherichia coli* chloride channel
EDC	*N*-(3-dimethylaminopropyl)-*N′*-ethylcarbodiimide hydrochloride
ESI	electrospray ionization
FFT	fast Fourier transform
FI	isotropic fluid
FL	full lenght
GPCR	G protein-coupled receptors
H	hexagonal
H_I	normal hexagonal
H_{II}	inverse hexagonal
HRMS	high resolution mass spectroscopy
Ia3d	gyroid
IM	inner membrane
Im3m	primitive

IPTG	isopropyl β-D-thiogalactopyranoside
L	micellar
L_1	normal micellar
L_2	inverse micellar
LB	Luria Broth
L_c	solid crystalline amellar
LCP	lipidic cubic phases
LLC	lyotropic liquid crystal
LPS	lipopolysaccharides
Lpt	lipopolysaccharide transporter
$L\alpha$	liquid crystalline lamellar
m	multiplet
MAG	monoacylglycerols
MDS	monodihydrosterculin
ME	monoelaidin
ML	monolinolein
MLB	monolactobacillin
MO	monoolein
MP	monopalmitolein
MV	monovaccein
NMR	nuclear magnetic resonance
NPPB	5-nitro-2-(3-phenylpropylamino)benzoic acid
OADS	4,4’-octanamidostilbene2,2’-disufnate
OG	n-octyl-β-D-glucopyranoside
OM	outer membrane
ompF	outer membrane protein F
PDB	protein data bank
PM	purple membrane
$Pn3m$	double diamond
Q	cubic
q	quadruplet

quint	quintet
Rm1ClC	*Ralstonia metallidurans* chloride channel
s	singlet
SAXS	small angle x-ray scattering
StClC	*Salmonella typhimurium* chloride channel
t	triplet
TB	Terrific Broth
TEM	transmission electron microscopy
TLC	thin-layer chromatography
TM	transmembrane domain
TPMS	triply-periodic minimal surface
XFEL	X-ray free electron laser

Appendix 2

NMR characterization

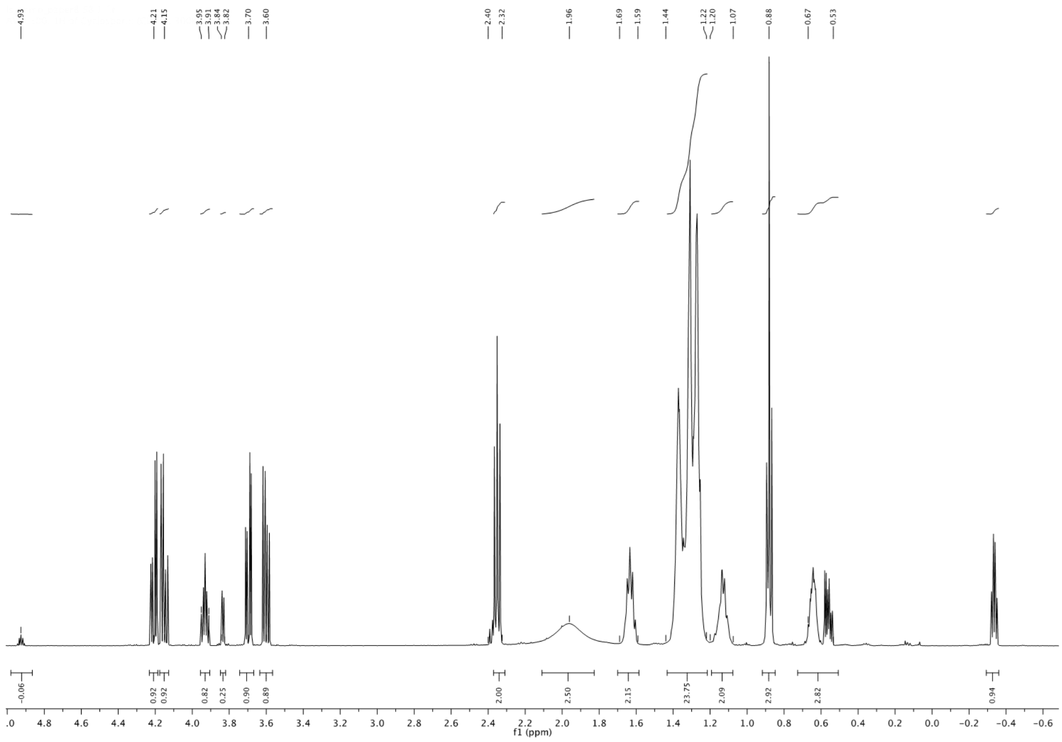

Spectrum 1. ^{1}H NMR (500 MHz, $CDCl_3$) of 1-MDS and 2-MDS (6-8%) mixture

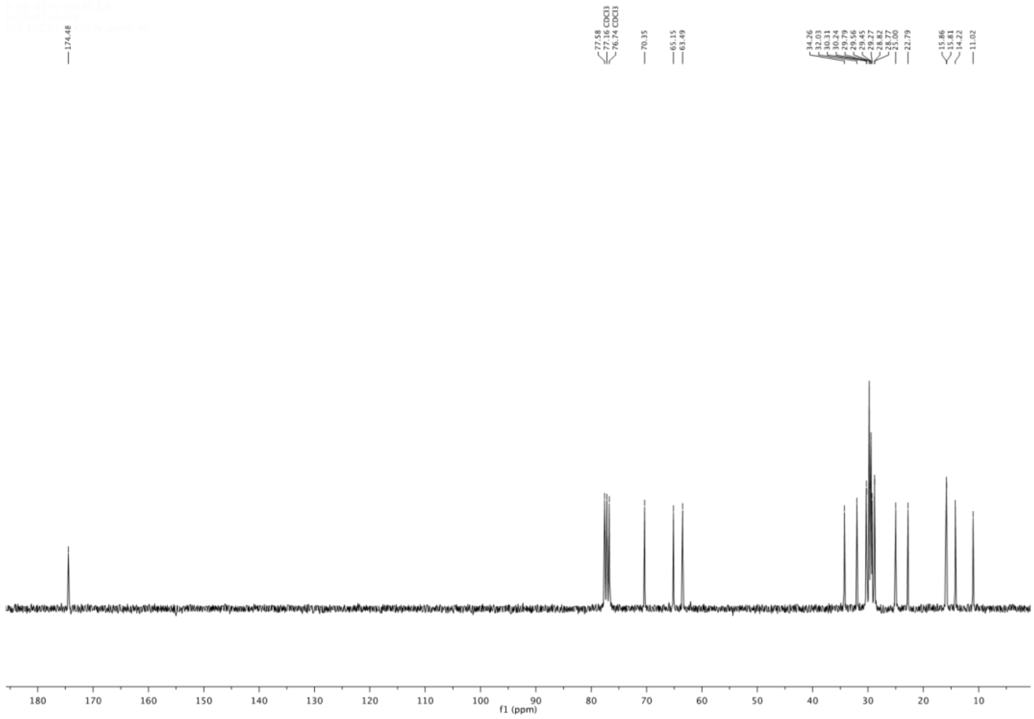

Spectrum 2 . ^{13}C NMR (125 MHz, $CDCl_3$) of 1-MDS and 2-MDS (6-8%) mixture

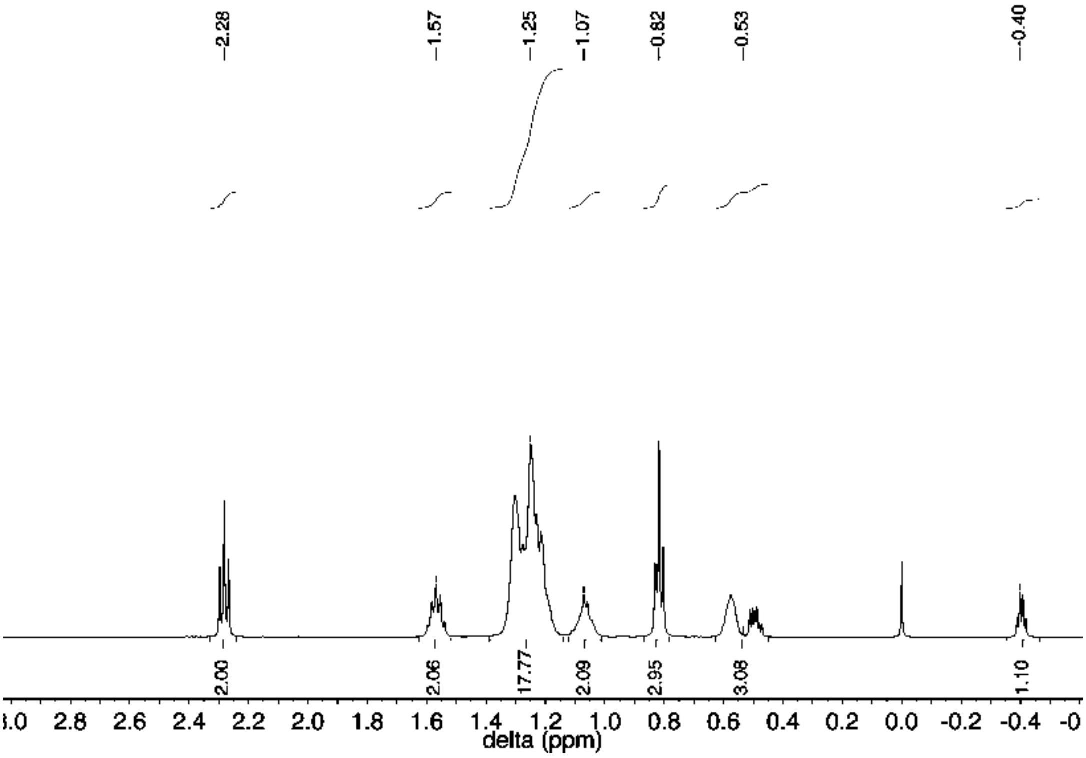

Spectrum 3. ^{1}H NMR (500 MHz, $CDCl_3$) of CP-palmitoleic acid

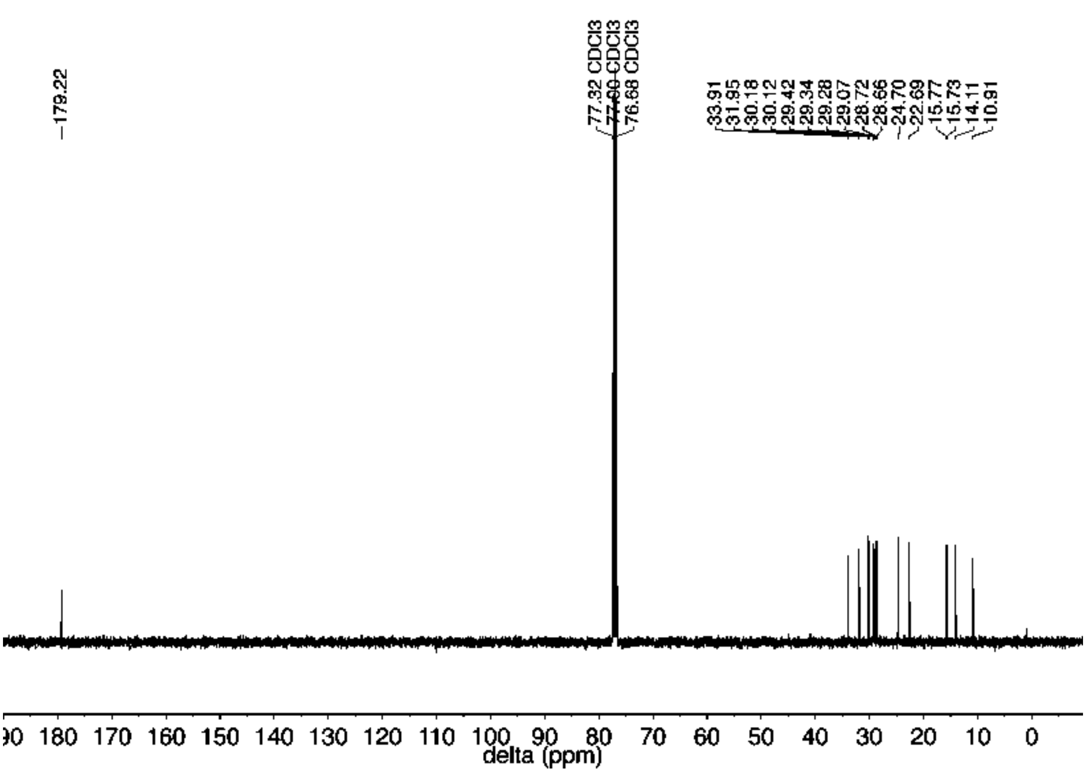

Spectrum 4. ^{13}C NMR (125 MHz, $CDCl_3$) of CP-palmitoleic acid

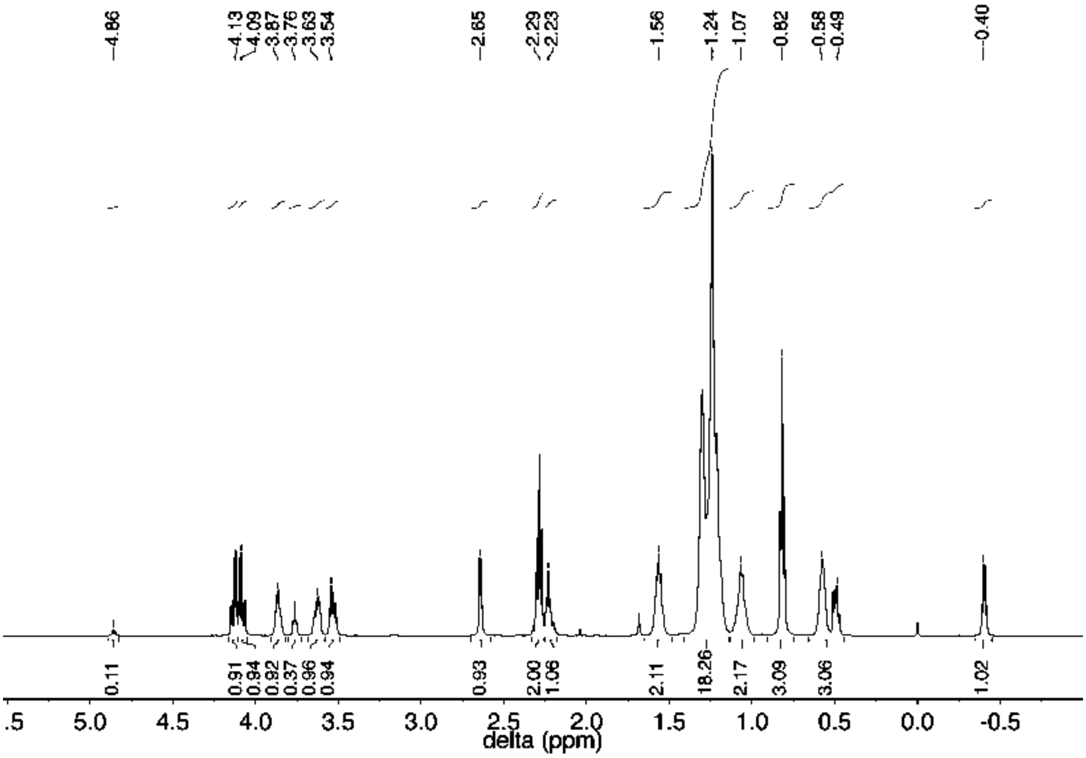

Spectrum 5. ^{1}H NMR (500 MHz, $CDCl_3$) of 1-CPMP and 2-CPMP (10%) mixture

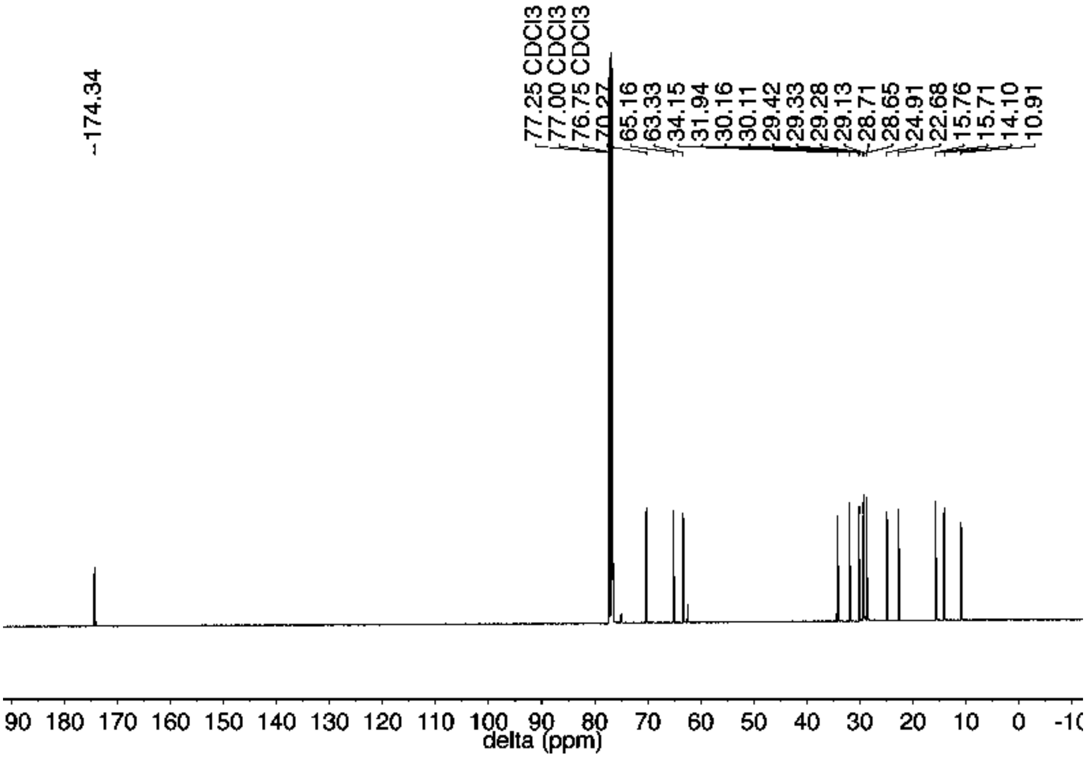

Spectrum 6. ^{13}C NMR (125 MHz, $CDCl_3$) of 1-CPMP and 2-CPMP (10%) mixture

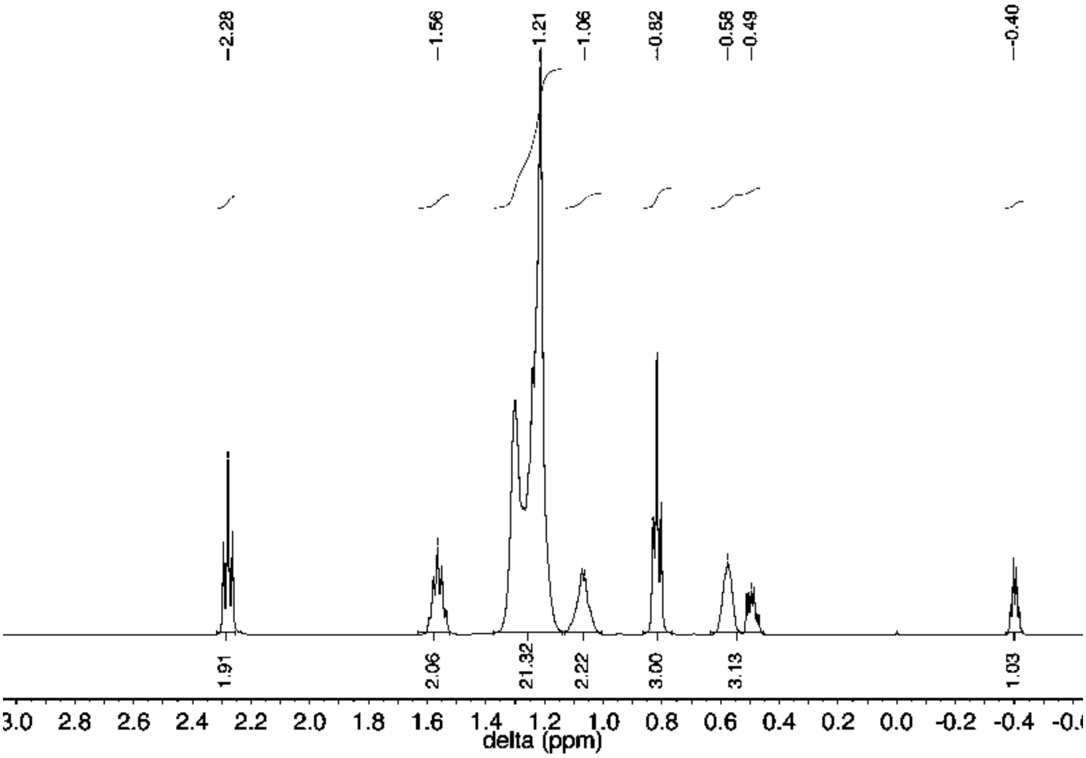

Spectrum 7. ^{1}H NMR (500 MHz, $CDCl_3$) of lactobacillic acid

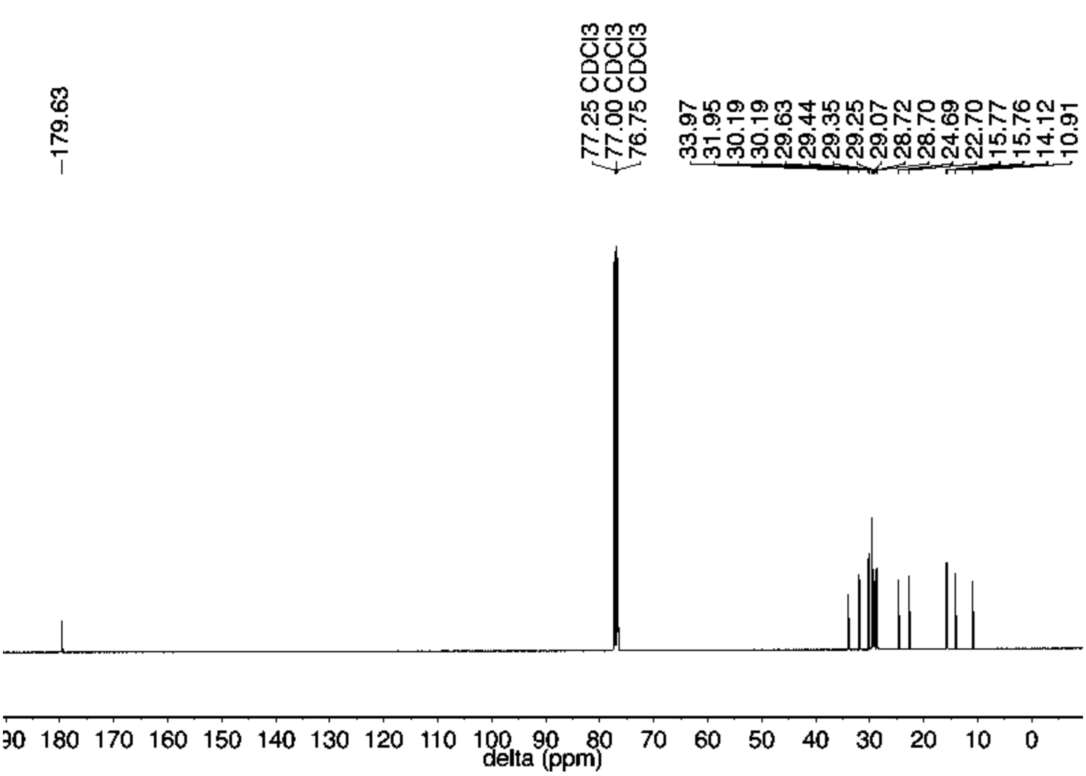

Spectrum 8. ^{13}C NMR (125 MHz, $CDCl_3$) of lactobacillic acid

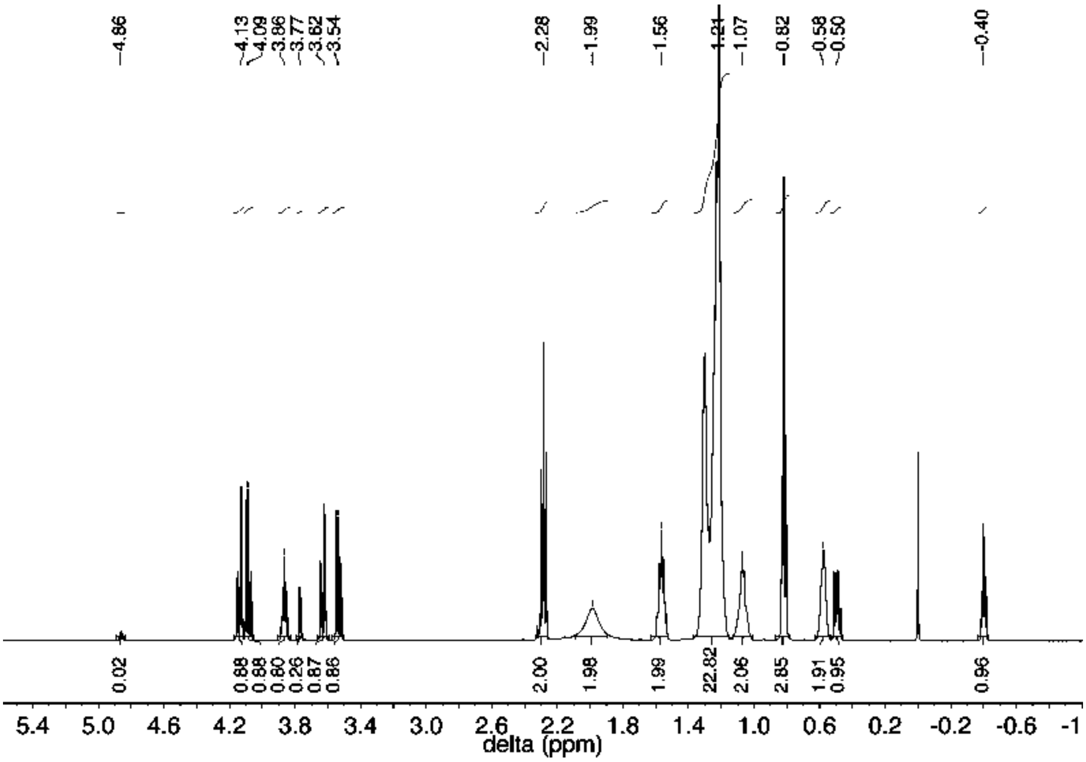

Spectrum 9. ^{1}H NMR (500 MHz, $CDCl_3$) of 1-MLB and 2-MLB (6-7%)

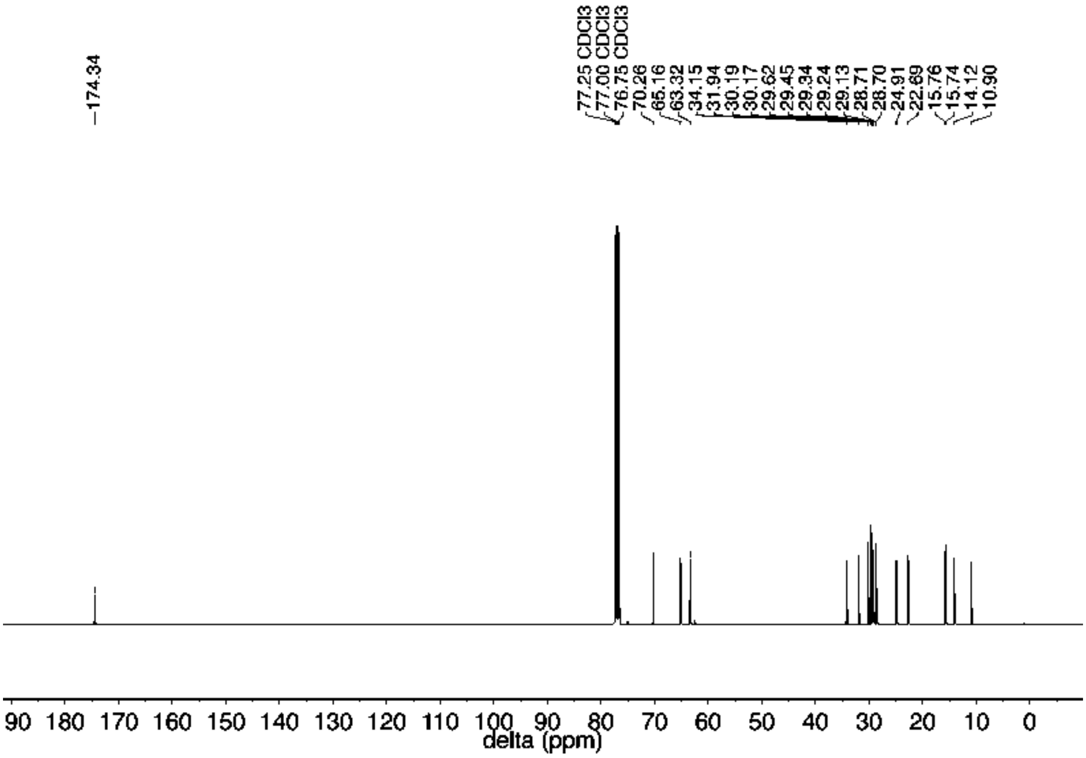

Spectrum 10. ^{13}C NMR (125 MHz, $CDCl_3$) of 1-MLB and 2-MLB (6-7%)

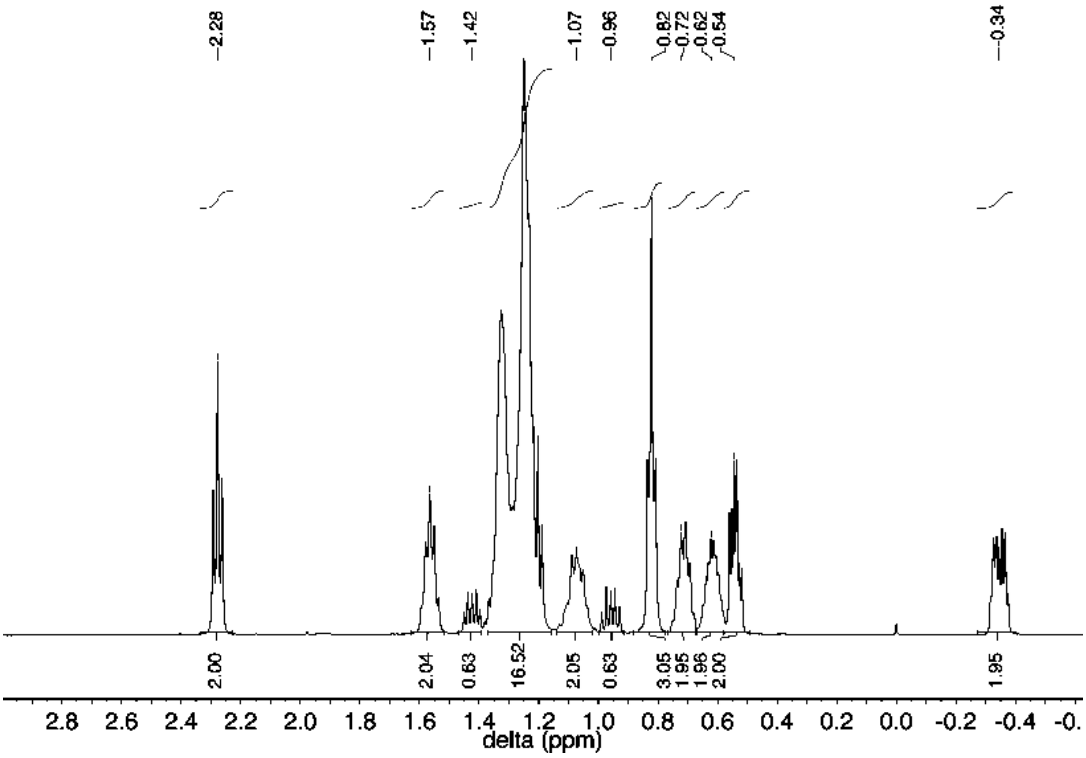

Spectrum 11. ^{1}H NMR (500 MHz, $CDCl_3$) of DCP-linoleic acid

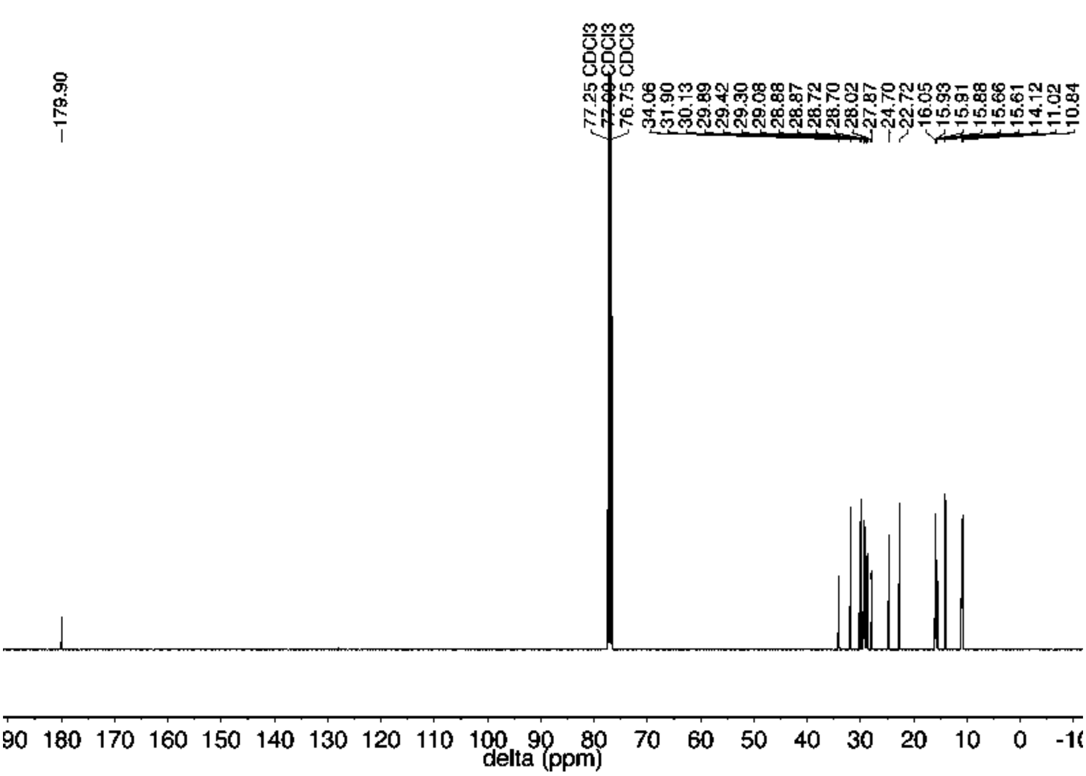

Spectrum 12. ^{13}C NMR (125 MHz, $CDCl_3$) of DCP-linoleic acid

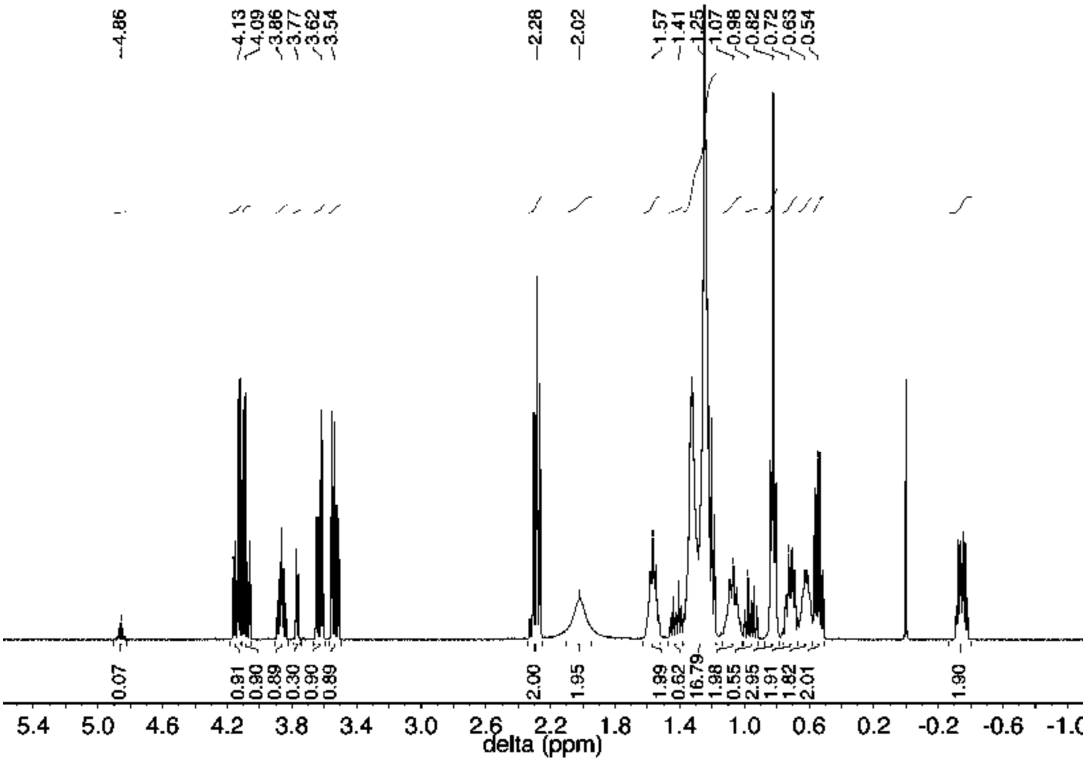

Spectrum 13. ^{1}H NMR (500 MHz, $CDCl_3$) of 1-DCPML and 2-DCPML (7-8%) mixture

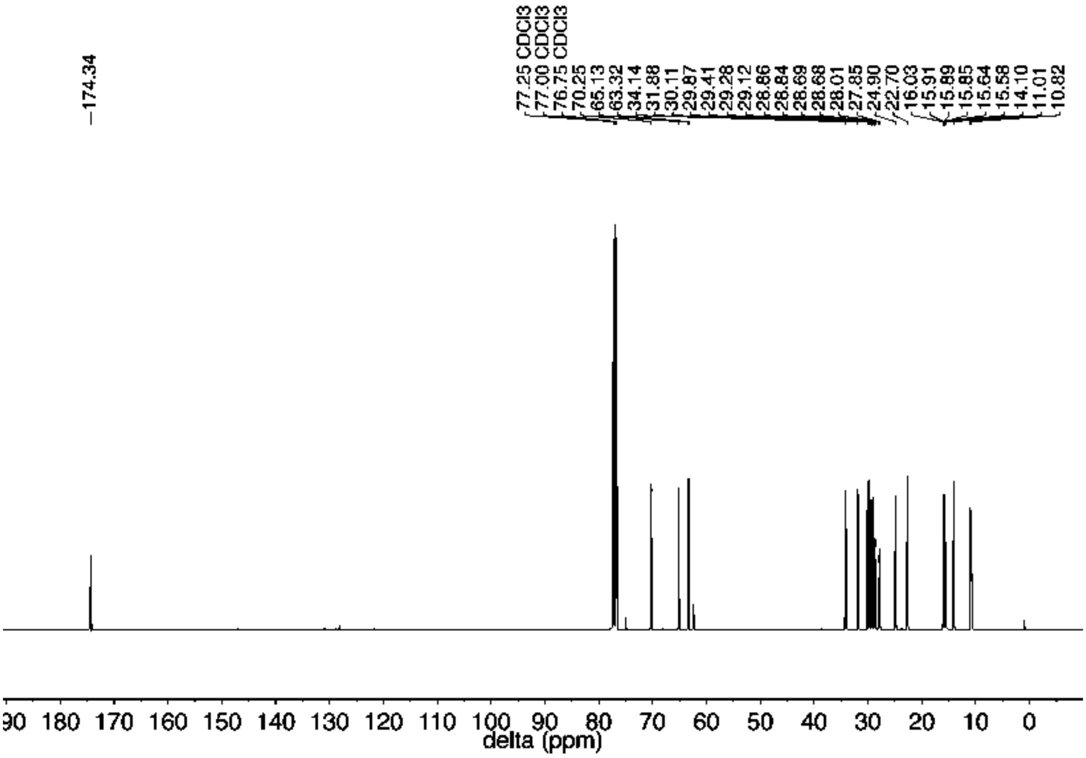

Spectrum 14. ^{13}C NMR (125 MHz, $CDCl_3$) of 1-DCPML and 2-DCPML (7-8%) mixture

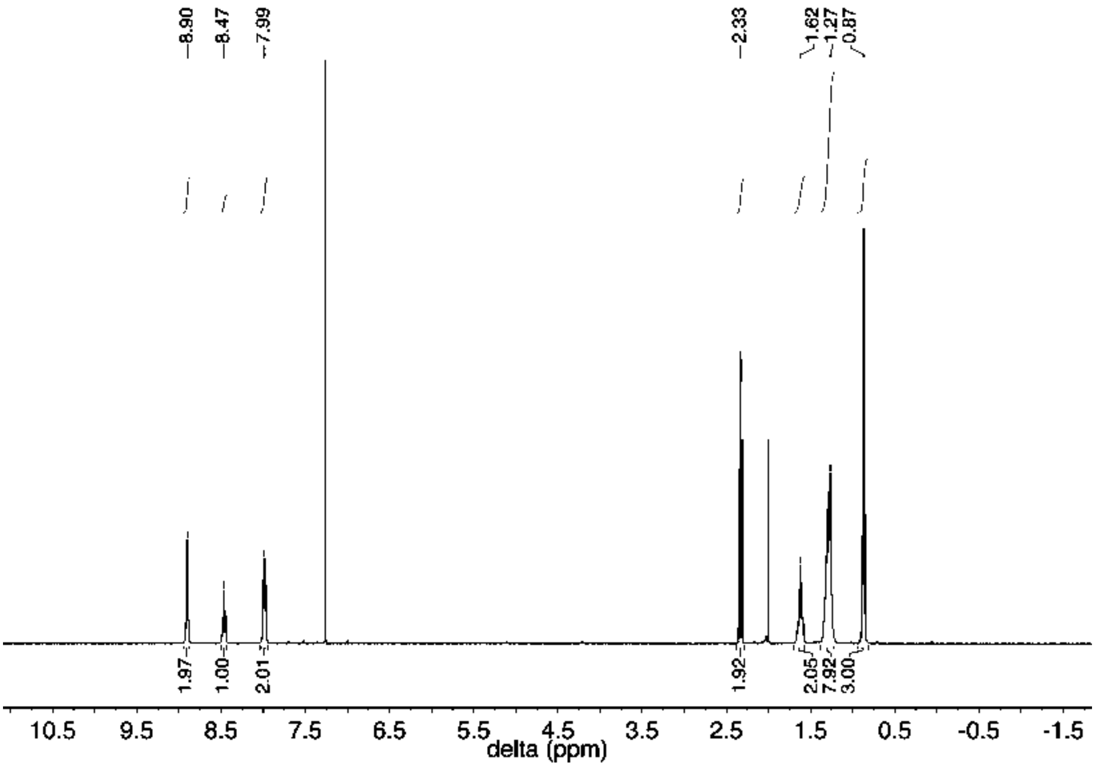

Spectrum 15. ^{1}H NMR (500 MHz, $CDCl_3$) of OADS

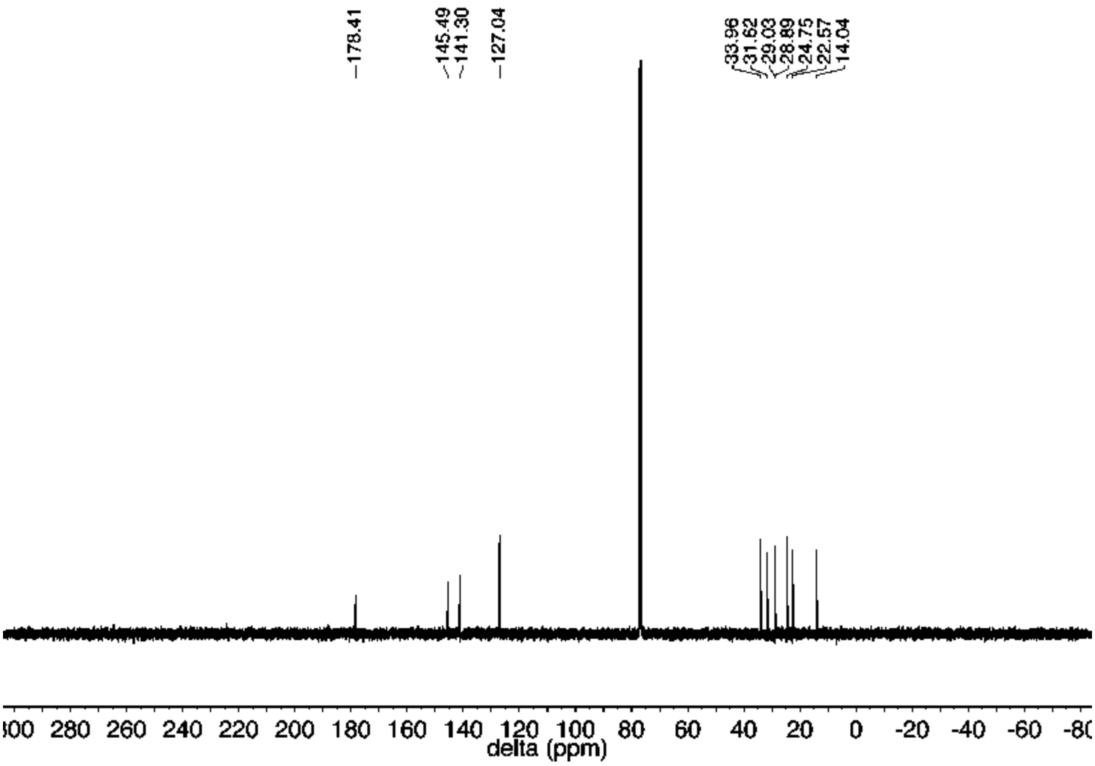

Spectrum 16. ^{13}C NMR (125 MHz, $CDCl_3$) of OADS

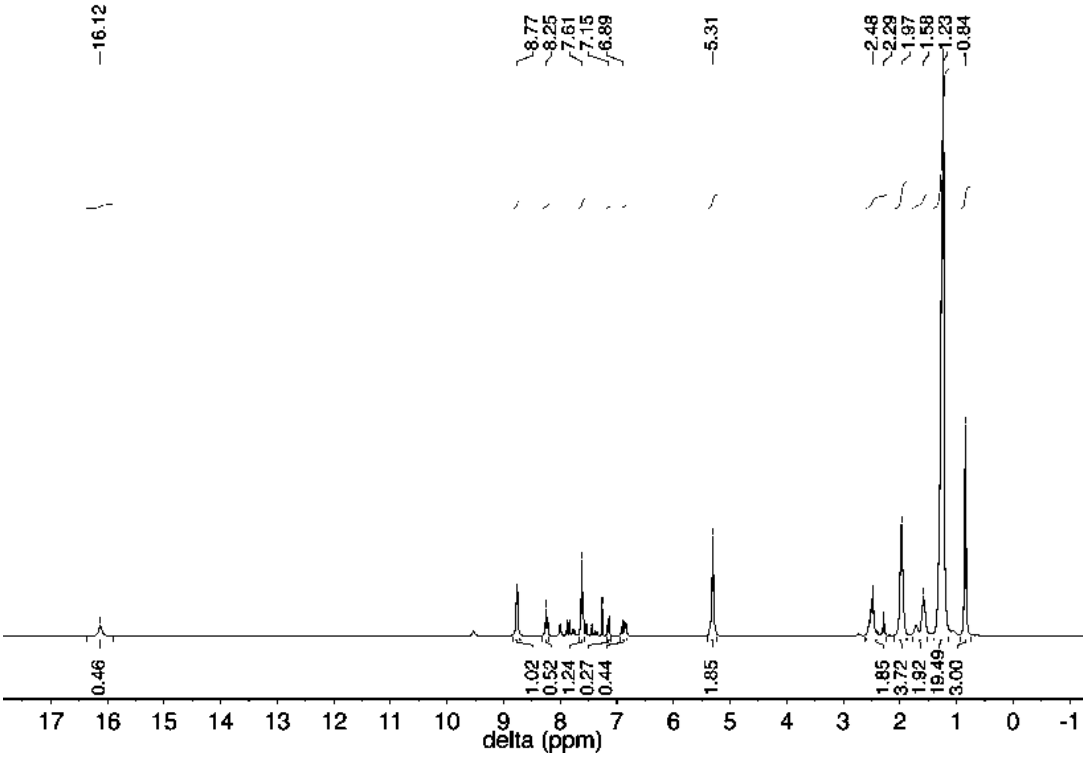

Spectrum 17. ^{1}H NMR (500 MHz, CD_3CN) of 4,4'-oleamidostilbene-2,2'-disulfonate

Appendix 3

Lattice parameters analysis

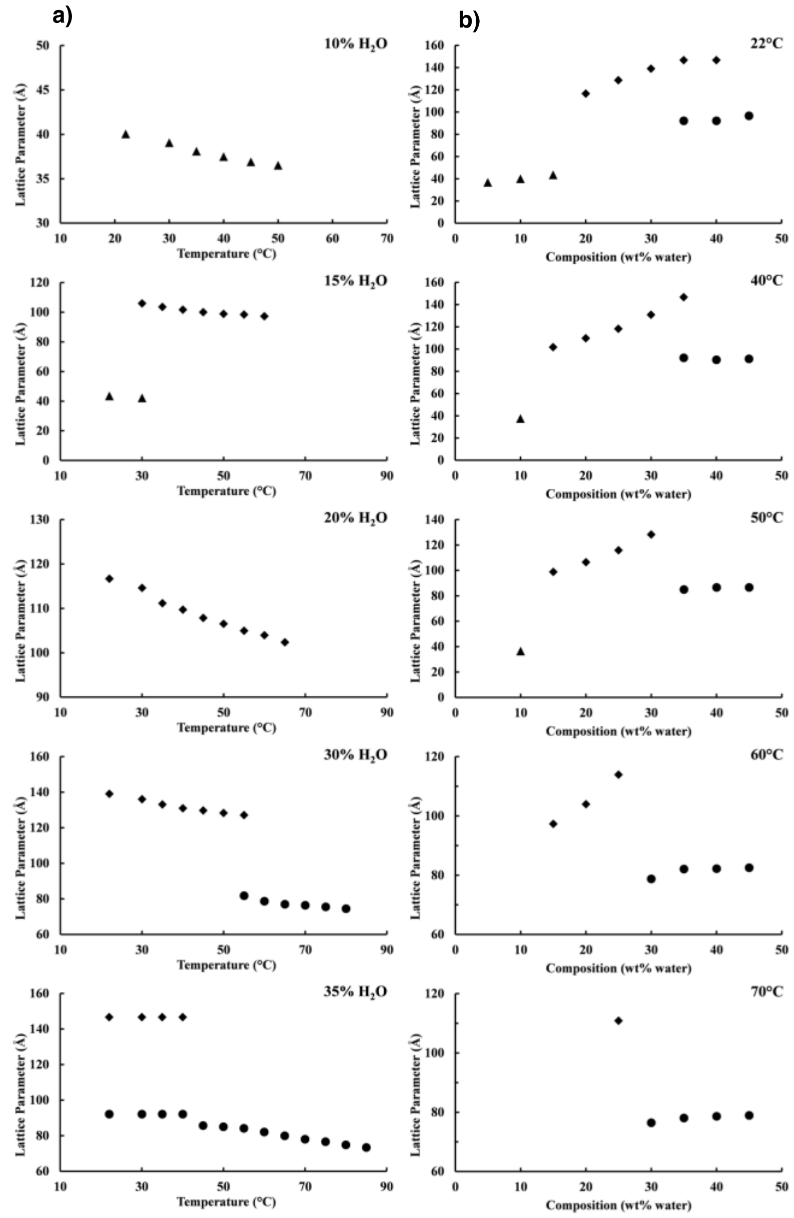

Figure 1. (a) Temperature dependence of the lattice parameters for the different phases (triangle=L_α, square=*Ia3d*, circle=*Pn3m*) observed in the MDS:water system at the indicated sample compositions (% (w/w) water). (b) Composition dependence of the different MDS:water mesophase lattice parameters at the indicated temperatures.

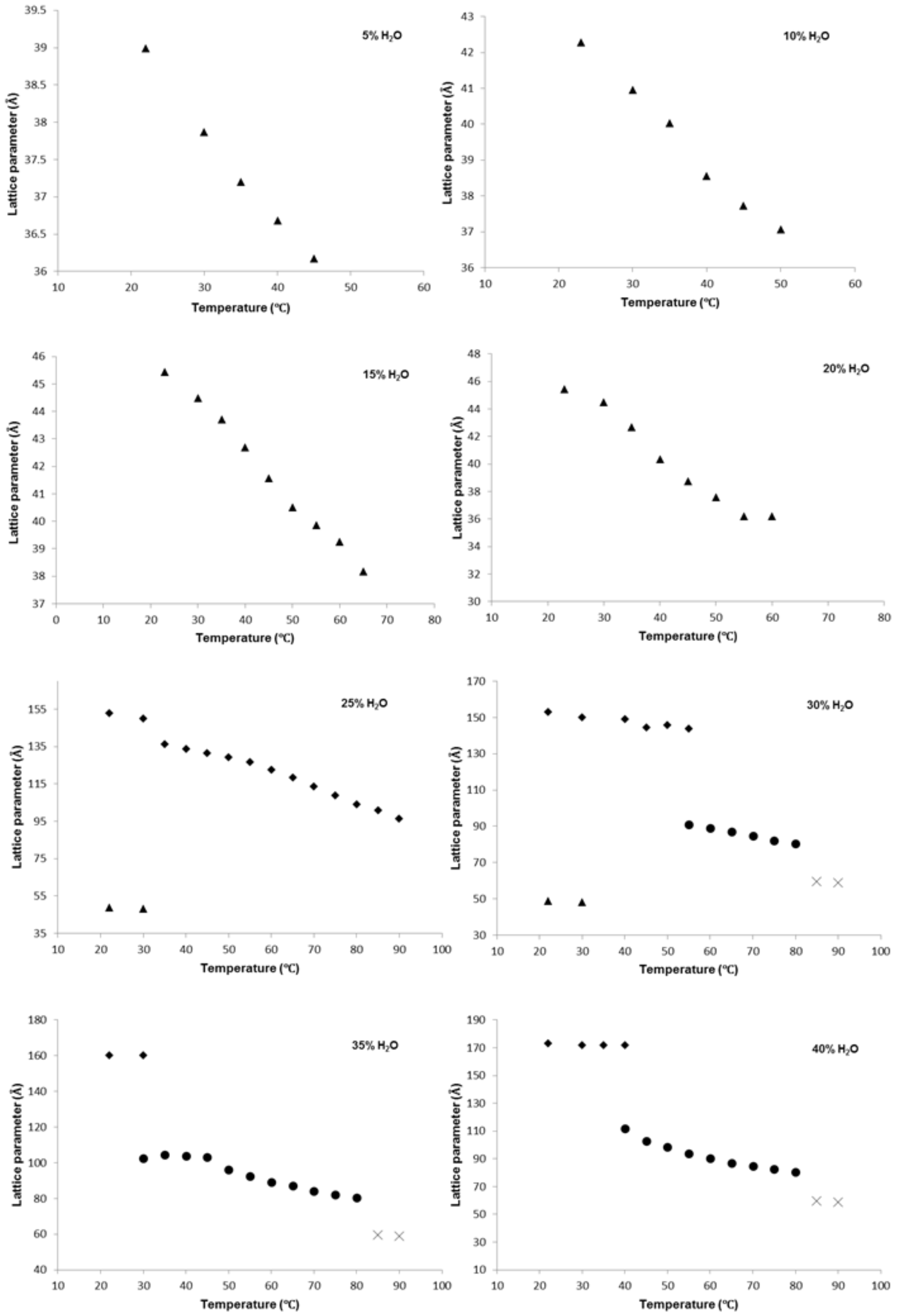

Figure 2. Temperature dependence of the lattice parameters for the different phases (triangle=*L*$_\alpha$, square=*Ia3d*, circle=*Pn3m*) observed in the MLB:water system at the indicated sample compositions (% (w/w) water).

Aknowledgements

I would like to thank the many people that contributed with their knowledge and their support to the realization of this work.

First of all Prof. Dr. Ehud M. Landau for giving me the possibility to work in his group, and for the guidance and advice during these four years.

I would like to thank Prof. Dr. Kim K. Baldridge for her thoughtful consideration and her extremely efficient support, and also for being one of the few female role models that PhD students have in this department.

Thank you to Prof. Dr. Jay S. Siegel for the interesting discussions and his contagious optimism: it was a real pleasure to start working in your group.

Thank you to Prof. Dr. Anthony Linden for his advices and for being part of my PhD committee.

I would like to thank also Prof. Dr. Raffaele Mezzenga for “adopting” me as part of his group, for his useful inputs, the good suggestions and for his constantly open door.

Thank you to Prof. Dr. Raimund Dutzler for his generous support, for the opportunity of working and learning in his group, for the time he spent teaching me and helping my research.

This work would not be possible without the scientific support of Prof. Dr. Andreas Plückthun, Prof. Dr. Oliver Zerbe and Prof. Dr. John A. Robinson. Thank you for your collaborations.

I would like to thank Philipp Ansorge, Jendrik Schöppe, Dr. Gloria Andolina and Simon Jurt for their important inputs into our scientific collaborations and their helpful attitude.

Beat Blattman for his positivism and his expert scientific assistance.

Dr. Alexander Batyuk for the “nerd moments”, for the crystal fishing, the nights at the synchrotron, but also the discussion, the laughs and the beers.

Dr. Cristina Manatschal for her teaching skills, her patience and her smiley help. It was a pleasure to work with you.

All the members of Landau's group, Dr. Yazmin M. Osornio for the initial guidance; Michael Duss for his ability to discerning between important and not important things in science and life and for teaching them to me, Dr. Simone Aleandri for his critical scientific approach, for being always open to discussion and to give suggestions. Marco Etter for his help and advice with any problem a foreigner student can have in Switzerland (including finding good whiskey), and Nicole Kieliger for bringing kindness in the group.

All the members of Mezzenga's group with a particular acknowledgment to Dr. Jijo Vallooran for his friendly help, Dr. Salvatore Assenza for the long evening discussions with good music as a background, Reza Ghanbari for the historical chats and the fun in the office and der Zauber Horst for his fixing everything including my morale.

Thank you to Dr. Giovanna Mancini and Dr. Cecilia Bombelli for being the first people believing I would have make it.

I would like to thank the people that have been my family during these four years: Chiara Speziale because "insieme siamo una forza" brought me here and because having you in Zurich was like bringing with me a piece of home. Dr. Luis Fernández Sánchez, Dr. Igor Pavlović and Giulia Rusconi for the funniest nights in Zurich abd for never letting me down. Dr. Renata Negrini that made me discover Zurich and its beautiful summers. Dr. Arman Nilforoushan and Dr. Alexandru Zabara for being my Swiss brothers, for giving me advice in the most difficult steps of this adventure and for celebrating every single success with me. Dr. Mahsa Taheri for being the sweetest member of our crazy family. Dr. Prof. Dr. Alessandra Iozzi, Prof. Dr. Marc Burger, Gabriel and Raffaello Poritz for the stimulating company, the attention and the warmth that made me feel home during this time here. Dr. Wye Khay Fong for being a smiling encouraging partner in science and life.

Un grazie speciale a tutta la mia grande famiglia che mi s(u)opporta da sempre. A mia nonna, che mi ha insegnato che la saggezza si affina col tempo; a mio fratello, per la sua costante e

rassicurante presenza e ai miei genitori, esempio e punto di riferimento della mia vita.

Curriculum vitae

Personal information

First name - Surname	**Livia Salvati Manni**
Telephone	+41-766830774
E-mail	livia.salvati@chem.uzh.ch or livia.salvati@gmail.com
Nationality	Italian
Date of birth	11/02/1988

Education

Since Jan. 2013: PhD student. Expected graduation date: 20/3/2017

PhD student at University of Zurich and visiting student at ETH Zurich

Thesis Title: “Design of novel lipidic cubic phases for membrane protein crystallization”

Supervisor: Prof. Ehud Landau

2012: **Masters of Chemistry,** University of Rome “Sapienza”

Thesis Title: “Transfer of chirality using lipidic aggregates”

Supervisor: Dr. G. Mancini.

Final mark: 110/110.

2010: **Bachelor of Chemistry,** University of Rome “Sapienza”

Thesis Title: “Regioselective azidolysis of vinylepoxides”.

Supervisor: Dr. G. Righi.

Final mark: 103/110.

2007: **High School Graduation**, Liceo Classico Statale “Amedeo di Savoia”, Tivoli.

Final mark: 100/100.

Languages

Italian (mother tongue), English (fluent).

Conferences

- “Nanodrug delivery: from the bench to the patient”. Rome, Italy, October 10-13, 2011.
- “Nanomedicine: from molecules to diagnosis and therapy”. Rome, Italy, October 1- 3, 2012.
- “Bicontinuous Cubics Satellite Conference 2014”. Noosa, Australia, 30th July - 2nd August, 2014. (poster presentation)
- “International Biophysics Congress (IUPAB)”. Brisbane, Australia, August 3-7, 2014. (poster presentation)

Scientific Schools/Courses

Swiss summer school in Chemical Biology. Villars, Switzerland, September 1-5, 2014.

Winter school in microscopy. Zurich, Switzerland, January 17-22, 2016.

Publications

1) Righi, G.; Salvati Manni, L.; Bovicelli, P.; Pelagalli, R. A New, simple, and mild azidolysis of vinylepoxides. *Tetrahedron Letters,* **2011,** 52, 3895- 3896.

2) Mauceri, A; Borocci, S.; Galantini, L.; Giansanti, L.; Mancini, G.; Martino, A.; Salvati Manni, L.; Sperduto C. Recognition of Concanavalin A by Cationic Glucosylated Liposomes. *Langmuir* **2014**, 30, 11301−11306.

3) Salvati Manni, L.; Zabara, A.; Osornio, Y. M.; Schöppe, J.; Batyuk, A.; Plückthun, A.; Siegel, J. S.; Mezzenga, R.; Landau, E. M. Phase Behavior of a Designed Cyclopropyl Analogue of Monoolein: Implications for Low-Temperature Membrane Protein Crystallization. *Angew. Chem. Int. Ed.* **2015**, 54, 1027- 1031.

4) Speziale, C.; Salvati Manni, L.; Manatschal, C.; Landau, E.M.; Mezzenga, R. A macroscopic H+ and Cl- ions pump via reconstitution of EcClC membrane proteins in lipidic cubic mesophases. *P Natl Acad Sci USA* **2016**, *113*, 7491-7496.

My research has been featured in the following scientific commentaries:

1) Dahl, C. Membrane Protein Won't Crystallize? Try This. *Chem. Eng. News* **2014**, 92, 24.

2) Yeston, J. A more stable phase via triangulation. *Science* **2015,** 347, 245.

Awards and grants

SCNAT/SCS Chemistry Travel Award 2014

Accommodation bursary for Bicontinuous Cubics Satellite Conference 2014

University of Zurich, Forschungskredit 2014

Best Talk Award, Doktorandentag 2015, University of Zurich